European School for Advanced Studies
in Reduction of Seismic Risk

Research Report No. ROSE-2005/02

Dynamic Behaviour of Reinforced Concrete Frames Designed with Direct Displacement-Based Design

by

J. Didier Pettinga
Graduate Student

M.J. Nigel Priestley
Co-Director

ROSE School
c/o EUCENTRE
Via Ferrata 1, 27100, Pavia, Italy

May 2005

TABLE OF CONTENTS

1. INTRODUCTION

Reinforced concrete frame structures are a common building form in seismically active regions. However, the use of such structural forms and the inherent variability in geometric proportions, sectional shapes and material properties means that the dynamic behaviour under earthquake loading has been, and remains, difficult to consistently evaluate.

Developments in seismic design of reinforced concrete structures can largely be attributed to research aimed at better understanding the mechanics of concrete behaviour and thus improving the detail design methods applied to structural and non structural elements. This has reached the extent that in some forms, code requirements are such that newly designed buildings can be considered sufficiently safe under seismic excitation.

Fundamental to the process of seismic design, has been the use of force-based design whereby a set of external forces, seen as equivalent to the inertial forces induced by ground accelerations, are applied to the structure. These design methods are often based on the key assumption that dynamically, the structure will behave principally with first mode response, with requirements for using multi-modal analysis when certain limits structural behaviour are not met. In many situations the first mode dominance is a valid assumption, however it is not necessarily satisfactory to disregard the presence of vibration modes above the fundamental, the so called 'higher modes'.

Studies reported by Paulay (1977), and further presented by Paulay and Priestley (1992), showed that higher modes do in fact play a significant role in reinforced concrete frame and wall behaviour, and that approaches to encompass these effects must be considered, especially when using simplified analysis methods such as the equivalent static lateral force-based approach.

Current code provisions in New Zealand (NZS 4203;1992 and NZS 3101;1995) have adopted the procedures described by Paulay and Priestley (1992), thereby accounting for the presence of higher mode effects using simplified equations that act to scale-up the design moments and shears such that the design envelope should provide sufficient capacity to prevent exceedance under earthquake demands.

Recent work presented by Priestley and Amaris (2002) looked at the dynamic behaviour of reinforced concrete structural walls designed using direct displacement-based design. The results added further emphasis to the importance of dynamic amplification, and emphasises that the current code provisions are in many cases insufficient. As a result of this work a modified form of the commonly used elastic modal superposition, was put forward as a simple and generally very effective approach to accounting for dynamic amplification of wall shear forces and bending moments.

Preliminary studies on frame behaviour designed with direct displacement-based design by Priestley (2003) have however suggested that the method found for wall structures does not transfer to frames in a succinct manner. Results were generally inconsistent and often gave a poor fit to mean envelopes found from inelastic time-history analyses. Hence the need for further work to develop a rational and simple approach for frame structures.

1.1 OBJECTIVES AND INTENT

Because the equations applied in design codes for frame dynamic behaviour were developed using force-based design procedures, it is important to check these methods with displacement-based design approaches to verify if and what differences there are in the dynamic behaviour of buildings designed with such processes.

The apparent inability of the modified modal superposition approach to accurately predict the dynamic behaviour of frame structures is due to many factors. However, one particular issue is that of the variability in geometric parameters. To this extent the research results presented here, attempts to narrow the geometric bounds, such that the behaviour of one particular form of simple frame structure can be assessed. The use of relatively deep beams and short spans has been adopted in what might be termed a 'tube-frame' structure, where by the perimeter frames are intended to act as the principal lateral deformation resisting components. This definition has also been made to ensure reasonable ductility demands by generating relatively stiff structures with low yield displacements. Using code drift limits normal reinforced concrete 2-way frames have ductility demands of about two, hence they would not provide a rigorous investigation of ductile dynamic behaviour.

The intent of this work is to investigate some key aspects of the direct displacement-based design method, using designs for 2, 4, 8, 12, 16 and 20 storey frames. The following points define the objectives and general method.

Using design spectrum compatible accelerograms, a series of inelastic time-history analyses of varying intensity are used to help assess the demands resulting from dynamic amplification.

A systematic investigation of the design displacement profiles and their application to ensure that drift demands satisfy the specified design drift limits. This is particularly important with respect to the ability of the method to control higher mode drift effects.

An examination of the significance of higher mode contributions to column shear forces and bending moments, in particular with respect to ductility demands and earthquake intensity.

2. CURRENT DESIGN APPROACHES

2.1 INTRODUCTION

The standard approach for seismic design of structures, specified in many design codes, involves the development of a base shear value corresponding to a given design spectrum. This design value is often derived for a reduced level of excitation on the proviso that ductile inelastic behaviour is acceptable and allowed for at section and member levels by providing adequate detailing to ensure material behaviour that accommodates the strain demands.

From the reduced design spectrum a set of lateral force vectors can be developed to represent first mode response only, as is the case for equivalent static methods, or as a series of force vectors representing a number of modes as specified in code requirements. These lateral forces are then applied to the structure as external forces and the member actions resulting, taken directly for design or statistically combined to give final design values.

Thus the underlying intent of force-based design involves the specification and attainment of a minimum strength, based on assumptions of initial stiffness, design earthquake intensity and ductile capacity of the structure, as applied through a force reduction factor. In some cases it is required to check the structural deformations, often in the form of storey drifts, against code defined limitations, to verify the deformation behaviour of the structure. This approach contrasts strongly to that of direct displacement-based design whereby structures are designed to attain a specified level of damage commensurate with a given limit state. By specifying a target displacement-based on an equivalent single degree of freedom system, it is possible to derive values of strength, stiffness and thus structural period. This method is further outlined in Chapters 3 and 4.

2.2 FORCE-BASED DESIGN METHODS

The following sections outline the methods of generating design forces described above, including code recommendations for the application of the methods.

2.2.1 Equivalent Static Lateral Force Method

This approach utilises the key assumption that the first mode dominates the structural response to the extent that a direct account of higher modes is not required. Code limitations on the use of this method generally centre around having a first mode period less than a specified maximum and maintaining the vertical and horizontal regularity of the structure.

If a structure satisfies these requirements then the force vector is defined such that the distribution varies linearly up the structure as an 'inverted triangle'. This profile thus matches the fundamental mode shape with no direct account for the higher modes. Some provision can be made, through the use of an additional proportion of force at the roof level. This extra force is specified as 8% in NZS 4203, 10 % by Paulay and Priestley (1992), and ranges from 0 to 25% for the UBC. It is noted that Eurocode 8 (EC8) does not specify this additional force.

The fundamental period of the structure can be estimated through the use of established equations such as that of the Rayleigh Method (NZS 4203:1992, EC8, UBC):

$$T_1 = 2\pi \sqrt{\frac{\sum_1^N \left(W_i \Delta_i^2\right)}{g \sum_1^N \left(F_i \Delta_i\right)}} \tag{2.1}$$

or with simple correlated approximations as suggested in EC8:

$$T_1 = C_t \cdot H^{3/4} \tag{2.2}$$

In which $C_t = 0.075$ for moment resisting concrete frames up to 40m in height and H being the height in meters.

Using design spectra, a value of Spectral Acceleration $S_a(T_1)$ is obtained from which the base shear can be calculated using the total seismic weight of the structure W_t.

$$V_b = S_a(T_1) \cdot W_t \tag{2.3}$$

The base shear can then be distributed as an equivalent lateral force vector at each level *i* using a generalised form:

$$F_i = V_b \frac{W_i h_i}{\sum_{i=1}^{N} (W_i h_i)} \tag{2.4}$$

This form is altered in NZS 4203 to give the additional proportion of base shear applied at the roof level, intended to account for increases in shear and moment values due to higher modes:

$$F_i = F_t + 0.92 \cdot V_b \frac{W_i h_i}{\sum_{i=1}^{N} (W_i h_i)} \tag{2.5}$$

where $F_t = 0.08V_b$ at roof level and 0 for all other levels. The lateral force distribution resulting from this equation is seen in Figure 2-1.

With this distribution of forces the global overturning and storey shear forces can be found along with individual member actions.

2.2.1.1 Methods of Dynamic Amplification.

It is clear that for taller structures this simplified approach is not adequate to account for modes above the fundamental, which tend to take greater participation as overall height increases. Thus it is foreseeable that further account could be made at a later stage of the design process. This has been used in NZS 3101 following the methods presented by Paulay and Priestley (1992) for frames and walls.

Moment Amplification: Equations are presented in NZS 3101 for both one-way and two-way frames, to account for concurrent moment capacity development in beams framing into a column, shifts in column point of contraflexure and in the case of two-way frames the reduced section efficiency for moments applied about the section diagonal axis. The amplification factor is given by ω and takes the following forms and limits for each frame type:

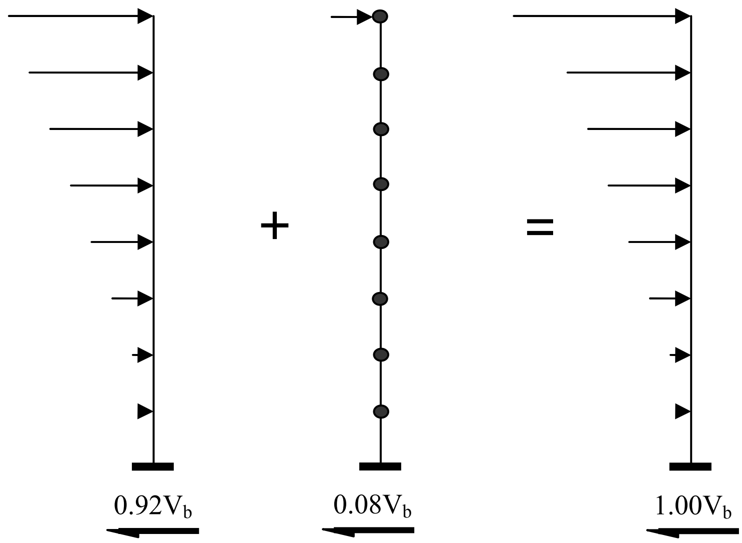

Figure 2-1. The concept of the Equivalent Lateral Force method with additional roof level force

$$\text{One-way frames } 1.3 \le \omega = 0.6T_1 + 0.85 \le 1.8 \tag{2.6a}$$

$$\text{Two-way frames } 1.5 \le \omega = 0.5T_1 + 1.1 \le 1.9 \tag{2.6b}$$

Here T_1 is the fundamental period found by the methods above or some other means such as dynamic modelling with a computer program. As higher mode responses do not affect the required strength at column bases, the value of ω is taken as 1.0 for one-way frames and 1.1 for two-way frames to account for the reduced section efficiency about the diagonal section axis. These factors are also applicable at roof level where it is deemed acceptable for plastic hinges to form in the columns. With the intent of providing a gradual reduction in amplification, the minimum factor allowed in Eq.(2.6a & b) is used for the floor level immediately below the roof.

Because higher mode response is seen to be significant in the upper storeys of a structure, Eq.(2.6a & b) is applied to the upper 70% of the building. From the base to 0.3*H*, a linear variation in ω from 1.0 or 1.1 at the base, to the value calculated from Eq.(2.6a & b) is used.

Thus the distribution of values for the dynamic amplification factor ω can be represented schematically as in Figure 2-2.

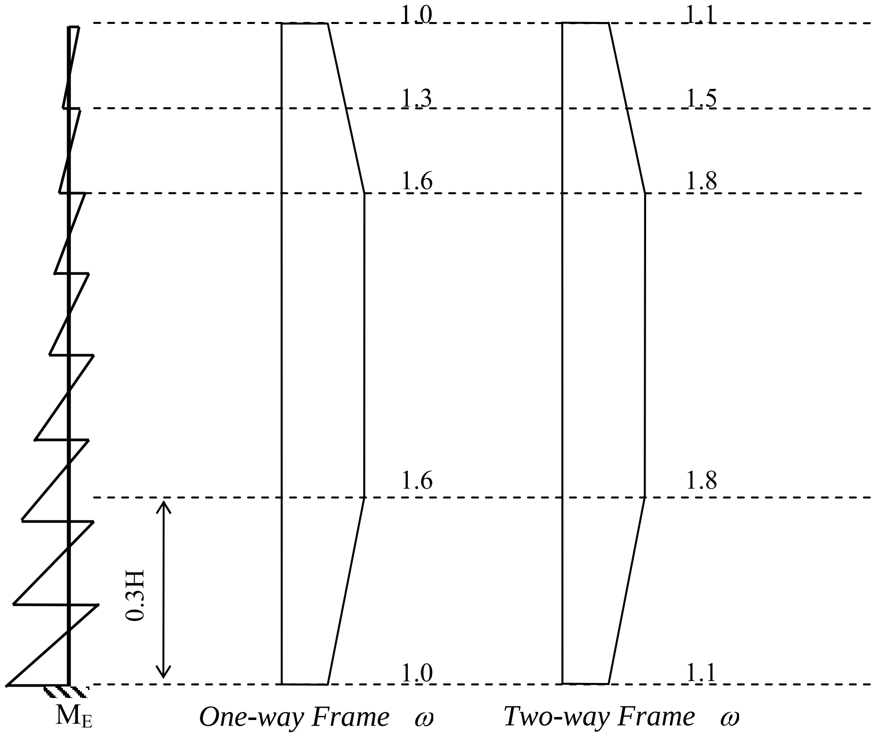

Figure 2-2. Schematic representation of column bending moment dynamic amplification as suggested by Paulay and Priestley (1992) for use with simplified lateral force methods

The dynamic amplification factor is applied in the design moment equation as shown:

$$M_u = \omega \phi_o M_E \tag{2.7}$$

where M_E is the moment value from the equivalent lateral force analysis and ϕ_o is the flexural overstrength factor for plastic hinges that accounts for material overstrength and strain hardening effects. In design this factor is typically specified in relevant material design codes, such as NZS 3101 where a minimum value is defined as:

$$\phi_o = \frac{M_o}{M_E} = \frac{\lambda_o}{\phi} = \frac{1.25}{0.85} = 1.47 \tag{2.8}$$

This value of overstrength is often higher due to practical limitations on available reinforcing bar sizes leading to excess provisions of nominal strength.

For the purposes of this study the flexural reduction factor is taken equal to 1.0, thus $M_o = \lambda_o M_E$, with λ_o calculated and removed from the time-history results following the procedure defined in Section 7.2.2.2.

Shear Amplification: It is possible to make an estimate of column shear by taking the amplified moment gradient found using the method above. It is likely that such an estimate could be excessively conservative. Therefore, with the probability of maximum amplified moments occurring simultaneously at each end of a column being sufficiently low, it is reasonable to consider another method of shear amplification.

Paulay and Priestley (1992) suggested a simple multiplicative factor that accounts for beam moment distribution into columns not following that given by an elastic analysis and thus generating a moment gradient, or shear force, larger than anticipated. This can be interpreted as a shift in the position of the point of contraflexure, and hence an account for dynamic magnification as suggested in the previous section. This approach has been adopted in NZS 3101 in the following forms:

One-way frame upper storeys $V_u = 1.3\phi_o V_E$ (2.9a)

Two-way frame upper storeys $V_u = 1.6\phi_o V_E$ (2.9b)

With typical values of ϕ_o this can result in design values of approximately $1.8V_E$ and $2.2V_E$ for one-way frames and two-way frames respectively.

In first storey columns where hinging is expected at the base, and should be anticipated at the top (due to inelastic first floor beam elongation), shear demands are calculated using the overstrength moments from top $M_{o(top)}$ and bottom $M_{o(bottom)}$ hinging:

$$V_{col} = \frac{M_{o(top)} + M_{o(bottom)}}{L_n} \tag{2.10}$$

where L_n is the clear height of the column from the first floor soffit to the base. Note this should also be applied to the top storey, where it is possible that columns may form plastic hinges before the top floor beams.

2.2.2 Multi-modal Superposition

When a structure does not satisfy code requirements for any one of the following: maximum height, period, and horizontal or vertical regularity, a modal analysis and subsequent combination is generally required (NZS 4203:1992, EC8, UBC). This procedure requires the determination of a number of vibration periods in order to include a sufficient proportion of the structural mass in the analysis. EC8 specifies this proportion to be greater than 90%, with all modes contributing greater than 5% being included (NZS 4203 is similar). Because of the consideration of the modal contributions, this method is assumed to directly account for higher mode effects, especially in the upper levels of a structure, and hence no further amplification is specified for design purposes.

Having determined these values of period and the corresponding mode shapes, the mass participation factors for each mode m can be found by the following:

$$\rho_m = \frac{\left(\sum_{i,m=1}^{N} \phi_{im} m_i\right)^2}{\sum_{i,m=1}^{N} \phi_{im}^2 m_i} \frac{1}{\sum_{i=1}^{N} m_i} \tag{2.11}$$

It is possible to obtain values of Spectral Acceleration, $S_a(T)$, from appropriate design spectra. From these values the base shear corresponding to each participating mode is found by:

$$V_{Bm} = S_a(T_m) g \left(\rho_m \sum_{i=1}^{N} m_i \right) \tag{2.12}$$

In a similar fashion to the equivalent static lateral forces described above, the base shear for each mode is distributed as:

$$F_{im} = V_{Bm} \frac{\phi_{im} m_i}{\sum_{i,m=1}^{N} (\phi_{im} m_i)} \tag{2.13}$$

These forces are applied to the structure as external loads, thus giving the modal member actions. Maximum modal displacements are found from the pseudo displacement spectrum that can be directly calculated from the design spectral accelerations by:

$$\Delta_m = S_a(T_m)g\frac{T_m^2}{4\pi^2} \tag{2.14}$$

This maximum displacement is used to find the modal displacement at each floor level i by the following:

$$\Delta_{im} = \phi_{im}\frac{\sum_{i,m=1}^{N}\phi_{im}m_i\Delta_m}{\sum_{i,m=1}^{N}\phi_{im}^2 m_i} \tag{2.15}$$

The results obtained from the above equations are specific to each vibration mode. Under excitation such as that due to earthquake ground motion, it is unlikely that the modal maxima will occur simultaneously. Thus it is considered that a direct summation of modal quantities will produce design values that are excessively conservative. For this reason it is common to apply one of two statistical combination methods; either the Square Root Sum of the Squares (SRSS) or Complete Quadratic Combination (CQC).

The application of SRSS is limited to some extent by the requirement that two modes of vibration, i and j, are sufficiently separated in periods T_i and T_j, such that correlation between the two modes is not significant. EC8 specifies that SRSS may be used if this separation is such that $T_j \leq 0.9T_i$. The form of the SRSS combinations for equivalent lateral forces, shears and displacements are as follows:

$$F_i = \sqrt{\sum_{i,m=1}^{N}F_{im}^2} \quad V_i = \sqrt{\sum_{i,m=1}^{N}V_{im}^2} \quad \Delta_i = \sqrt{\sum_{i,m=1}^{N}\Delta_{im}^2} \tag{2.16}$$

If the structure does not satisfy this constraint then a more rigorous combination that accounts for modal correlations using cross modal coefficients ρ_{ij} can be used with the following form:

$$F_m = \sqrt{\sum_i \sum_j F_{mi}\rho_{ij}F_{mj}} \tag{2.17}$$

Because the modal superposition method uses values of spectral acceleration, it is common to reduce the design base shear and thus applied lateral forces to allow for ductile structural response. Assuming the equal displacement approximation is valid, this reduction can simply be taken as a direct division of the elastic forces (for all the modes used) by R (the force reduction factor) or q (the behaviour factor) equal to μ_Δ, the design structural displacement ductility. This value is specified in design codes for various structural forms depending on the anticipated ductile capacity of the structure. For reinforced concrete frames the value of μ_Δ is usually taken between 3 and 6.

3. DISPLACEMENT-BASED DESIGN METHOD

3.1 DIRECT DISPLACEMENT-BASED DESIGN

3.1.1 Introduction

Recent developments in seismic design philosophy have centred around the concept of performance-based design. In the past 10 years many researchers have proposed methods of design focusing on performance-based techniques (as summarised and compared by Sullivan et al., 2003). In its purest form this is an approach whereby a structure is designed, not to satisfy a set of performance requirements, but instead to meet the given criteria. In this way a structure is designed and expected to reach a specified acceptable amount of damage under one or more levels of 'design intensity' earthquake. Structures designed in this manner can be expected to exhibit more of a uniform risk, something that is not easily achieved using force-based procedures. It should be noted that most performance-based methods check displacements at the end of the design process, or require transverse reinforcement detailing to match calculated rotations, few procedures proposed actually design to target drift amounts.

Material strain limits are commonly used to define damage limit states. For reinforced concrete these can be defined by concrete compression strains and steel tension (or compression) strains. Often the serviceability limit state (SLS) is defined such that concrete compression strains remain lower than ε_c = 0.004 above which point cover spalling may occur, and corresponding steel tension strains are low enough that residual crack widths are acceptably low, for example ε_s = 0.010 to 0.015. In a similar fashion, a damage control limit state can be defined based on larger strain levels. For concrete compression strains this can be a function of confined concrete strains that can be estimated from allowable transverse reinforcement tension strains caused by lateral concrete expansion, such that:

$$\varepsilon_{cm} = 0.004 + \frac{\left(1.4\rho_s f_{yh}\varepsilon_{suh}\right)}{f'_{cc}} \tag{3.1}$$

Where ρ_s is the confinement volumetric ratio, f_{yh} the transverse steel yield strength, ε_{suh} the transverse steel strain at maximum stress and f_{cc}' the confined concrete compression strength (Mander et al. 1988).

Maximum longitudinal steel tensile strains can be set at any desired level, however for reasons relating to buckling (under reversed loading) and avoidance of low cycle fatigue (Priestley and Kowalsky, 2000) it is prudent to limit this level to the following:

$$\varepsilon_{sm} = 0.6\varepsilon_{su} \tag{3.2}$$

Further to the specification of material strain limits, it is possible, and conceptually more straightforward, to define limit states by drift amounts. For serviceability limits this could be set at $\theta = 0.01$ to avoid non-structural damage, while for damage-control limit states, the amount of structural damage deemed acceptable, is left to choice, however, in many cases this drift limit will be specified in design codes. For instance NZS 4203 limits inter-storey drifts to $\theta = 0.02$ for designs completed without inelastic time-history analysis (for which $\theta = 0.025$ is acceptable).

Underlying the displacement-based design methods is the use of displacement design spectra. Often these are a simple conversion of spectral accelerations given in design codes. Of particular importance in the definition of a displacement spectrum is the so called 'corner-period' beyond which peak displacements are assumed constant for increasing structural period. This reflects the fact that as structural period increases, maximum displacements tend to that of the peak ground displacement, thus for periods over a defined limit, peak displacements can be considered independent of structural period.

The following section outlines one particular form of displacement-based design, namely 'Direct Displacement-Based Design' (Priestley, 1993). The general method is described and appropriate equations defined, along with important assumptions underlying the design process.

3.1.1 Direct Displacement-Based Design Method

The following relations are a summary of the design process developed and described in greater detail by Priestley and Kowalsky (2000) and Priestley et. al (2004).

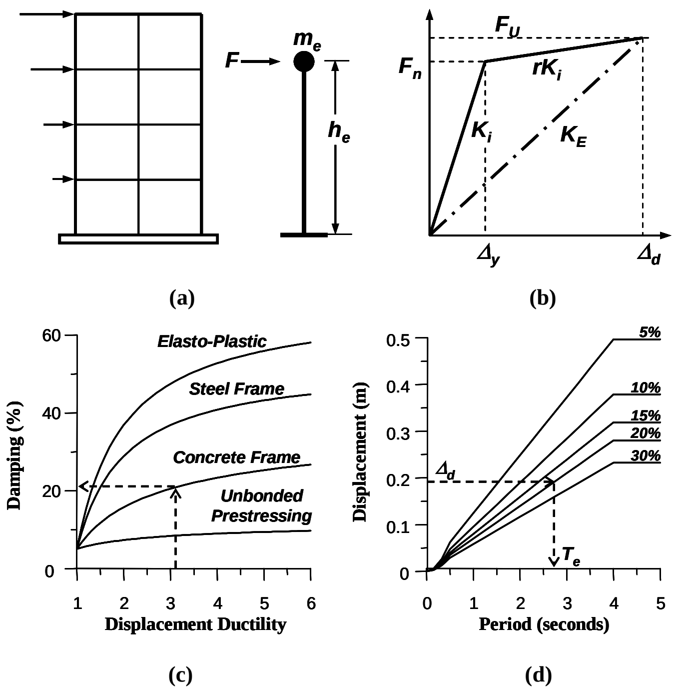

Figure 3-1. Fundamentals of Direct Displacement-Based Design [from Priestley et. al (2004)]

The method of direct displacement-based design is founded on the use of a "substitute structure" as proposed by Shibata and Sozen (1976) and shown in Figure 3-1. This uses an equivalent single degree of freedom (SDOF) representation of a multi-degree of freedom (MDOF) system such that the natural period of the SDOF is given by:

$$T_e = 2\pi\sqrt{\frac{m_e}{K_e}} \tag{3.3}$$

where m_e is the effective mass of the structure, K_e is the effective stiffness at the design displacement and therefore:

$$V_b = K_e \Delta_D \tag{3.4}$$

with Δ_D representing the maximum design displacement of the substitute structure. To incorporate the effects of inelastic action in the real structure, hysteretic damping is combined with elastic viscous damping to give an equivalent viscous damping of the form:

$$\xi_d = 5 + \xi_{hyst}\,\% \text{ which for concrete beams becomes } \xi_d = 5 + 120\left(\frac{1-\mu^{-0.5}}{\pi}\right)\% \qquad (3.5)$$

and is thus applied to reinforced concrete frames as beam plastic hinging is the primary source of inelastic action. Note that μ is defined as the displacement ductility at the design displacement; $\mu = \Delta_D / \Delta_y$. Priestley (1998) showed that the yield drift θ_y can be calculated with sufficient accuracy for design purposes using the relation:

$$\theta_y = 0.5\varepsilon_y \frac{l_b}{h_b} \text{ which multiplied by the } H_e \text{ gives } \Delta_y = 0.5\varepsilon_y \frac{l_b}{h_b} H_e \qquad (3.6)$$

With H_e equal to the effective height. Thus the substitute structure yield displacement can be used to calculate the system displacement ductility, where l_b is the beam length and h_b the storey height. Note that this relation can also be applied to individual storey heights to allow for changes in design drift and beam depth up the height of the building.

The displacement spectrum is used to directly evaluate the displacement demand of the equivalent substitute structure. However, for direct displacement-based design it may be necessary to adjust the displacement spectra for such use. Code based design spectra are normally developed for 5% damping (NZS 4203, EC8, UBC), hence to modify the spectra for damping levels ξ_d other than 5%, the following equation from EC8 is used to give a corrected value of displacement demand for normal accelerograms recorded more than 10km from the fault rupture (the exponent $\beta = ½$):

$$\Delta_{(T,\xi)} = \Delta_{(T,5)}\left(\frac{10}{5+\xi_d}\right)^{1/2} \qquad (3.7)$$

Where $\Delta_{(T,\xi)}$ and $\Delta_{(T,5)}$ are the design spectrum corner displacements at the calculated equivalent viscous damping level and 5% design level spectrum respectively. EC8 gives two values for the corner-period T_D, depending on the earthquake type defined for a given region. For Type 1 spectra, T_D = 2.0 seconds, while for Type 2 spectra T_D = 1.2 seconds. However, recent work (Faccioli et al., 2004) has shown that the corner period is dependent on magnitude and epicentral distance, hence it would seem appropriate to extend the corner period beyond such low values as given by EC8 in order to develop results applicable to regions of higher seismicity.

The equivalent substitute structure approximates the multi-degree of freedom structure at peak response, thus the effective stiffness of the structure is significantly lower than that for an 'elastic' structure. Therefore the effective period T_e is significantly longer and the displacement response spectra should be adjusted accordingly to account for this phenomenon. This is another reason for the extension of the corner period beyond that specified in many codes.

Assuming a linear displacement spectrum (note this is not always the case) and an appropriate corner period with corresponding displacement demand, Eq.(3.3) and (3.7) can be substituted into Eq.(3.4) to give:

$$V_b = K_e \Delta_D = \frac{4\pi^2 m_e}{T_c^2} \frac{\Delta_{(c,5)}^2}{\Delta_D^2} \left(\frac{10}{5+\xi_d} \right)^{1/2} \tag{3.8}$$

with Δ_D found from:

$$\Delta_D = \frac{\sum_{i=1}^{n} m_i \Delta_i^2}{\sum_{i=1}^{n} m_i \Delta_i} \tag{3.9}$$

where m_i and Δ_i are the masses and design displacements at each significant level i of the structure up to n storeys. The effective mass m_e is calculated in a similar fashion:

$$m_e = \frac{\sum_{i=1}^{n} m_i \Delta_i}{\Delta_D} \tag{3.10}$$

Further, the effective height of the substitute structure is found from:

$$H_e = \frac{\sum_{i=1}^{n} m_i \Delta_i H_i}{\sum_{i=1}^{n} m_i \Delta_i} \tag{3.11}$$

The final component of the direct displacement-based design process is an assumed displacement profile for the structure. As the equivalent substitute structure seeks to model peak response, the profile needs to reflect the inelastic deformed shape of the building. Earlier studies (Priestley, 1993; Loeding et al., 1998) proposed three separate normalised equations for reinforced concrete frame buildings that are applied individually depending on the number of storeys, as follows:

for $n \leq 4$: $$\phi_i = \frac{H_i}{H_n} \tag{3.12a}$$

for $4 \leq n < 20$: $$\phi_i = \frac{H_i}{H_n}\left(\frac{16-0.5\frac{H_i}{H_n}\cdot(n-4)}{16-0.5(n-4)}\right) \tag{3.12b}$$

for $n > 20$: $$\phi_i = \frac{2H_i}{H_n}\left(1-0.5\frac{H_i}{H_n}\right) \tag{3.12c}$$

Where H_n is the total height of the structure, H_i the height to each storey i and n the number of storeys.

The storey displacements are found using:

$$\Delta_i = \phi_i \cdot \left(\frac{\Delta_c}{\phi_c}\right) \tag{3.13}$$

Where Δ_c and ϕ_c are the critical storey displacement and critical normalised design profile displacement. Having calculated a value of base shear using the above equations, it remains to distribute this force up the height of the building. In a similar fashion to the equivalent lateral force methods described previously this is done in proportion to the masses and displacements at each level of significant mass i:

$$F_i = V_B \frac{\Delta_i m_i}{\sum_{i=1}^{n} \Delta_i m_i} \tag{3.14}$$

It is possible to apply this lateral force distribution to an elastic computer model with correct stiffness definitions, to generate the member shears and moments under this loading. However, one principal intent in the development of direct displacement-based design is to maintain simplicity and clarity in the design procedure; in effect avoiding where possible, the potential for inappropriate computer modelling. Therefore, with some reasonable assumptions (described in Chapter 4), it is possible to find the member design actions using the process developed in the following section.

Finally, by designing the frame so that yield displacements, displacement ductilities and equivalent viscous damping are calculated at each level of the structure, it is possible to use a relation similar to that used for buildings with multiple structural walls, to calculate the overall effective damping of the substitute structure. Using an average value of damping, weighted in proportion to the beam design moments (found using the method described in Section 4.1) the changes in damping at each level (from varying beam yield curvatures and displacement profile) can be taken into account. While the beam design moments are not known at this stage of the process, they can be related to the equivalent lateral force distribution found from Eq.(3.14). Thus the damping contribution can be seen to relate to the storey displacements, therefore this weighted average becomes:

$$\xi_{eff} = \sum_{i=1}^{n} \left[\frac{\sum_{j=i}^{n} \Delta_j m_j}{\sum_{i=1}^{n} \left(\sum_{j=i}^{n} \Delta_j m_j \right)} \cdot \xi_{d,i} \right] \tag{3.15}$$

This value of effective damping is that used in Eq.(3.8) ($\xi_d = \xi_{eff}$) to evaluate the design base shear.

4. DDBD FRAME DESIGN PROCEDURES

4.1 GENERALISED DESIGN PROCEDURE

In a simplified form, the overturning moment at the building base can be determined by:

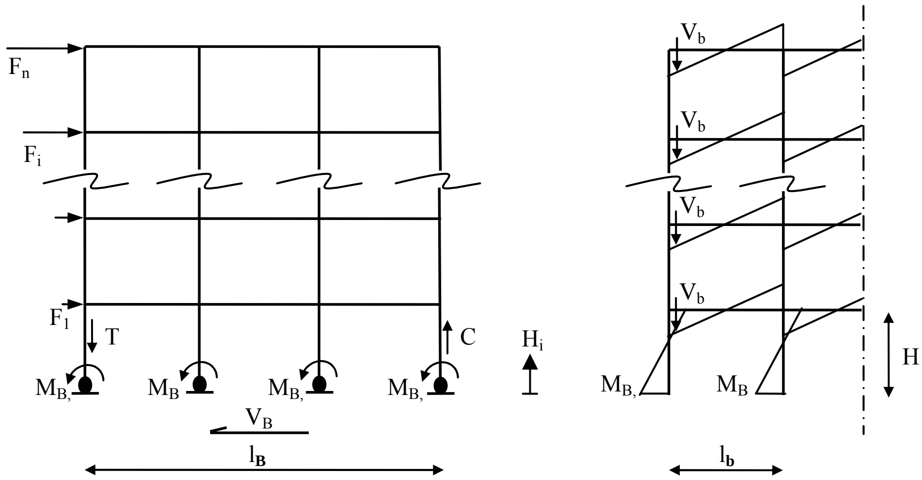

Figure 4-1. Schematic representation of the simplified design approach used for this study

$$OTM = \sum F_i H_i \tag{4.1}$$

Therefore assuming that for a regular frame structure (Figure 4-1 and Figure 4-2) significant variations in seismic axial load only occur in the outside columns, the following relation can be rearranged and used to find the seismic axial tension force *T* in the outer column.

$$OTM = \sum M_B + T \cdot L_B \tag{4.2}$$

Note that the proportion of overturning moment resisted by column base bending, ΣM_B, is an arbitrary design decision. Priestley and Kowalsky (2000) assume a point of contraflexure in the bottom storey columns of $0.6H_1$ from the base. Therefore the column base flexural contribution for k columns is:

$$\sum M_B = M_1 + M_2 + \ldots + M_k = V_B(0.6H_1) \tag{4.3}$$

As the outer column tension force is the sum of the seismic beam shears up the building $T_c = \sum V_{bi}$; it is possible to determine a distribution of beam shears, which under the assumption of seismically dominated beam flexural behaviour can be used to calculate the beam end moment demands. While the distribution of beam shears is also an arbitrary decision, and to some extent appears to have minimal influence, it is proposed that these forces be allocated in proportion to the column storey shear of the level below the beam level i being considered, which can be represented as the following:

$$V_{Bi} = T \frac{V_{C,i,i-1}}{\sum_{i=1}^{n} V_{C,i,i-1}} \quad \text{with} \quad V_{C,i,i-1} = \sum_{j=1}^{j=n} F_j \tag{4.4}$$

Here j denotes the storey below the beam level being considered and $V_{C,i,i-1}$ is the storey shear force below the particular beam level. With the seismic beam shears defined, the corresponding beam end moments at the column centreline are simply:

$$M_{bi} = V_{bi} \frac{l_b}{2} \tag{4.5}$$

These seismic beam moments are taken as the design moments for the members, with the assumption of moment-redistribution being used to account for gravity moment contribution. However in some cases this may not be appropriate, particularly when dealing with long-span beams that are dominated by gravity load demands.

To assign moment distributions to the columns, the proportion of base shear β resisted by each column must be decided. This is a design decision and will vary for different structures, however, for the case of the regular frames used in this study, proportions were set such that the moment distributions were close to those found using an elastic lateral force analysis. For the frames studied, where four columns were present (Figure 4-2), the proportions were kept at $0.17V_B$ to each of the outside columns and $0.33V_B$ to each inside column.

To derive the distribution of moments above the column base, joint equilibrium was maintained using the cumulative storey shear found by Eq.(4.4). Thus having set the individual column base moment as:

$$M_{B,k} = \beta \cdot V_B \left(0.6H_1\right) \tag{4.6}$$

the bottom storey top moment $M_{i,top,k}$ can be found to satisfy the value of βV_B and therefore knowing the first floor beam moment, by equilibrium the value of the column design moment above the first floor joint can be calculated so that:

$$M_{i+1,bottom,k} = M_{bi} - M_{i,top,k} \tag{4.7}$$

In a similar fashion to the first storey column, the second storey top moment can be found from:

$$M_{i+1,top,k} = \beta V_{C,i} \cdot h_{i+1} - M_{i+1,bottom,k} \tag{4.8}$$

The process follows in the same manner to each successive storey above. It is possible that initial assumptions of base shear distribution between columns may produce unrealistic bending moment distributions in the upper levels of the frame, in which case the proportions can be adjusted to achieve values suitable for design.

Having determined the design moments and shears for the frame, it is then a matter to develop the reinforcement detailing suitable for the given demands, as follows using current methods of reinforced concrete Capacity Design.

4.2 DESIGN PROCEDURE AS APPLIED TO THIS STUDY

4.2.1 Frame Descriptions

The intent of this study was to assess the dynamic behaviour of moment resisting reinforced concrete perimeter frames, or 'tube-frames' that have become a common form of lateral force resistance. These frames are generally characterised by the use of short spans with deeper than usual beams, relative to the columns. Thus they are comparatively stiff, commonly with a low yield displacement. In comparison the internal frames for such systems are required only for gravity support, and are therefore more slender and flexible.

For this study the following frame properties (Table 4-1) and geometries (Table 4-4) were used, with values of concrete compressive strength f_c' and steel yield strength f_y defined so that material overstrength was already accounted for in the design and therefore could be ignored in looking at the results from the analyses. The Modulus of Elasticity for concrete was calculated using $E_c = 4700\sqrt{f_c'}$.

Table 4-1. Basic material parameters assumed in frame design and modelling

Property	f_c'	E_c	ρ	ν	f_y	ε_y
Value	35 MPa	27800 MPa	2.4 t/m3	0.3	450 MPa	0.00225

The definition of a tube-frame implies that under seismic attack, the exterior frames provide the dominant form of lateral resistance. Therefore, in this study the seismic weights are somewhat higher than are expected for normal flexible frames. Table 4-2 outlines how the seismic weight was assumed to be distributed up the height of the structure, to represent dead and live load contributions.

Table 4-2. Frame seismic weight parameters

Levels *n*	Seismic Weight	Gravity Weight
Roof: *n*	2500 kN	1250 kN
All levels: 1 to *n*-1	3000 kN	1500 kN

Thus the frames are modelled as lumped mass systems, with the mass at each level mass being distributed to the beam-column joints to represent the proportion carried laterally and vertically, based on tributary member lengths. To these weights the beam and column self weights are added at each joint in a similar fashion.

Figure 4-2 schematically presents the six frames investigated, ranging from two to twenty storeys in height, with a constant inter-storey height of 3.5 meters and beam span length of 5 meters for all beam bays. Table 4-4 defines the beam and column section sizes used at each level in each of the frames.

4.2.2 Displacement Design Spectrum

The design displacement spectrum was defined using the forthcoming version of EC8 (based on the May 2002 draft). Previous studies using direct displacement-based design have tended to use values of Peak Ground Acceleration around 0.4*g*, however for this study a somewhat higher value of 0.6*g* was used with the assumption of "moderately soft ground" which can be characterised by Soil Type *B*.

Therefore to generate the generic 5% damping, elastic response spectrum the following parameters apply:

Table 4-3. EC8 elastic response spectrum parameters for Soil Type B

PGA	S	γ	η	T_b	T_c	T_d
0.6g	1.2	1	1	0.15	0.5	5

Note that the corner period of the displacement spectrum that can be derived from the acceleration spectrum was extended to 5 seconds, from the code specified maximum of 2 seconds. This is because for large magnitude earthquakes found in many regions of the world, the assumption of constant displacement demand for structural periods beyond 2 seconds, has been found inappropriate (Faccioli et al., 2004) and is summarised with respect to direct displacement-based design by Priestley et al. (2004). Also, the use of an effective period as defined in Section 3.1.1 can require the extension of the design displacement spectrum in order to accommodate differences in response due to the influence of ductility, as effective periods can be significantly longer than the corresponding elastic period (Priestley and Kowalsky, 2000).

Based on the following equations [Eq.(4.9)] defined in EC8, the design spectrum is presented in Figure 4-3.

$$\begin{aligned}
&0 \leq T \leq T_B: && S_e(T) = a_g \cdot S \cdot \gamma \cdot \left[1 + \frac{T}{T_B} \cdot (\eta \cdot 2.5 - 1)\right] \\
&T_B \leq T \leq T_C: && S_e(T) = a_g \cdot S \cdot \gamma \cdot \eta \cdot 2.5 \\
&T_C \leq T \leq T_D: && S_e(T) = a_g \cdot S \cdot \gamma \cdot \eta \cdot 2.5 \left[\frac{T_C}{T}\right] \\
&T \geq T_D: && S_e(T) = a_g \cdot S \cdot \gamma \cdot \eta \cdot 2.5 \left[\frac{T_C T_D}{T^2}\right]
\end{aligned} \tag{4.9}$$

The design spectral accelerations can then be converted to the design displacement spectrum using the relation in Eq.(4.10).

$$S_d = S_a(T) \cdot \left(\frac{T}{2\pi}\right)^2 \tag{4.10}$$

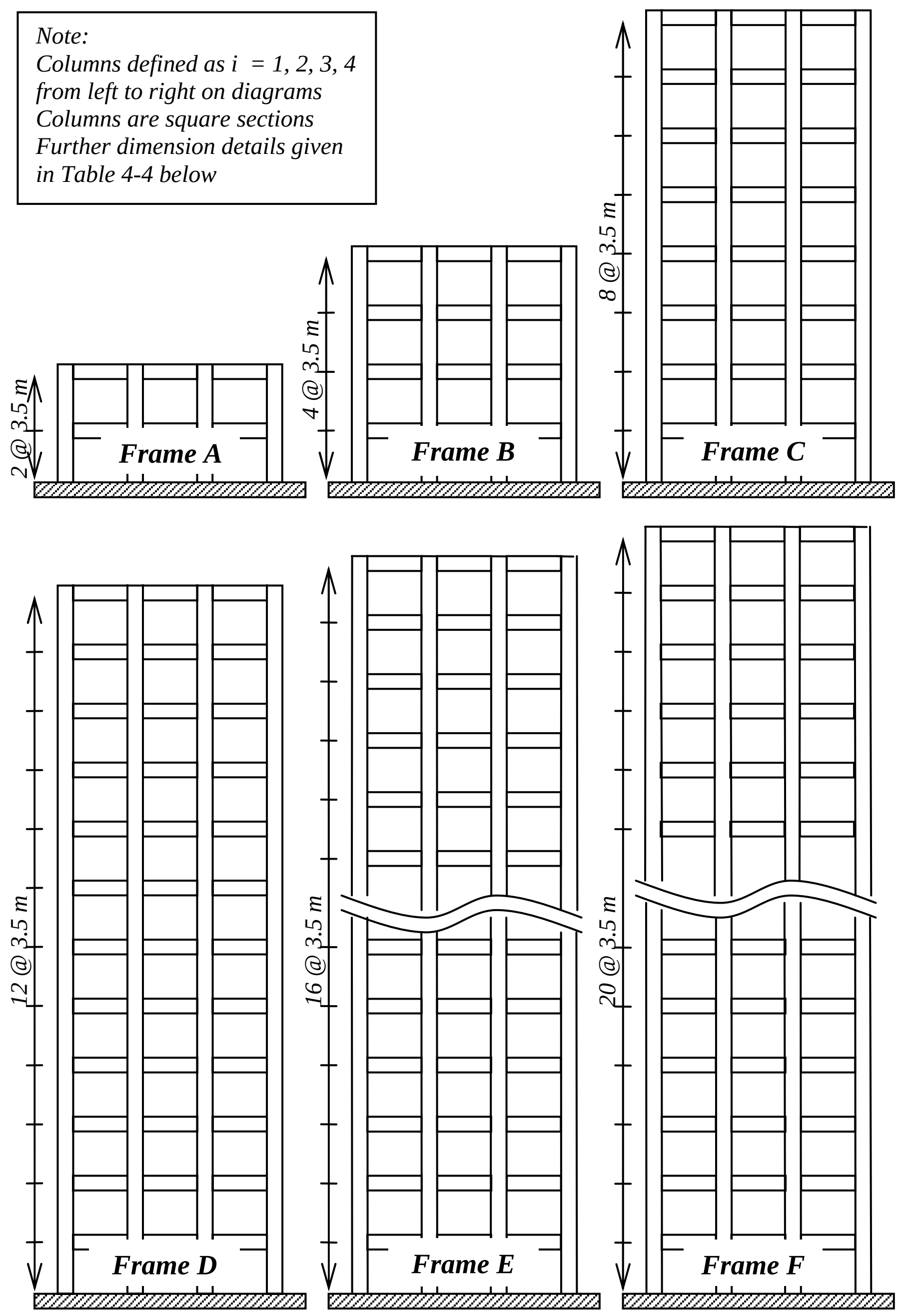

Figure 4-2. Building frame geometries

Table 4-4. Frame member geometries

n	Frame A				Frame B				Frame C				Frame D				Frame E				Frame F			
	Columns (square)		Beams		Columns (square)		Beams		Columns (square)		Beams		Columns (square)		Beams		Columns (square)		Beams		Columns (square)		Beams	
i	**1&2**	**3&4**	b_w	h_b	**1&2**	**3&4**	b_w	h_b	**1&2**	**3&4**	b_w	h_b	**1&2**	**3&4**	b_w	h_b	**1&2**	**3&4**	b_w	h_b	**1&2**	**3&4**	b_w	h_b
20																					950	950	400	900
19																					950	950	400	900
18																					950	950	400	900
17																					950	950	400	900
16																	850	850	400	900	950	950	400	900
15																	850	850	400	900	950	950	400	900
14																	850	850	400	900	950	950	400	1200
13																	850	850	400	900	950	950	400	1200
12													800	800	400	900	850	850	400	900	950	950	400	1200
11													800	800	400	900	850	850	400	900	950	950	400	1200
10													800	800	400	900	850	850	400	1200	950	950	400	1200
9													800	800	400	900	850	850	400	1200	950	950	400	1200
8									700	700	400	900	800	800	400	900	850	850	400	1200	950	950	400	1400
7									700	700	400	900	800	800	400	900	850	850	400	1200	950	950	400	1400
6									700	700	400	900	800	800	400	900	850	850	400	1200	950	950	400	1400
5									700	700	400	900	800	800	400	900	850	850	400	1200	950	950	400	1400
4					700	700	400	900	700	700	400	900	800	800	400	900	850	850	400	1200	950	950	400	1400
3					700	700	400	900	700	700	400	900	800	800	400	900	850	850	400	1200	950	950	400	1400
2	650	650	400	900	700	700	400	900	700	700	400	900	800	800	400	900	850	850	400	1200	950	950	400	1400
1	650	650	400	900	700	700	400	900	700	700	400	900	800	800	400	900	850	850	400	1200	950	950	400	1400

NB: b_w is the beam shear width; h_b is the total beam depth

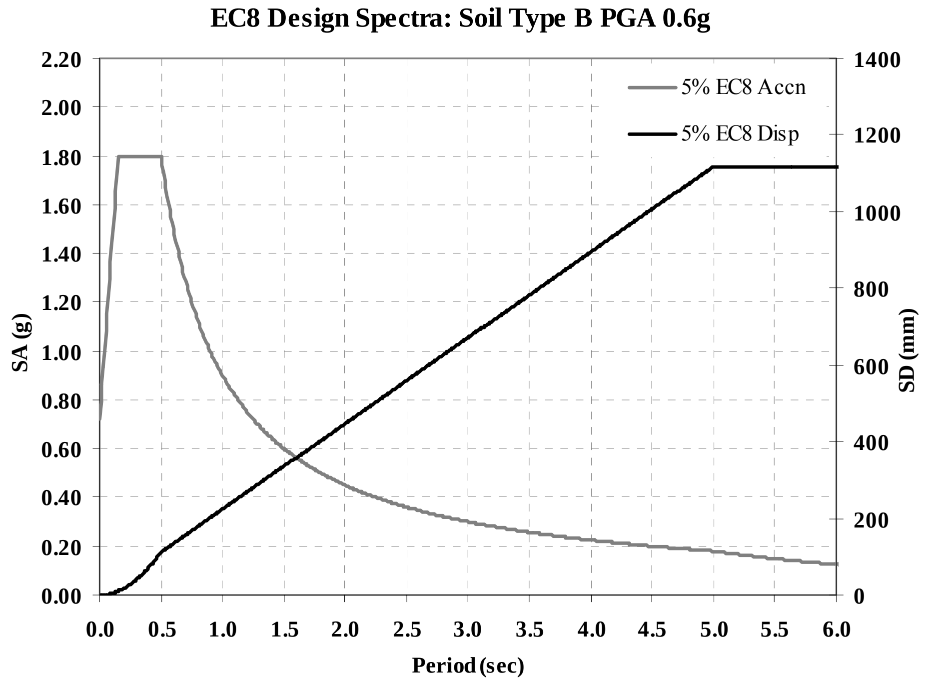

Figure 4-3. EC8 5% Acceleration and Displacement Spectra for Soil Type B (modified for a Corner Period = 5.0 seconds) ; PGA = 0.6g

The parameters $\Delta_{C,5}$ and T_c used in Eq.(3.8) at the 5% damping level, are 1.118 meters and 5 seconds respectively.

4.2.3 Direct Displacement-based Design Parameters

The key objective of this study is to develop a method of accounting for higher mode amplification in reinforced concrete frames that does not require the need for inelastic time-history analysis. Therefore a critical design inter-storey drift of $\theta = 2\%$ was assigned, in accordance with the recommendations in NZS 4203. For a constant storey height of 3.5 meters, this corresponds to an inter-storey displacement of 0.07 meters at the critical storey level, assumed to be the lowest level.

The yield displacements, ductilities and equivalent viscous damping values were calculated at each level and combined using Eq.(3.15) to give the substitute structure effective damping level. Finally using Eqs.(3.8) to (11) the following direct displacement-based design parameters were found for each frame, as shown in Table 4-5.

Table 4-5. Direct displacement-based design parameters for initial study frames

Frame	θ_d	Δ_d (m)	M_e (t)	H_e (m)	ξ_{eff} (%)	T_e (sec)	K_e (kN/m)	V_b (kN)
A: n = 2	2 %	0.114	547	5.7	21.8	0.83	31191	3542
B: n = 4	2 %	0.205	1066	10.2	21.8	1.50	18701	3828
C: n = 8	2 %	0.317	2216	19.0	17.6	2.13	19276	6103
D: n = 12	2 %	0.465	3266	28.1	17.4	3.11	13338	6196
E: n = 16	2 %	0.613	4382	37.2	18.6	4.21	9761	5979
F: n = 20	2 %	0.721	5515	46.2	19.0	5.35	8710	6281

NB: T_e for Frame F exceeds T_c therefore iteration was required for actual displacement and equivalent damping

The variation in equivalent viscous damping values is a reflection of the changes in design displacement profile, with the large difference between Frames B and C due to the introduction of the parabolic profile for $n > 4$. However the increase in the damping value for the 16 and 20 storey frames is due to an error in the calculation of the weighted average, later found in the design calculations and is explained further in Chapter 6.

With these parameters defined, the equivalent lateral force distributions and overturning moments were calculated. The method described in Section 4.1 is then used with values of base shear proportion β, to give sensible column bending moment distributions. The equivalent lateral forces, storey shears and overturning moment distributions are given in Table 4-6 and Table 4-7, resulting member design bending moments and shears in Table 4-8 and Table 4-9, and comparatively in Figure 4-4.

Table 4-6. DDBD equivalent lateral forces, storey shears, overturning moments and displacements; Frames A, B & C

Storey	Frame A				Frame B				Frame C			
	F_i (kN)	V_{icol} (kN)	OTM (kNm)	Δ_i (m)	F_i (kN)	V_{icol} (kN)	OTM (kNm)	Δ_i (m)	F_i (kN)	V_{icol} (kN)	OTM (kNm)	Δ_i (m)
20												
19												
18												
17												
16												
15												
14												
13												
12												
11												
10												
9												
8									865	865	0	0.498
7									936	1800	3027	0.443
6									816	2616	9329	0.387
5									692	3308	18487	0.328
4					1357	1357	0	0.280	563	3871	30065	0.267
3					1236	2592	4748	0.210	429	4300	43613	0.203
2	2215	2215	0	0.140	824	3416	13820	0.140	291	4591	58663	0.138
1	1349	3564	7753	0.070	412	3828	25775	0.070	148	4738	74731	0.070
0	0	3564	20228	0.000	0	3828	39172	0.000	0	4738	91315	0.000

Table 4-7. DDBD equivalent lateral forces, storey shears, overturning moments and displacements; Frames D, E & F

Storey	Frame A				Frame B				Frame C			
	F_i (kN)	V_{icol} (kN)	OTM (kNm)	Δ_i (m)	F_i (kN)	V_{icol} (kN)	OTM (kNm)	Δ_i (m)	F_i (kN)	V_{icol} (kN)	OTM (kNm)	Δ_i (m)
20									707	707	0	0.718
19									826	1532	2474	0.716
18									819	2352	7838	0.711
17									809	3161	16069	0.702
16					693	693	0	0.717	795	3956	27133	0.689
15					825	1518	2424	0.697	776	4732	40977	0.673
14					798	2316	7737	0.674	763	5494	57538	0.653
13					767	3083	15844	0.648	735	6229	76767	0.630
12	732	732	0	0.643	732	3815	26635	0.618	704	6933	98569	0.603
11	842	1575	2562	0.606	693	4508	39989	0.585	668	7601	122836	0.573
10	787	2361	8073	0.566	658	5166	55768	0.549	628	8230	149441	0.538
9	727	3088	16337	0.523	610	5776	73849	0.509	584	8814	178246	0.501
8	662	3750	27144	0.477	559	6335	94066	0.466	541	9355	209096	0.459
7	594	4344	40270	0.427	503	6838	116239	0.419	488	9843	241838	0.415
6	522	4866	55474	0.375	443	7281	140171	0.370	431	10274	276289	0.366
5	445	5311	72505	0.320	379	7660	165654	0.316	370	10643	312247	0.314
4	364	5675	91093	0.262	312	7972	192465	0.260	304	10947	349498	0.258
3	279	5955	110956	0.201	240	8211	220366	0.200	234	11182	387814	0.199
2	190	6145	131798	0.137	164	8375	249106	0.137	161	11342	426951	0.136
1	97	6242	153306	0.070	84	8459	278419	0.070	82	11425	466649	0.070
0	0	6242	175154	0.000	0	8459	308026	0.000	0	11425	506635	0.000

Table 4-8. Beam design shear forces and bending moments

Storey	Frame A		Frame B		Frame C		Frame D		Frame E		Frame F	
	V_{bi} (kN)	M_{bi} (kNm)	V_{bi} (kN)	M_{bi} (kNm)	V_{bi} (kN)	M_{bi} (kNm)	V_{bi} (kN)	M_{bi} (kNm)	V_{bi} (kN)	M_{bi} (kNm)	V_{bi} (kN)	M_{bi} (kNm)
20											157	393
19											341	852
18											523	1307
17											703	1757
16									152	381	879	2198
15									334	834	1052	2629
14									509	1273	1221	3053
13									678	1695	1385	3462
12							158	395	839	2097	1541	3853
11							340	850	991	2478	1690	4224
10							510	1274	1136	2840	1829	4573
9							667	1666	1270	3175	1959	4898
8					180	450	810	2024	1393	3482	2079	5199
7					374	936	938	2344	1503	3759	2188	5470
6					544	1360	1050	2626	1601	4002	2284	5709
5					688	1719	1146	2866	1684	4211	2366	5915
4			252	629	805	2012	1225	3063	1753	4382	2433	6084
3			481	1202	894	2235	1285	3214	1805	4514	2486	6214
2	326	814	633	1584	954	2386	1327	3316	1842	4604	2521	6303
1	524	1310	710	1775	985	2463	1348	3369	1860	4650	2540	6349
Column Tension Force	850	-	2076	-	5424	-	10803	-	19351	-	32176	-

4.2.4 Section Analysis

For the inelastic time-history analyses, it was required to design the reinforcing details in both the columns and beams. This was accomplished using the GW-BASIC program, RECMAN2, that implements the concrete confinement and reinforcement stress-strain model presented by Mander et al. (1988). This program was used to calculate reinforcement requirements, and then to perform a moment-curvature analysis on the section with the designed reinforcement layout.

A bilinear approximation was made to the moment-curvature curve following the definitions of Paulay and Priestley (1992) for yield curvature, nominal moment capacity, ultimate curvature and ultimate capacity. For this process the limiting material strains suggested in Section 3.1.1 were applied and are summarised in Table 4-10. While RECMAN2 calculates the confinement effect of the steel design, according to the equation in Table 4-10, the ultimate concrete compression strain resulting from the assumed transverse reinforcement was manually checked for each frame.

Table 4-9. DDBD column moment distributions for Outer (1 & 4) and Inner (2 & 3) columns (kNm; positive values are anticlockwise moment)

	Frame A		Frame B		Frame C		Frame D		Frame E		Frame F	
Storey	Outer	Inner	Outer	Inner	Outer	Inner	Outer	Inner	Outer	Inner	Outer	Inner
20											2002	823
19											-1581	1640
19											2433	64
18											-1521	1706
18											2828	908
17											-1428	1809
17											3185	1704
16											-1304	1947
16									1348	206	3502	2450
15									-936	1006	-1149	2119
15									1771	663	3778	3140
14									-867	1090	-963	2325
14									2141	1456	4016	3781
13									-762	1219	-747	2565
13									2457	2170	4209	4359
12									-623	1391	-502	2836
12							449	736	2720	2804	4355	4870
11							-21	117	-450	1603	-230	3138
11							871	1582	2928	3353	4454	5310
10							49	253	-246	1854	69	3470
10							1225	2296	3085	3826	4505	5677
9							155	456	-12	2141	392	3828
9							1511	2877	3187	4209	4506	5968
8							294	722	250	2462	738	4212
8					1534	186	1730	3326	3232	4502	4460	6185
7					-990	1154	462	1045	537	2815	1106	4620
7					1925	717	1883	3644	3221	4703	4364	6319
6					-791	1299	656	1419	847	3195	1493	5049
6					2151	1421	1970	3832	3155	4810	4216	6369
5					-503	1510	875	1839	1177	3600	1896	5497
5					2222	1929	1992	3894	3034	4822	4018	6332
4					-138	1776	1113	2296	1524	4026	2315	5961
4			1667	220	2150	2248	1950	3829	2858	4738	3769	6206
3			-717	1204	289	2088	1367	2785	1885	4469	2745	6438
3			1919	1199	1946	2382	1847	3642	2629	4558	3469	5990
2			-104	1522	763	2434	1634	3298	2257	4926	3184	6925
2	1239	1203	1688	1645	1623	2339	1682	3335	2347	4282	3119	5681
1	312	1123	703	1942	1269	2803	1909	3828	2637	5392	3630	7419
1	998	1497	1072	1608	1194	2123	1459	2910	2013	3908	2719	5278
0	1497	2245	1608	2411	1791	3184	2189	4365	3020	5862	4079	7917

For the purposes of consistency, the transverse steel detailing was assumed to remain constant throughout the structure, for each frame, however, it was set so that basic requirements specified in NZS 3101 were satisfied. Thus with the assumption that longitudinal reinforcing has a nominal diameter (d_b) of 28mm, the required maximum spacing was the smaller of $6d_b$ or $d/4$; in all cases the former governed, and under practical considerations the transverse reinforcement centre to centre spacing was set at 150mm.

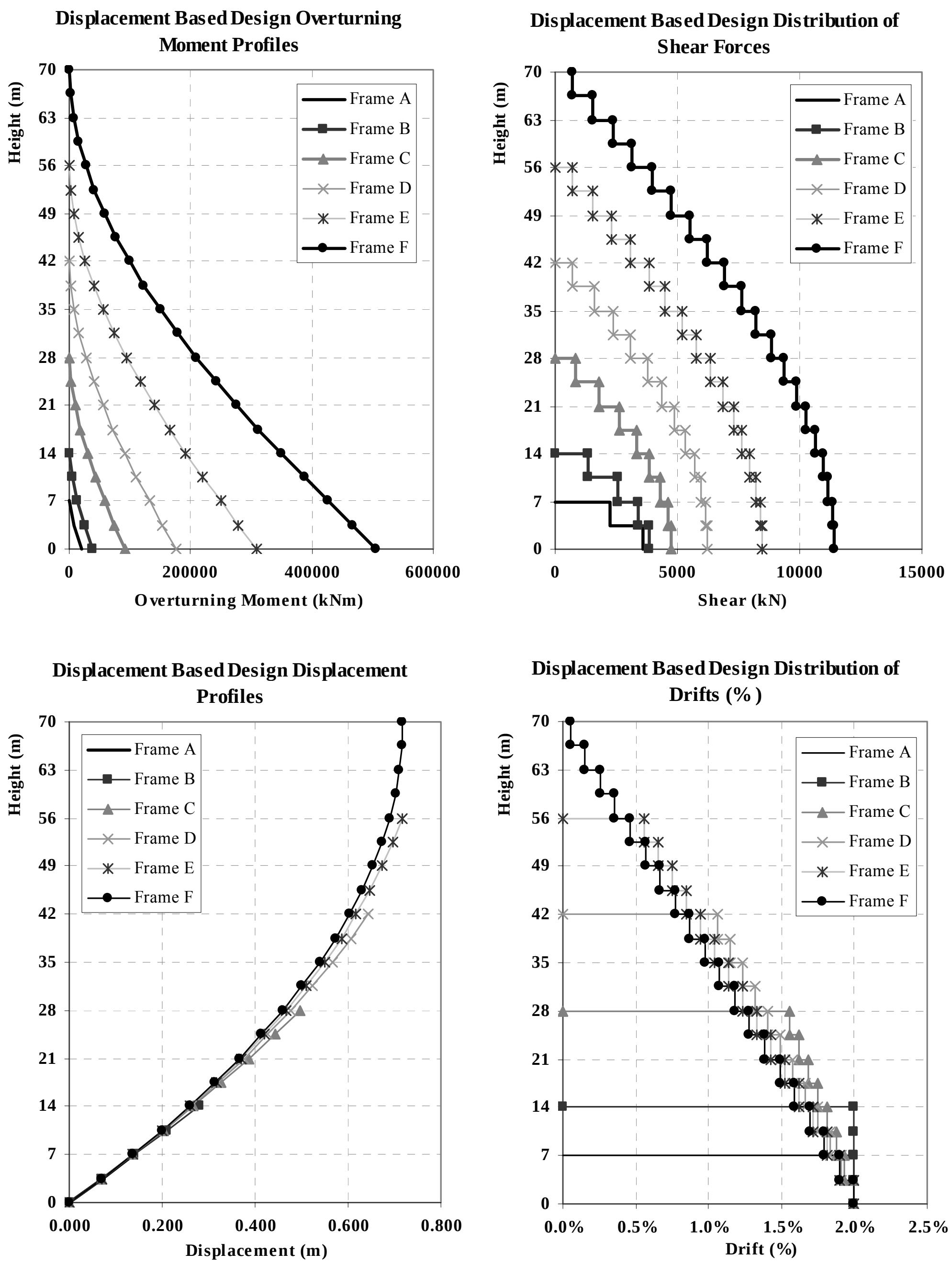

Figure 4-4. Displacement-based designs for Frames A to F

Table 4-10. Limiting material strain conditions to determine bilinear approximation to Moment-Curvature relations

	Concrete: ε_c	Steel: ε_s
'First Yield': M_y & ϕ_y'	0.002	$f_y/E_s = 0.00225$
'Nominal Capacity': M_N	0.004	0.015
'Yield': ϕ_y	Extrapolated from origin through 'First Yield' to M_N	
'Ultimate Capacity': M_N & ϕ_u	$\varepsilon_{cm} = 0.004 + \frac{(1.4\rho_s f_{yh} \varepsilon_{suh})}{f'_{cc}}$	$0.6\varepsilon_{su} = 0.06$

Mander et al. (1988) proposed the following equation to calculate the confined concrete strength:

$$f'_{cc} = \left(-1.254 + 2.254\sqrt{1 + \frac{7.94 f'_l}{f'_c} - \frac{2 f'_l}{f'_c}} \right) f'_c \tag{4.11}$$

where *fl'* is applied using $f'_{lx} = K_e \rho_x f_{yh}$ and $f'_{ly} = K_e \rho_y f_{yh}$ to account for different confinement levels in orthogonal directions. For this study the confinement in each direction was considered equal.

Preliminary trials of the frame designs suggested that the moment-curvature behaviour of the beams did not vary significantly, in particular the post yield stiffness of the section was found to be reasonably consistent. Therefore it was considered appropriate to set the ratio of the bilinear moment-curvature post-yield stiffness to initial stiffness, r_ϕ, equal to 0.015 for the beams.

As described by Priestley (2003), the initial flexural stiffness can be determined using the bilinear approximation to the moment-curvature curve:

$$I_{cr} = \frac{M_N}{E_c \phi_y} \tag{4.12}$$

Using the simplified equation for the yield curvature in T-section beams proposed by Priestley (1998):

$$\phi_y = 1.70\frac{\varepsilon_y}{h_b} \tag{4.13}$$

and assuming that $M_N = M_E$ (values from Table 4-8) then the value of I_{cr} can be found (within acceptable levels of variation for design) without the need for a full section analysis.

Table 4-11 and Table 4-12 present the values of beam yield curvature, the corresponding values of I_{cr}, and r_ϕ.

Column post-yield behaviour is significantly dependent on the axial load ratio, therefore in all cases a full reinforcement design and moment-curvature analysis was carried out to determine the bilinear approximation parameters as defined in Figure 4-5. Using the material strain limits defined in Table 4-10 the bilinear parameters I_{cr} and r_ϕ, along with confined concrete strength and ultimate strain were found (Table 4-13).

Table 4-11. DDBD beam Yield Curvature, cracked Second Moment of Area and bilinear flexural factor for frames A, B & C

	Frame A			Frame B			Frame C		
Level	f_y	I_{cr}	r_f	f_y	I_{cr}	r_f	f_y	I_{cr}	r_f
20									
19									
18									
17									
16									
15									
14									
13									
12									
11									
10									
9									
8							0.00425	0.0038	0.015
7							0.00425	0.0079	0.015
6							0.00425	0.0115	0.015
5							0.00425	0.0146	0.015
4				0.00425	0.0053	0.015	0.00425	0.0170	0.015
3				0.00425	0.0102	0.015	0.00425	0.0189	0.015
2	0.00425	0.0110	0.015	0.00425	0.0134	0.015	0.00425	0.0202	0.015
1	0.00425	0.0069	0.015	0.00425	0.0150	0.015	0.00425	0.0208	0.015
0	-	-	-	-	-	-	-	-	-

Table 4-12. DDBD beam Yield Curvature, initial Second Moment of Area and bilinear flexural factor for frames D, E & F

	Frame D			Frame E			Frame F		
Level	f_y	I_{cr}	r_f	f_y	I_{cr}	r_f	f_y	I_{cr}	r_f
20							0.00425	0.0033	0.015
19							0.00425	0.0072	0.015
18							0.00425	0.0111	0.015
17							0.00425	0.0149	0.015
16				0.00425	0.0032	0.015	0.00425	0.0186	0.015
15				0.00425	0.0071	0.015	0.00425	0.0222	0.015
14				0.00425	0.0108	0.015	0.00319	0.0344	0.015
13				0.00425	0.0143	0.015	0.00319	0.0391	0.015
12	0.00425	0.0033	0.015	0.00425	0.0177	0.015	0.00319	0.0435	0.015
11	0.00425	0.0072	0.015	0.00425	0.0210	0.015	0.00319	0.0477	0.015
10	0.00425	0.0108	0.015	0.00319	0.0320	0.015	0.00319	0.0516	0.015
9	0.00425	0.0141	0.015	0.00319	0.0358	0.015	0.00319	0.0553	0.015
8	0.00425	0.0171	0.015	0.00319	0.0393	0.015	0.00273	0.0684	0.015
7	0.00425	0.0198	0.015	0.00319	0.0424	0.015	0.00273	0.0720	0.015
6	0.00425	0.0222	0.015	0.00319	0.0452	0.015	0.00273	0.0752	0.015
5	0.00425	0.0243	0.015	0.00319	0.0475	0.015	0.00273	0.0779	0.015
4	0.00425	0.0259	0.015	0.00319	0.0494	0.015	0.00273	0.0801	0.015
3	0.00425	0.0272	0.015	0.00319	0.0509	0.015	0.00273	0.0818	0.015
2	0.00425	0.0281	0.015	0.00319	0.0519	0.015	0.00273	0.0830	0.015
1	0.00425	0.0285	0.015	0.00319	0.0525	0.015	0.00273	0.0836	0.015
0	-	-	-	-	-	-	-	-	-

Table 4-13. DDBD confined concrete column values and M-ϕ bilinear approximation parameters

		f_{cc}' (MPa)	ε_{cu}	N_{Grav} kN	M_y kNm	ϕ_y' /m	M_N kNm	ϕ_y /m	M_u kNm	ϕ_u /m	I_{cr} m4	r_ϕ
Frame A												
	Outer	48.2	0.0228	490	980	0.0052	1405	0.0070	1620	0.1150	0.0081	0.0099
	Inner	49.0	0.0223	980	1890	0.0058	2050	0.0078	2102	0.1050	0.0103	0.0020
Frame B												
	Outer	48.2	0.0227	1048	1262	0.0053	1594	0.0068	1802	0.1214	0.0085	0.0077
	Inner	49.1	0.0224	2096	1937	0.0060	2393	0.0074	2586	0.1115	0.0116	0.0057
Frame C												
	Outer	50.2	0.0220	2144	1475	0.0058	1800	0.0071	1952	0.1218	0.0092	0.0052
	Inner	50.6	0.0218	4288	2555	0.0061	3215	0.0077	3224	0.0853	0.0151	0.0003
Frame D												
	Outer	49.1	0.0199	3288	3769	0.0054	4584	0.0066	4737	0.0784	0.0249	0.0031
	Inner	49.0	0.0199	6575	3453	0.0051	4400	0.0065	4347	0.0666	0.0244	-0.0013
Frame E												
	Outer	48.1	0.0191	4471	2558	0.0049	3027	0.0057	3123	0.0846	0.0189	0.0023
	Inner	48.5	0.0190	8942	4387	0.0044	5921	0.0059	5899	0.0539	0.0358	-0.0005
Frame F												
	Outer	47.0	0.0178	5734	3246	0.0043	3800	0.0050	3870	0.0733	0.0273	0.0014
	Inner	47.2	0.0177	11469	5557	0.0039	7414	0.0052	7329	0.0450	0.0517	-0.0015

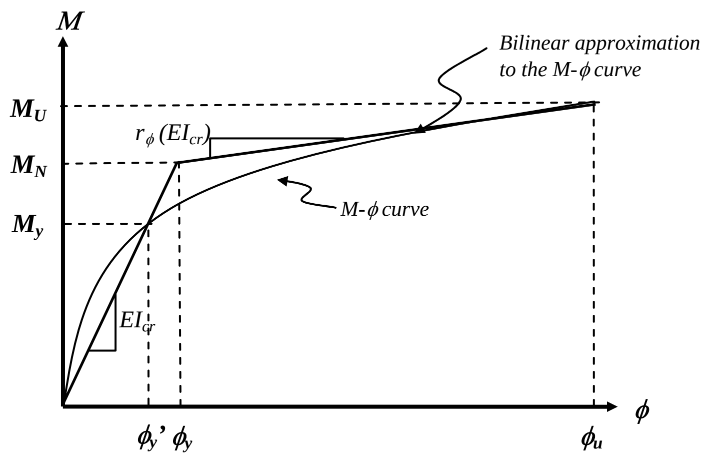

Figure 4-5. Schematic representation of the bilinear approximation to the Moment-Curvature curve, used to determine member and section properties.

5. INELASTIC TIME-HISTORY ANALYSES

For each frame a series of inelastic time-history simulations were performed using spectrum-compatible accelerograms at intensities of 0.5x, 1.0x and 1.5x (later changed to 2.0x in subsequent sets of analyses). The variations were included to assess the sensitivity of the dynamic behaviour to intensity, in particular with respect to the commonly held notion that Capacity Design (Paulay and Priestley, 1992) effectively desensitises the structure to variations in earthquake characteristics. The program Ruaumoko 2D (Carr, 2002) was used for this purpose with appropriate modelling assumptions and hysteretic models, defined below, that reflect inelastic reinforced concrete behaviour.

5.1 MODELLING ASSUMPTIONS

In order to simplify the analyses and isolate the particular dynamic effects sought in this study the following assumptions were made with respect to the models used:

- All columns were assumed to have fully fixed base boundary conditions with foundations remaining elastic and rigid.

- Floor diaphragms were assumed in-plane with adequate system connections to transfer floor inertia forces to the perimeter frame.

- The tube frame provided the only form of lateral response resistance.

- Member material properties were taken as homogeneous unless specified in certain areas.

- Member strengths and stiffness were idealised based on the principles outlined in preceding sections of this study.

- Frame design is carried out such that capacity design principles are followed, allowing inelastic action to occur only at column bases and beam ends to form a weak-beam strong-column mechanism.

- Member properties were concentrated along element centrelines and weights concentrated at appropriate nodal points as described in Section 4.2.1.

- Shear deformations were allowed for in the definition of both beam and the column elements. The shear area A_s was taken as $5/6\,h \cdot b_w$ with h and b_w as defined in Table 4-4

5.2 SPECIFIC MODEL DETAILS AND DEFINITIONS

5.2.1 Model type and geometry

Ruaumoko 2D utilises a concentrated plasticity representation of prototype structures with potential inelastic behaviour limited to specifically defined regions of the structure. Therefore care must be taken in defining the model geometry such that plasticity can occur where and as expected. As the frames in this study were assumed to form a weak beam-strong column mechanism the model geometry around beam-column joints was as shown in Figure 5-1.

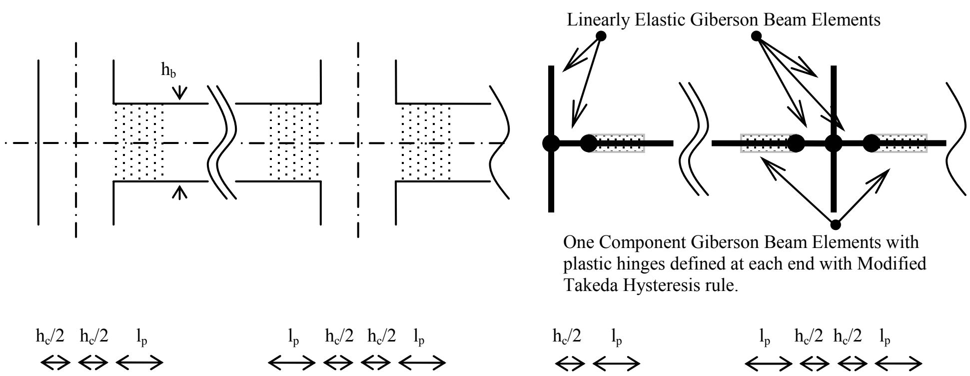

Figure 5-1. Element geometry used to model the building frame beam-column intersections in Ruaumoko

The use of the One Component Giberson Beam element required the definition of positive and negative yield moments for each plastic hinge. For this elements axial yield conditions were ignored. The linear elastic elements used to model the beam ends within the joint region were given the same elastic section properties as the clear span portion of the corresponding beam.

The first storey columns were modelled using Concrete Beam-Column elements requiring the definition of plastic hinge lengths, bilinear factors and the yield interaction surface to account for axial load variation during the earthquake. To prevent unwanted yielding at the top of these columns the upper end of the elements were provided with a yield surface up to five times stronger than that at the base (In practice this strength would be defined by dynamic overstrength factors. It will be recalled that the quantification of these factors was one of the aims of this study).

Design of the required reinforcing for the Concrete Beam-Column elements was carried out assuming bending moment and axial load design values based on the assigned earthquake moments (M_E) and gravity axial compression loads (N_G), as suggested by Priestley and Kowalsky (2000) and represented in Figure 5-2(a & b). Principally this is an intermediate axial load approximation (shown as point (a) in Figure 5-2b) that lies between the maximum earthquake compression axial force ($N_{E,C}$) and earthquake tension force ($N_{E,T}$) defined in Figure 4-1 and shown in Figure 5-2b. If the tension force was considered in the design with the same earthquake moment, the required reinforcing steel content would be significantly increased (point (b) in Figure 5-2b). It is noted that if the external columns were designed for the gravity plus seismic tension force, the external column with seismic compression force would have excess flexural strength and the resulting column base shear strength would be in excess of the design level. Provided the sum of the external column base moments matches the design value (which is essentially assured if the gravity axial force is used for both, and thus the outer column reinforcement layouts are equal) the design base shear strength is satisfied. It should be noted that this does not imply excessive ductility demand on the tension column, as flexural strength and stiffness are essentially proportional, and both tension and compression column can be expected to yield at essentially the same overall displacement [Priestley, 2003b].

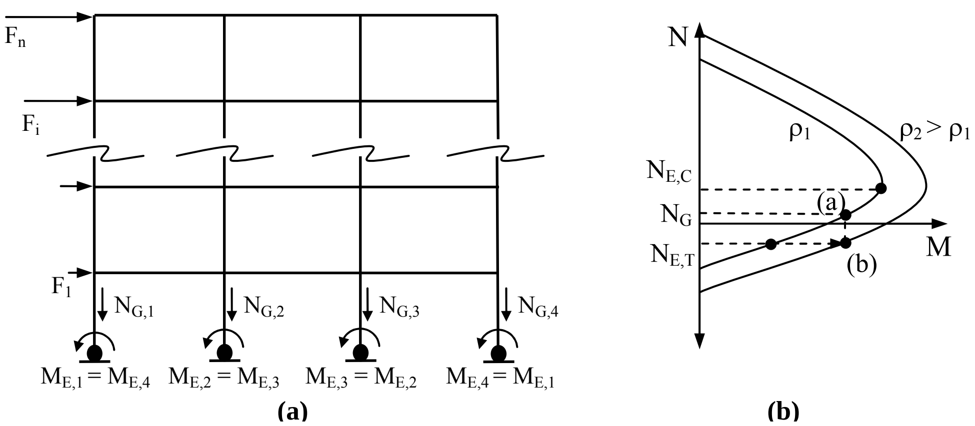

Figure 5-2. Bottom storey column design actions used for base hinge reinforcement design

5.2.2 Member bilinear factors and plastic hinge properties

Potential plastic hinge regions of each model required the definition of the bilinear factor for flexural inelastic behaviour and the length of the potential plastic hinge. Values for r_ϕ, the ratio of post yield stiffness to initial stiffness were taken from

Table 4-11, Table 4-12 and Table 4-13, with the initial stiffness being defined by the elastic section properties for Young's Modulus E_c and I_{cr}. No axial yield surface was included therefore no value for the axial bilinear factor was used.

The plastic hinge lengths were calculated using the equations suggested by Paulay and Priestley (1992) that accounts for strain penetration into the joint or base regions:

$$l_p = 0.08l + 0.022 d_b f_y \tag{5.1}$$

where f_y is given in MPa while l and d_b are in millimetres. The results from this equation were then rounded to the nearest ten centimetres. For beams with a clear span of 4300 mm, using 28 mm diameter bars, this gives a length of 500 mm, while for columns with a soffit height of 3050 mm, the estimate is 400 mm.

5.2.3 Modified Takeda Hysteresis rule

The Modified Takeda rule (Otani, 1974) is commonly used for modelling inelastic reinforced concrete behaviour. By varying the alpha and beta factors (α and β) which modify the unloading and reloading stiffnesses, it is possible to account for 'pinching' effects seen due to increased axial load. Thus the different contributions to hysteretic damping from beam hinges and column hinges can be modelled.

For this work the following values (Table 5-1) were used to define the hysteretic behaviour of beams and columns.

Table 5-1. Modified Takeda hysteresis rule parameters

Parameter	Alpha	Beta	NP	KKK
Beam Hinges	0.25	0	1	2
Column Hinges	0.50	0	1	2

With these values the beam hinges have a greater unloading stiffness (α = 0.25) to reflect the absence of significant axial load in the beams, while the 0.50 for the columns results in lower unloading stiffness as could be expected due to axial loading in these elements.

Further definition of these parameters is given in Appendix 1 of the Ruaumoko User Manual (Carr, 2002).

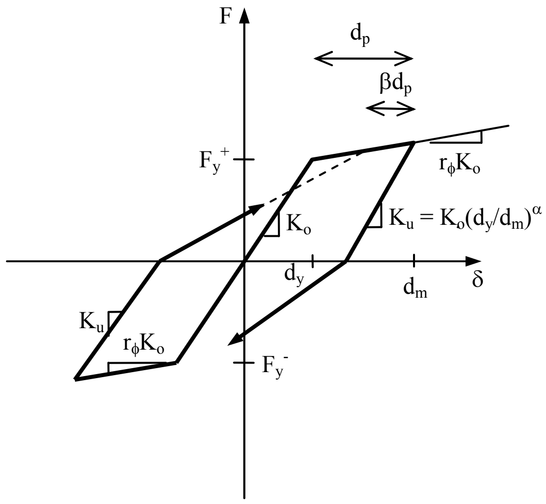

Figure 5-3. Schematic representation of the Modified Takeda hysteresis model used in Ruaumoko

5.2.4 Viscous damping

The presence of damping additional to that developed from hysteretic action is often accounted for in dynamic analyses. However the appropriateness of this assumed contribution, the values used and the form of application are not generally agreed on, making this a somewhat subjective decision. For the purposes of this study a Rayleigh damping model was used in proportion to the tangent stiffness, to model this apparent viscous damping. Thus the damping was calculated with respect to the mass and tangent stiffness terms, **M** and **K** in the form:

$$\mathbf{C} = a\mathbf{M} + b\mathbf{K} \tag{5.2}$$

where:

$$a = \frac{2\omega_i \omega_j \left(\omega_i \lambda_j - \omega_j \lambda_i\right)}{\omega_i^2 - \omega_j^2} \quad \text{and} \quad b = \frac{2\left(\omega_i \lambda_i - \omega_j \lambda_j\right)}{\omega_i^2 - \omega_j^2} \tag{5.3}$$

The values of a and b are calculated from two selected modes *i* and *j* for which the viscous damping is specified. For reinforced concrete structures the viscous damping level is often assumed to be 5% of critical damping and the selected modes are set at this value. However given the use of hysteretic models which generate their own form damping it is possible that this may overestimate damping slightly. Initial findings from recent numerical studies (Grant et. al, 2004) suggested that equivalent inelastic first mode viscous damping is dependent on the ductility developed in the structure, and that to achieve similitude with the equivalent viscous damping equation used in the design process [Eq.(3.5)], this may take the form of (note that since this study was completed the form and application of this adjustment has been significantly revised):

$$\lambda_{i=1} = \frac{5}{\sqrt{\mu_\Delta}}\% \tag{5.4}$$

where μ_Δ is the displacement-based design ductility. This approximation was adopted in the study, along with a third mode (for structures with n ≥ 4) damping value of 4%. With these inputs Ruaumoko calculates the proportionality constants a and b.

5.2.5 P-Δ Effects

This study did not include *P-Δ* effects. It is intended that this issue will be investigated separately.

5.2.6 Input ground motions

A set of artificial accelerograms was generated to be compatible with the EC8 spectrum defined in Section 4.2.2 (note that a suite of five real accelerograms, with details included in Appendix A, were scaled to match the design spectrum, and used as a final check to the method). The program SIMQKE was used for this purpose (provided as part of the Ruaumoko software package), in which the 5% Design Velocity spectrum was used as the target curve, along with the acceleration time envelope defined in Figure 5-4.

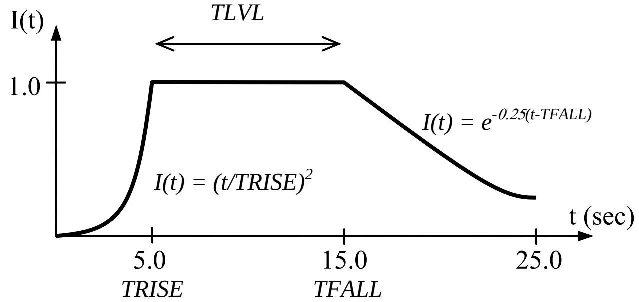

Figure 5-4. Ground acceleration time envelope used to generate artificial accelerograms for time-history analyses

The resulting suite of five selected accelerograms are shown in Figure 5-5 and Figure 5-6 with respect to the design spectral acceleration and displacement curves.

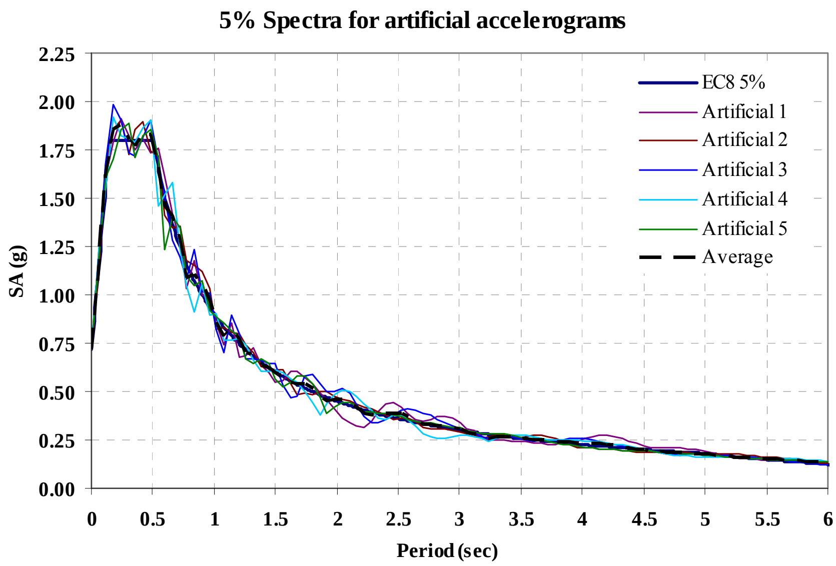

Figure 5-5. Comparison of artificial acceleration spectra with EC8 elastic design spectrum

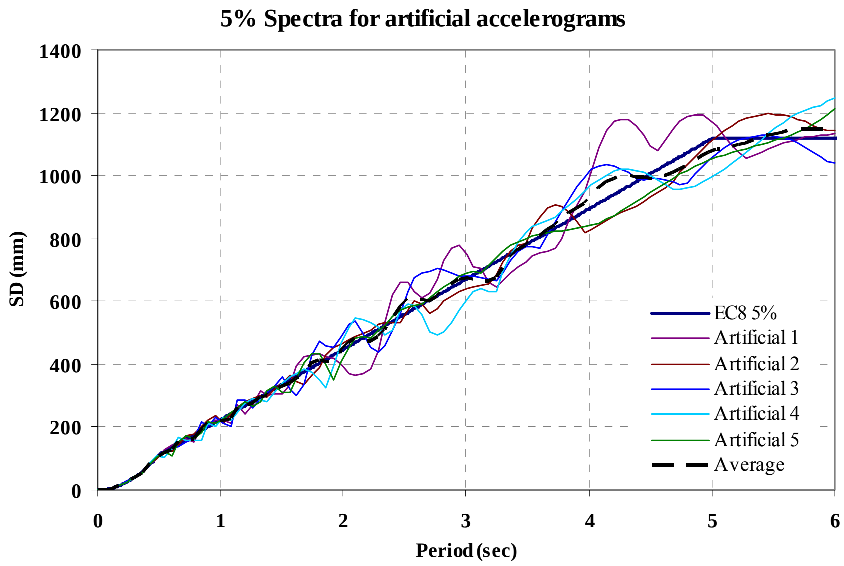

Figure 5-6. Comparison of artificial displacement spectra with EC8 elastic design spectrum

6. INITIAL INELASTIC TIME-HISTORY RESULTS

The following inelastic time-history results represent the structural model behaviour seen for the 4, 8, 12, 16 and 20 storey frames detailed in Chapter 4. It should be noted however that an error involving the weighted average procedure used to find the effective equivalent viscous damping, was found in the design calculations after these analyses were completed. For the buildings of more than four storeys, this error effectively under-weighted the contribution of larger lower level ductilities, while over-weighting the smaller upper level ductilities. Therefore the apparent system equivalent viscous damping was lowered (as presented in Table 4-5), making the design base shear larger than that required for the structure at the design level displacement, and therefore the overall strengths (and stiffness) were greater. This error was rectified from Section 6.2.2 onwards, with earlier designs and analyses not being re-evaluated as it was found that the general behaviour important to the following developments was not significantly altered.

6.1 MAXIMUM DRIFT AND DISPLACEMENT PROFILES

The time-history results were initially checked for maximum displacement and drift validity with respect to the assumed design displacement profiles and the target design drift of 2%. Figure 6-1 shows the mean envelopes for each of the frames simulated at this stage for earthquake intensities of 0.5x, 1.0x and 1.5x the design intensity (*I*).

The general behaviour of all the frames gives a useful comparison to assess whether the direct displacement-based design process as described in Chapter 4, produces structures with characteristics adequate to meet the limitations imposed during the design stages.

The 4, 8 and 12 storey frames show behaviour consistent with that expected from a moment resisting frame. In general the maximum storey drifts meet, or do not significantly exceed the suggested code limit of 2%, and average displacement profiles at the time of maximum displacement at the design effective height (H_e) approximate the assumed design profile reasonable well (note the effective height can be interpreted as the centre of force (*C.o.F*) height). Of note is that the 12 storey frame behaviour is somewhat influenced by a trial to test the effects of accounting for seismic axial tension forces during the column reinforcement design stages.

As mentioned in Section 5.2.1 column reinforcement was generally designed using the combination of bending moment and axial compression load $M_E + N_G$. The trial design used for the 12 storey frame accounted for the seismically induced column tension forces which for taller buildings becomes very significant in the structures ability to resist global overturning. In this case the axial load considered was $N_G – N_T$ where tension is taken as a negative quantity. This leads to increased design strength, implying significantly stiffer column sections, with the result that bottom storey rotations (storey drifts) are reduced, and in the extreme case found to step away from the design limit (in cantilever fashion) as clearly seen for intensities equal to 0.5x the design level.

The observed influence of column reinforcement design is an important issue as there is potential for significant deviation from the expected dynamic behaviour due to designers following common code requirements that various moment and axial load combinations be considered, including net column tension forces due to global overturning moments. This also has implications for code requirements on minimum steel ratios in column (and beam) sections. In specific cases (particularly for tall buildings with lower design ductility values), a design considering the $M_E + N_G$ combination may require a low amount of reinforcing in the outer columns, in which case minimum content specifications may govern (NZS 3101 limits columns to a minimum of 0.80%). If this is the case the designer is forced to provide excessive stiffness to the columns and hence can unintentionally alter the dynamic behaviour of the whole structure.

The 16 and 20 storey frames designed according to the described method, with no account for seismic axial tension, deviate significantly from the design profiles, both in terms of maximum displacement at the effective height and maximum storey drift. The upper quarter of each frame appears to behave in a cantilever fashion, with resulting drifts at the design intensity reaching approximately 3%, showing that higher mode displacement response is a significant issue for the taller buildings. The displacement envelopes are more linear than assumed by the design profiles, suggesting ductile behaviour is more evenly distributed than originally assumed.

The scatter between results using the different accelerograms was generally acceptable when compared to the dispersion of the input motion spectra. As shown in Figure 5-6, the five records used gave a good average with respect to the EC8 design spectra, over most of the constant velocity portion of the graph. However it is noticeable that for periods greater than four seconds the dispersion of the records increases significantly. The effect of this scatter is presented in Section 7.2.2.1 where it is seen that maximum storey drifts are particularly sensitive to the input motion characteristics, and also to some extent maximum displacements.

6.2 OBSERVATIONS AND DDBD METHOD CHANGES FOR FRAMES

The time-history results indicate that the simplified design method as applied with direct displacement-based design does not provide adequate control of displacements, in particular storey drifts which can be related to the material strain demands and thus structural (and non-structural) damage.

As mentioned the displacement profiles at the time of maximum displacement of the centre of force, were generally more linear for the taller structures than allowed for in the design equations. When this is considered with respect to Eq. (3.14) it is clear that a more linear design profile, resulting in greater upper level displacements will in turn distribute a more significant proportion of the base shear to those levels. Consideration of Eqs. (4.4) and (4.5) shows that this will result in greater design strengths for the beams and therefore a structure with greater stiffness in the upper levels. Therefore the development of an updated design profile, more linear than Eq. (3.12b & c), is a logical approach to introducing greater control to the upper storey displacements.

6.2.1 Design displacement profile developments

To investigate the influence of the design displacement profile, the extreme case of a pure linear equation as used for frames up to four storeys in height is first considered. For constant vertical stiffness and high ductility demand, this can be interpreted as the displacement response to a single point load of magnitude equal to the base shear V_b. Thus the storey shear forces become equal, as do the design beam shear forces, and therefore beam design bending moments. In comparison to the original parabolic displacement profiles this apportions greater strength and stiffness to the upper levels (and less to the lower levels).

To test this upper limit, the 16 storey frame was redesigned accordingly and tested under the same suite of artificial records. Figure 6-2 shows the displacement behaviour is significantly different from that seen in Figure 6-1 with the upper storey drift maxima reduced well below the design limit of 2% and in fact exhibiting behaviour similar to what was expected using the original parabolic design profile. However with the reduction in upper storey drift demands, the lower level maximum, now becomes critical with the bottom storey reaching approximately 3.7%. This concentration of displacement demand is also reflected in the displacement profiles.

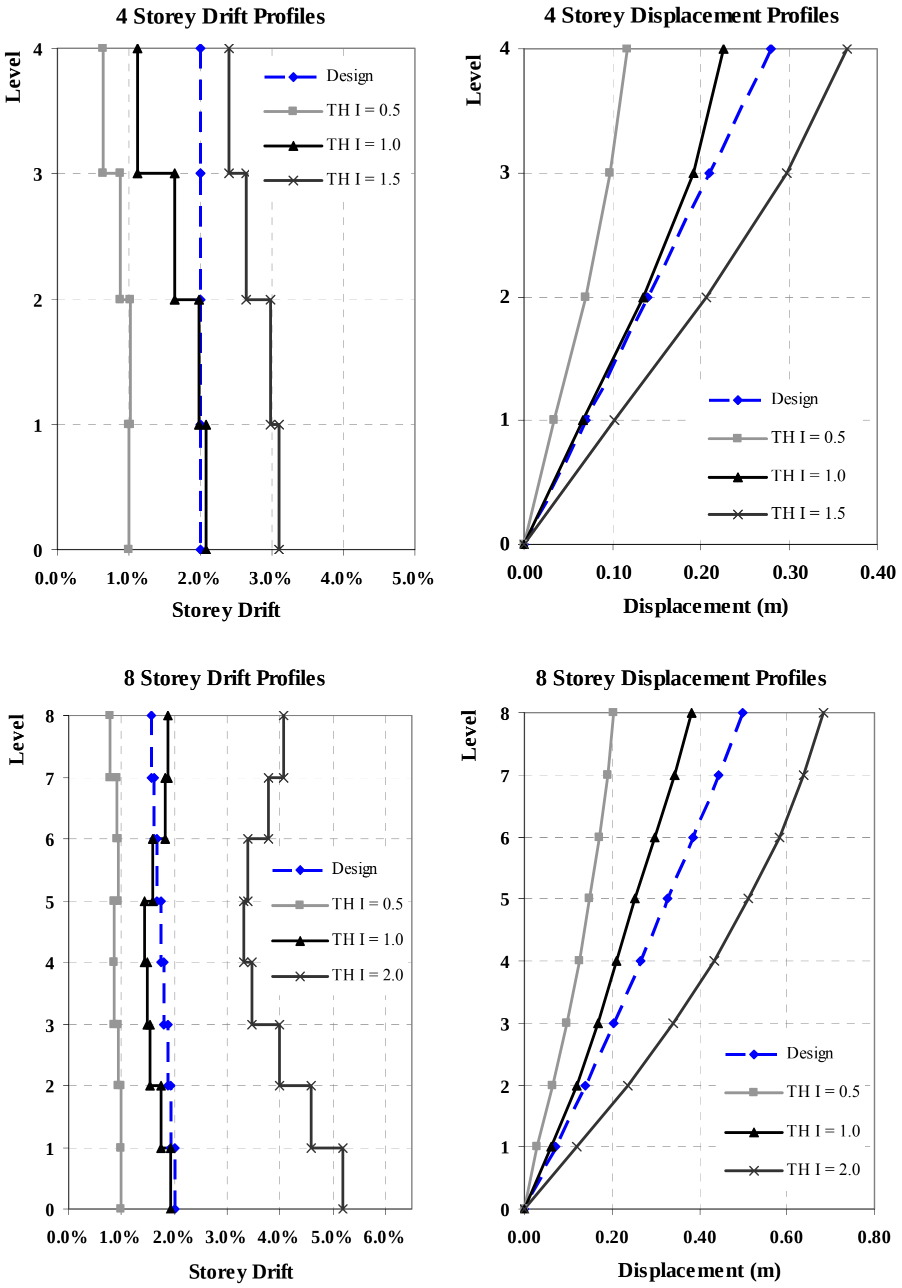

Figure 6-1. Inelastic time-history maximum storey drifts, and displacement profiles at the time of maximum displacement at the centre of force effective height (H_e)

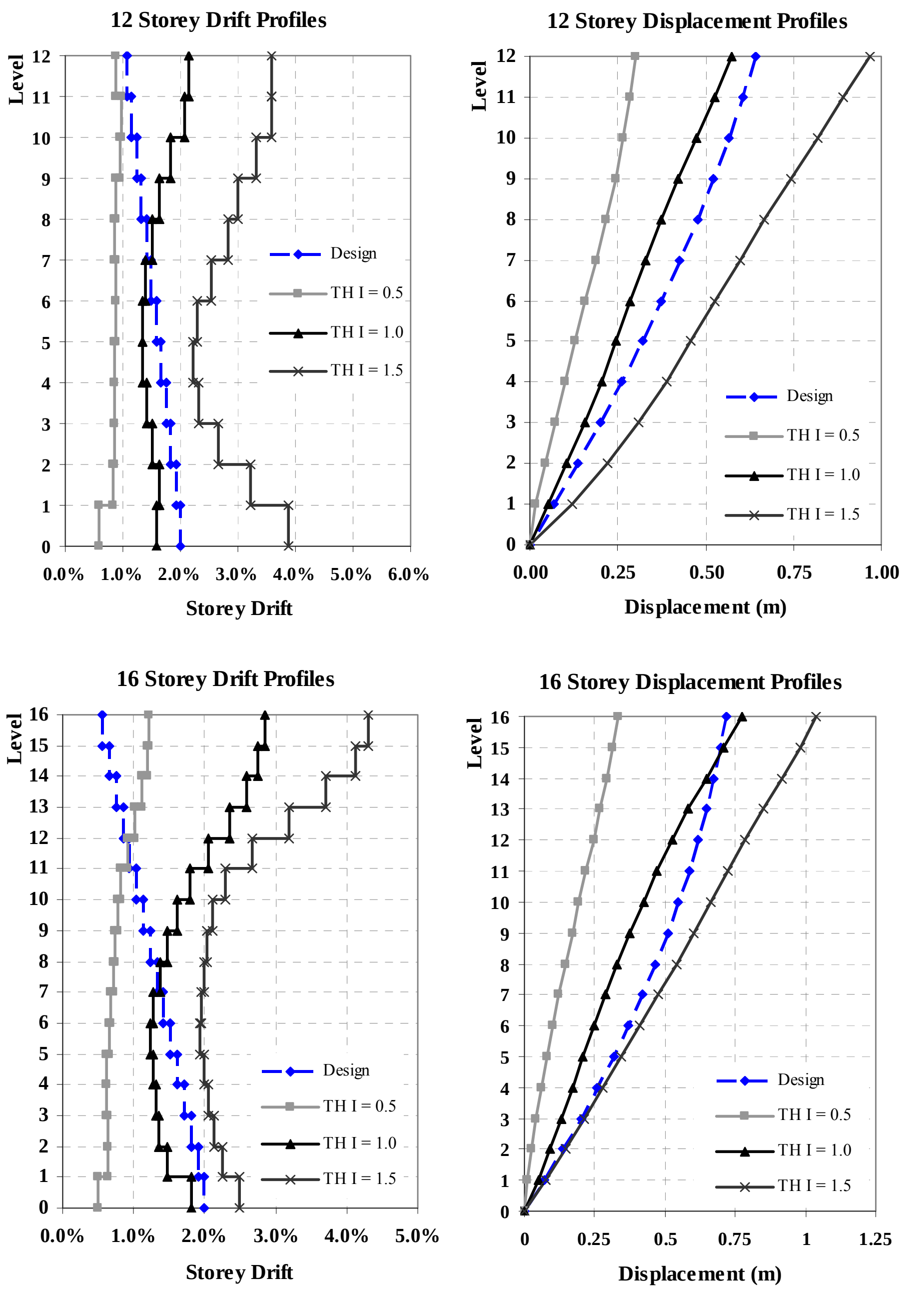

Figure 6.1. Inelastic time-history maximum storey drifts, and displacement profiles at the time of maximum displacement at the centre of force effective height (H_e) (cont.)

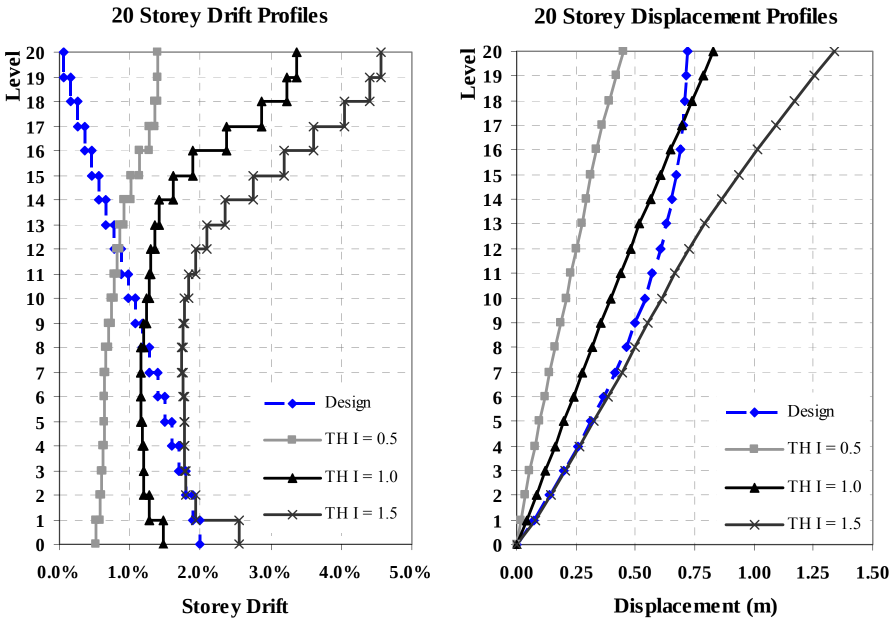

Figure 6.1. Inelastic time-history maximum storey drifts, and displacement profiles at the time of maximum displacement at the centre of force effective height (H_e) (cont.)

The result above suggests that a solution should lie at an intermediate stage between the parabolic profiles originally used and the linear profile with a single point load at the roof level. This would allow proportionally more strength to be distributed to the upper levels, while at the same time maintaining a reasonable overall strength pattern. Comparing the results in Figure 6-1, the design profile for the 12 storey structure appears to reflect well, the observed profiles of the 12, 16 and 20 storey frames.

Therefore substituting n = 12 into Eq. (3.12b) and simplifying, results in:

$$\phi_i = \frac{4}{3} \cdot \left(\frac{H_i}{H_n} \right) \cdot \left(1 - \frac{1}{4} \frac{H_i}{H_n} \right) \tag{6.1}$$

This equation is now assumed applicable to all structures regardless of the number of levels (possibly with a change in profile for smaller structures). Comparison of the resulting displacement profile using Eq.(6.1) with the original and linear profiles is given in Figure 6-3.

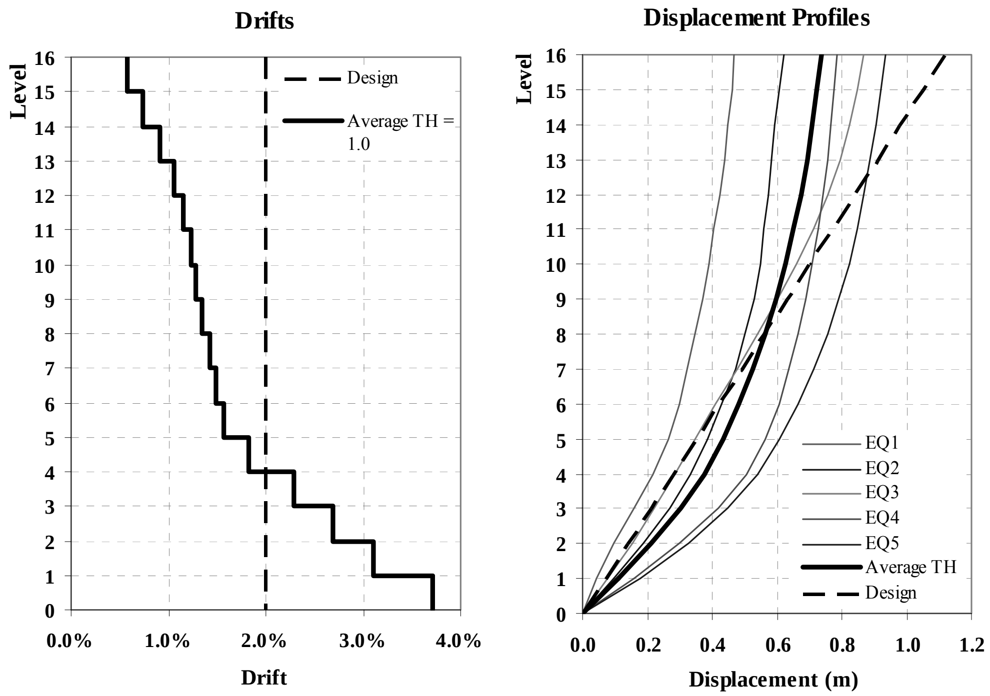

Figure 6-2. Maximum storey drifts and displacement profiles using a linear design profile and equal beam strengths

Figure 6-4 shows the resulting displacement responses for the 16 storey frame. While the design displacement profile and average time-history profiles give reasonable agreement, the upper level drifts still exceed the design limits and suggested code limit of 2%. The intended storey drift control using a more linear profile has not eventuated, indicating that further changes are required to develop better control of the upper levels.

It is noted that storey drifts over the lower half of the frame are somewhat constant, and that the bottom storey displacement tends to be significantly below the design displacement. These observations combined with the consideration that the distribution of beam strength over the frame height governs the storey stiffness, suggests that some amount of lower storey strength could be reassigned elsewhere in the frame, allowing lower storey displacements to move out towards the design level, while potentially further reducing the upper level displacement response.

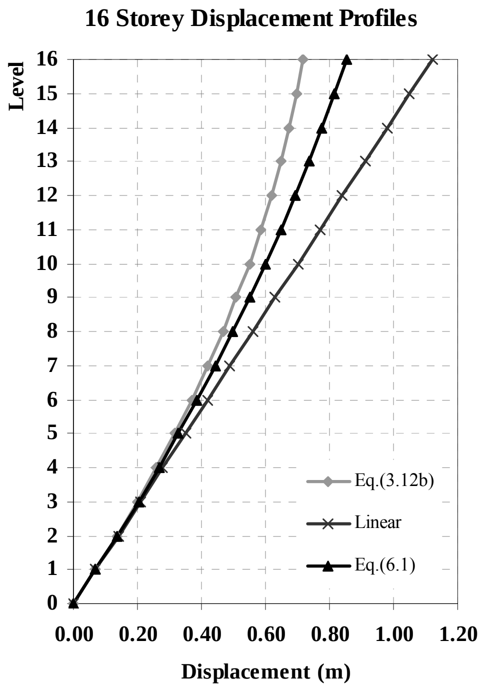

Figure 6-3. Comparison of original Eq. (3.12), suggested Eq. (6.1) and linear displacement profiles for a 16 storey frame

The profile in Eq.(6.1) is considered applicable to frames greater than four storeys in height and that as assumed in Eq.(3.12) a linear profile is still suitable for structures of four storeys or less. While Figure 6-1 shows maximum drifts less than the design level in the upper levels of the four storey frame, this behaviour is considered satisfactory given the apparent excess in upper level strength and stiffness. The use of Eq.(6.1) for buildings of less than four storeys would introduce significantly more curvature to the profile (that would match the drift demands closely), thus increasing the design base shear and resulting member actions. In such circumstances there is a substantial increase in reinforcing requirements that is unnecessary given that upper storey drifts are not exceeding the design limits. Therefore it is proposed that the design profiles be defined in a similar fashion to Eq.(3.12) such that:

$$\text{for } n \leq 4: \qquad \phi_i = \frac{H_i}{H_n} \tag{6.1a}$$

$$\text{for } n > 4: \qquad \phi_i = \frac{4}{3} \cdot \left(\frac{H_i}{H_n}\right) \cdot \left(1 - \frac{1}{4}\frac{H_i}{H_n}\right) \tag{6.1b}$$

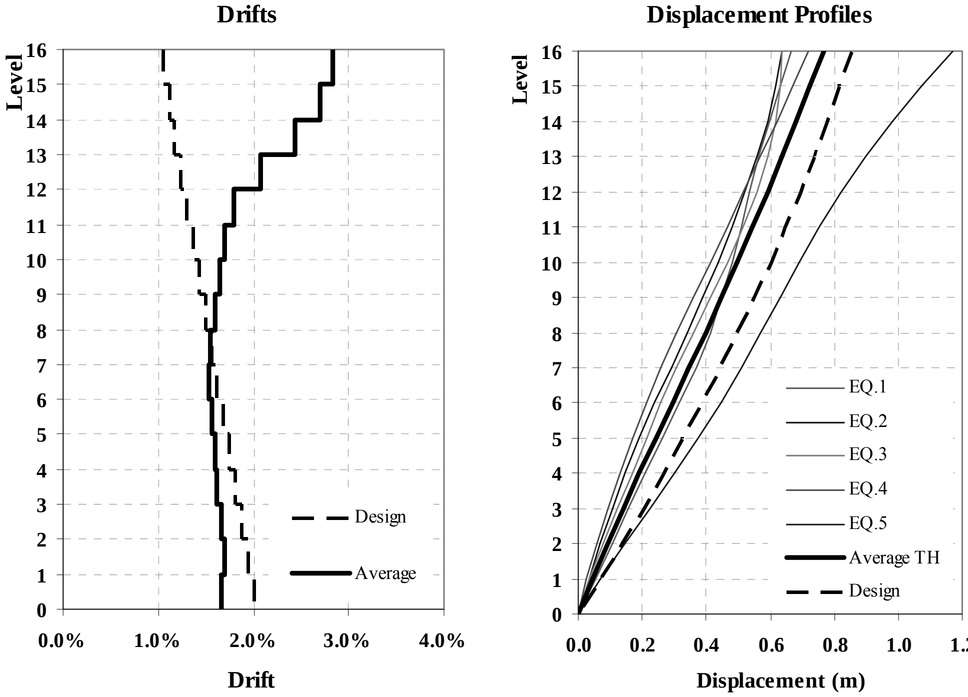

Figure 6-4. Maximum storey drifts and centre of force maximum displacement profiles using design based on Eq. (6.1)

6.2.2 Distribution of beam strengths

The method of distributing beam strength according to Eqs.(4.4) and (4.5) is considered logical and practical to maintain for this study, as it allows direct control and observation of changes in strength resulting from variations in earlier stages of the design method. To alter the distribution in beam strength, the profile of design storey shears is the principal variable which can be changed. Therefore changes to the lateral force distribution according to Eq.(3.14) would allow such an investigation.

Paulay and Priestley (1992) suggest that when designing for structures higher than 10 storeys using the equivalent static lateral force method, an additional portion of the base shear be applied at the roof level as a means of accounting for higher mode effects in the upper floors. With this in mind such an application at the lateral force distribution stage, of direct displacement-based design, might provide a simple means of controlling the displacement response of the frames in question. This approach is supported in recent work presented by Medina (2004) who showed that an additional lateral load with proportions varying between $0.03V_B$ and $0.35V_B$ (for frames with ductile behaviour) applied at the roof level, was a good approach for controlling and distributing ductility demands with greater equality.

Therefore Eq.(3.14) would take on a form similar to Eq.(2.5):

$$F_i = F_t + 0.9V_B \frac{\Delta_i m_i}{\sum_{i=1}^{n} \Delta_i m_i} \tag{6.2}$$

with $F_t = 0.1V_B$ at the roof level and 0 for all others.

From the results in Figure 6-1 this redistribution could also be seen to apply only to frames over 10 storeys in height. As mentioned, application of Eq.(6.1b) will lead to a profile with greater curvature than seen with Eq.(3.12) for buildings of less than 12 storeys. This will have two effects on the resulting design. First the upper level design displacements decrease, therefore the proportion of base shear (using Eq.(3.14)) assigned to these levels will decrease giving strength and stiffness reductions. Second, the reduction in overall displacement magnitude reduces the expected ductility development throughout the frame, in turn reducing the equivalent viscous damping and therefore resulting in a higher base shear value to be distributed. The extent of influence such changes would have on the dynamic behaviour of intermediate height frames needs to be verified.

Figure 6-4-6.6 and 6.7 plot the comparisons of design drift and displacement profile for the results from time-history analyses using a series of variations of design displacement profile and base shear distribution for the 8, 16 and 20 storey frames. The assumed drift limit of 2.0% is also presented in the graphs to highlight the acceptable limits of performance over the height of the buildings.

Figure 6-5 indicates that for intermediate height frames, it is valid to apply Eq.(6.2). The average maximum drift meets the 2% design limit, with one of the five artificial earthquakes producing a result in excess of this limit. Thus it appears reasonable to include intermediate height buildings in the application of Eq.(6.2), as a simple performance precaution that will reduce upper level drift demands while allowing lower storey demands to move closer to the design profile limits. This issue is discussed further with respect to procedures suggested in the following Section 6.2.3.

Application of Eqs.(6.1) and (6.2) in the direct displacement-based design process was trialed on the 16 storey frame. Figure 6-6 shows the comparatively good behaviour of the building, with the intended reductions in upper level drift demands occurring, such that they no longer exhibit the uncontrolled cantilever behaviour seen in Figure 6-1. The 2% code limit is still exceeded in the upper levels, while the bottom half of the building generally follows the design drift profile, with a peak value of 2.27% (14% exceedance) occuring at the second storey. Even though the upper level drifts are now controlled, higher mode effects are still clearly visible in the deviation from the first mode drift profile used in design.

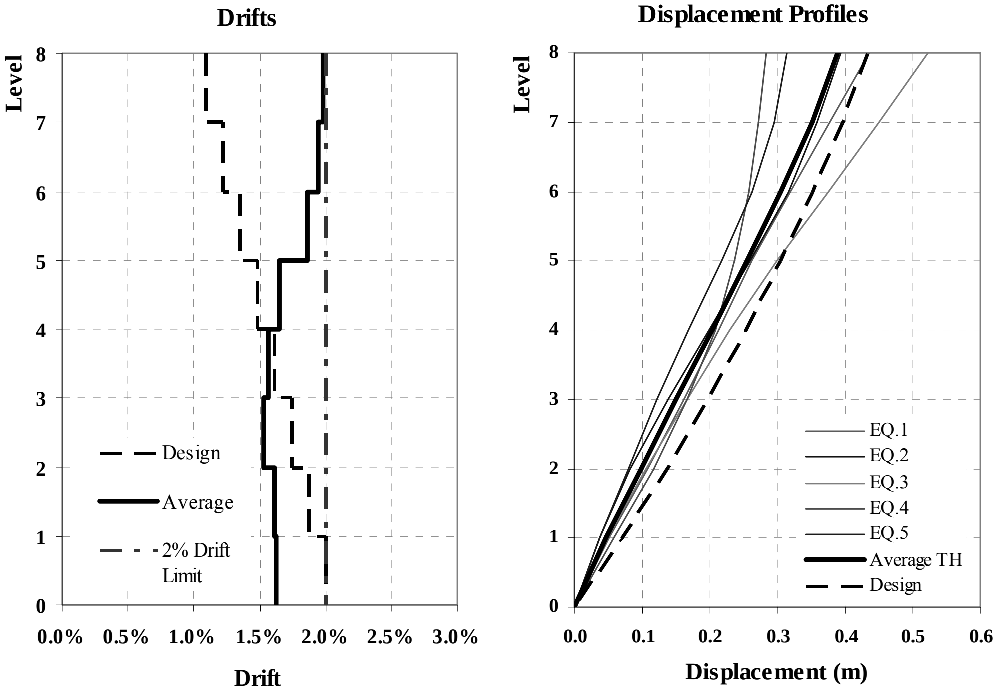

Figure 6-5. Maximum drift and displacement profiles; 8 storey frame using the displacement profile from Eq. (6.1) and lateral force distribution of Eq. (3.14)

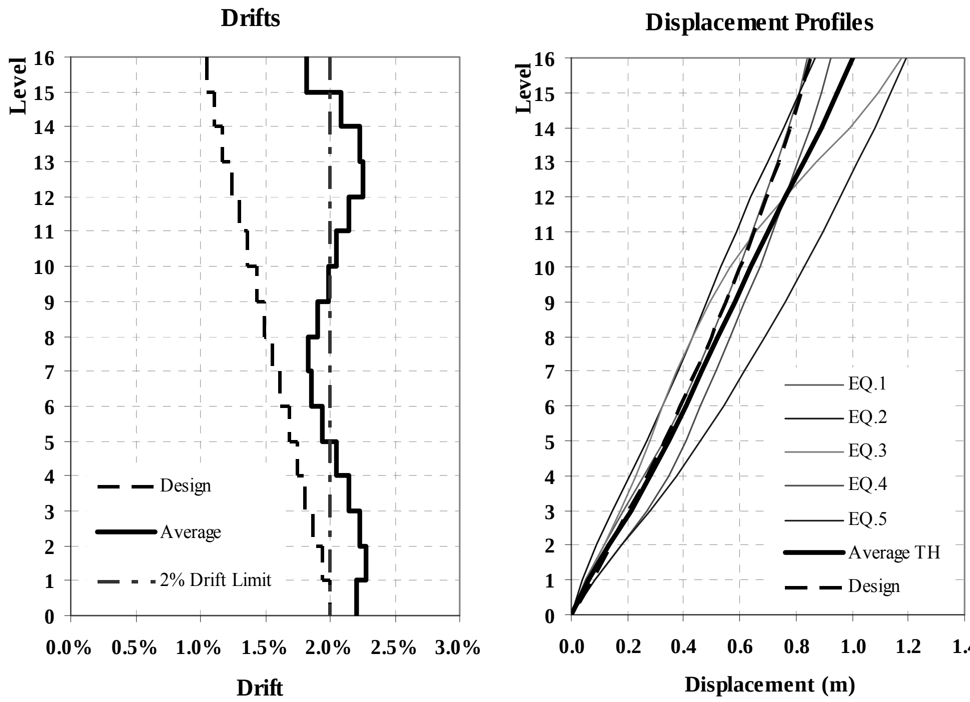

Figure 6-6. Maximum drifts and displacements; 16 storey frame using the displacement profile from Eq. (6.1) and lateral force distribution of Eq. (6.2)

In Figure 6-6 the plot of the maximum displacement (at the effective height) profiles also shows on average, very good agreement with the suggested design profile. There is some scatter around this average, however it is within the likely variation expected from time-history analysis, and is acceptable

To further verify the improvement in dynamic displacement response using Eqs. (6.1) and (6.2), the 20 storey frame was also redesigned accordingly; results are shown in Figure 6-7.

Similar mean behaviour to Figure 6-6 is observed for the 20 storey frame with a small drift exceedance over levels 15 to 17 due to higher mode effects, and a critical drift of 2.35% at the bottom storey. As with the 16 storey frame, the cantilever behaviour of the upper floors has been reduced, and the peak drifts follow the design profile over the lower half of the frame very closely. The average displacement profile also gives consistent agreement with the design profile given by Eq.(6.1).

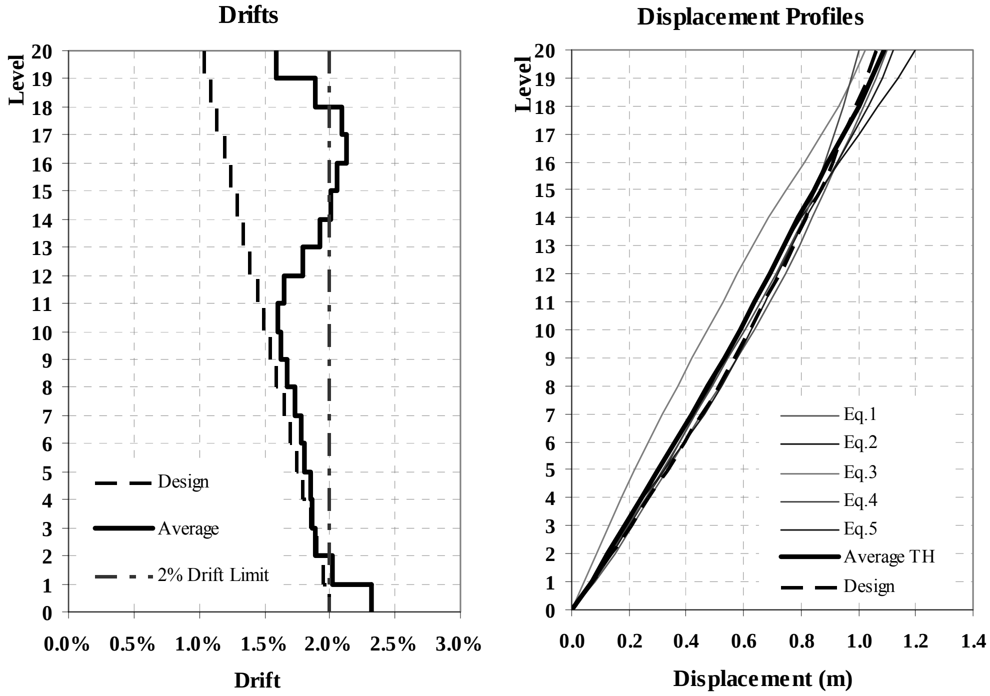

Figure 6-7. Maximum drifts and displacements; 20 storey frame using the displacement profile from Eq. (6.1) and and lateral force distribution of Eq. (6.2)

Figure 6-6 and 6.7 show consistently better dynamic behaviour with respect to drifts and displacement profiles than attained previously (Figure 6-1, 6.2 and 6.4). The developments presented show that the distribution of beam strength is clearly the governing factor of displacement response; a result of the stiffness dependency on section strength (Priestley, 1998). The combination of increased linearity in the design displacement profile and an adjusted distribution of seismic beam design shears (and thus moment strengths) has lead to a greater proportion of base shear being assigned to the upper levels of the structure. Thus the design strength of these previously critical upper levels has been increased and consequently the structure has greater stiffness in such regions.

6.2.3 Dynamic amplification of storey drifts

The suggested developments in Sections 6.2.1 and 6.2.2 have produced significant improvements in the dynamic displacement behaviour of the 16 and 20 storey frames which had demonstrated critical behaviour using the original methods Sections 3.1.1 and 4.1. The drift demands are now generally satisfactory, however the maximum values in the bottom storey consistently exceed the design limit of 2% in both buildings. To a lesser extent this is true of the upper storeys around the ¾ height of the building.

The development of upper storey drifts greater than the assumed first mode inelastic drift profile used in design, are due to higher modes dominating the response of the top half of the structure. Therefore if the higher modes do not significantly alter the inelastic first mode drifts, a simple representation of the observed behaviour can be developed by considering the additional displacements from the second mode (found from an elastic modal analysis) directly summed (either added or subtracted) with the first mode displacement profile over the top half of the structure. Therefore Figure 6-8 shows both the first mode inelastic displacement and drift profiles and the profiles resulting from the addition of the second mode displacements. The heavy line in the plot of drifts, is the envelope of maximum storey drifts found by considering the first mode only for the bottom half of the structure, and the combined first and second mode drifts over the top half.

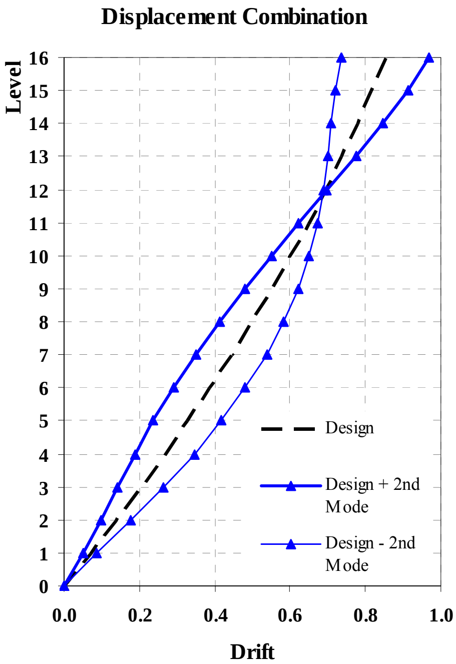

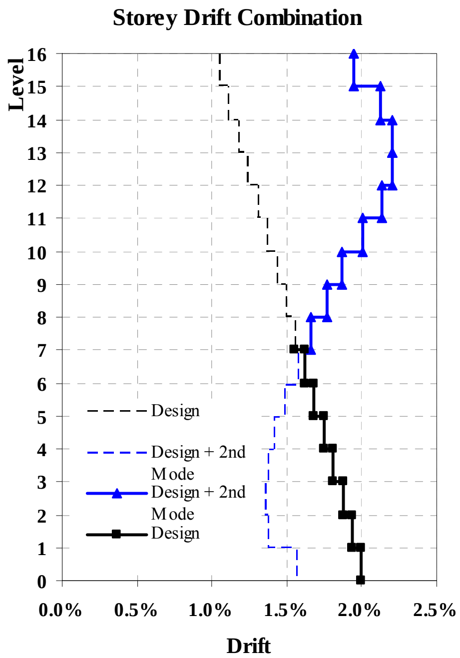

Figure 6-8. 16 storey inelastic first mode design displacement and drift profiles with combined with second mode elastic displacement and drift profiles; this represents the observed maximum drift behaviour seen in the time-history results.

The heavy line in Figure 6-8 can be interpreted as a basic representation of the maximum drift demands seen in the inelastic time-history analysis results, and shows the probable dominance of the second mode response in the upper half of the building. While the third (and possibly fourth) mode displacement behaviour may contribute further to the results above, it is seen that the inclusion of only the second mode replicates the observed dynamic behaviour well, and that the drift behaviour is influenced significantly by only the first and second modes.

The presence of higher mode effects in the displacement response of the taller structures and the slight drift limit (2%) exceedance, indicates that the general procedure is satisfactory, but that an account of the potential for higher mode demands should be included to provide a margin of conservatism such that the potential for these excesses is limited.

Possible means for providing such a margin include redistributing the lateral forces in a more complex manner such that the 10% placed at roof level is spread over the upper levels in some fashion, and potentially at the bottom storey level as well. Such an approach is seen to add complexity to the design method, in contrast to the intent of the methodology. Another approach is to apply a drift reduction factor that reduces the design drift so that the effective stiffness of the structure is adjusted to achieve a critical drift less than the assumed code limit of 2%. Thus any excessive drift demands above the design level should remain consistently within the code limit.

The drift reduction factor could be introduced at the point of choosing a design drift limit to therefore directly reduce the design drift from a suggested limit state drift as follows:

$$\theta_{d,\omega} = \omega_\theta \cdot \theta_d \tag{6.3}$$

However to maintain consistency in the design approach the application of this factor has been applied such that design displacements are directly reduced at each level:

$$\Delta_{i,\omega} = \omega_\theta \cdot \Delta_i \tag{6.4}$$

Combining with Eq.(3.13) gives:

$$\Delta_{i,\omega} = \omega_\theta \cdot \phi_i \cdot \left(\frac{\Delta_c}{\phi_c}\right) \tag{6.5}$$

Investigation of the results seen in Figure 6-6 and 6.7 shows average bottom storey drift values of 2.27% and 2.35%. To develop an appropriate value of ω_θ designs were made for 2, 4, 8 and 12 storey frames using Eq.(6.1a) for the 2 and 4 storey buildings, and Eq.(6.1b) for the intermediate height buildings. All designs used Eq.(6.2) for the lateral force distributions, however the requirement for this modification may not be necessary for the shorter structures.

Medina (2004) also commented that limiting the lower storey ductility demand (i.e. drift demands) was also beneficial for controlling the onset of global instability due to P-Δ effects in taller, more flexible structures. Thus the added effect of the proposed drift amplification factor would also be useful in this respect.

For the results shown in Figure 6-6, 6.7 and 6.9 the following bottom storey drift maxima were recorded (Table 6-1).

Table 6-1. Time-history maximum storey drifts using a linear design profile (for 2 and 4 storeys) and Eq. (6.1) for all others; Eq. (6.2) was applied in all cases

Num. Storeys	2	4	8	12	16	20	Average
Peak base Drift	2.21 %	2.35 %	1.82 %	2.20 %	2.27%	2.35 %	2.20 %

The average maximum drift of 2.19% is 9.5% in excess of the design drift limit of 2%. Therefore it is proposed that a value of ω_θ = 0.85 (a 15% reduction) is used, to give an effective design drift of 1.7%, which allows for a margin of conservatism to satisfactorily meet the assumed code limit. Note that the drifts in the bottom level of the four storey frame now exceed the design 2% compared to Figure 6-1. This is due to a shift in effective stiffness pushing the structure into portion of the displacement spectrum where one earthquake exhibited a displacement demand well in excess of the design spectrum.

The results from a trial of the 16 storey frame using Eqs.(6.1), (6.2) and (6.5) with ω_θ = 0.85 are presented in Figure 6-10.

The time-history results in Figure 6-10 show very good dynamic displacement behaviour with respect to the design profiles and code limits. When compared to Figure 6-6 the 2% drift limit is not excessively exceeded at any level (2.03% at the bottom level), and the design displacement profile gives good representation of the average maximum centre of force displacement profile. It should be noted that the average maximum drift and displacement results are compared to both the original and reduced design profiles. The

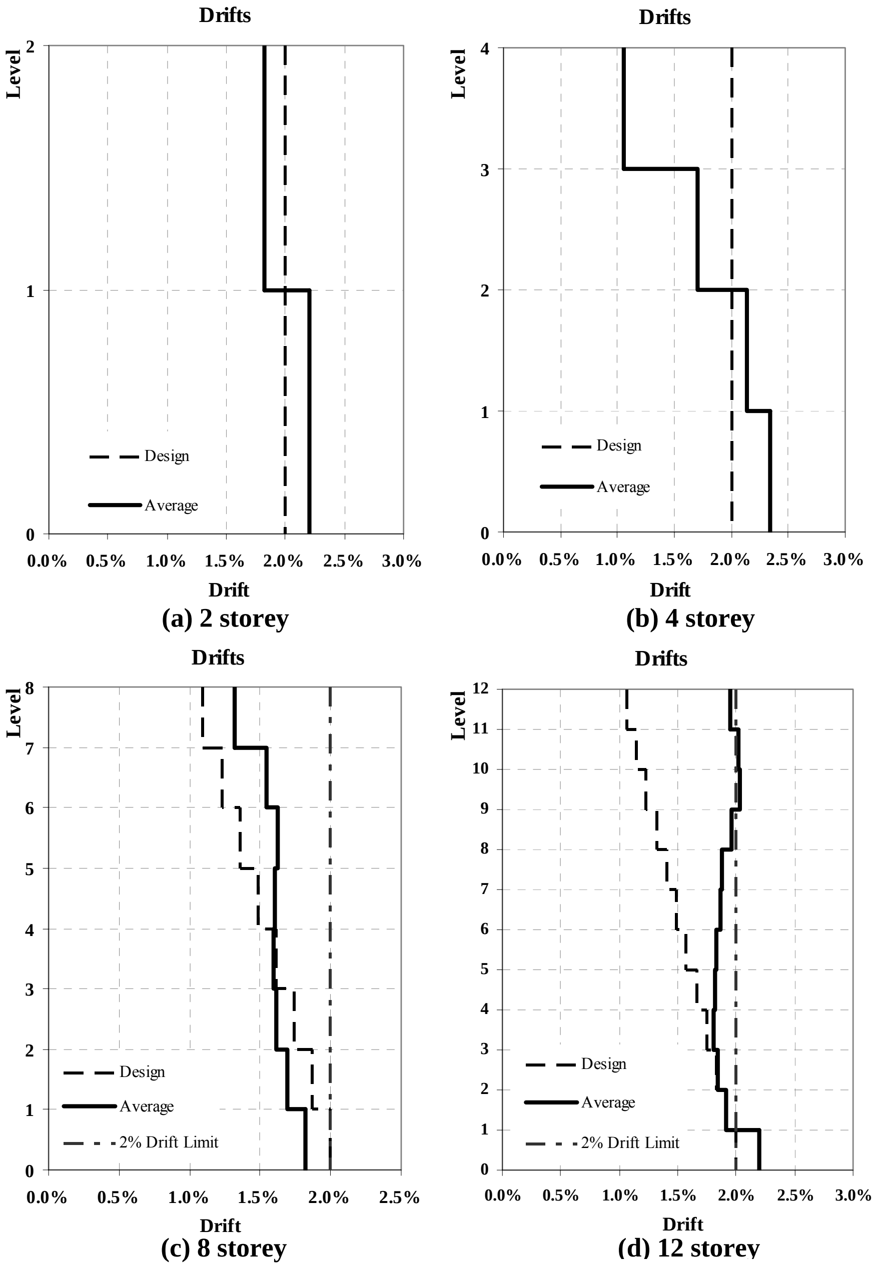

Figure 6-9. Maximum storey drift profile for 2, 4, 8 and 12 storey frames using Eq. (6.2) in the design process to identify a suitable value of ω_θ

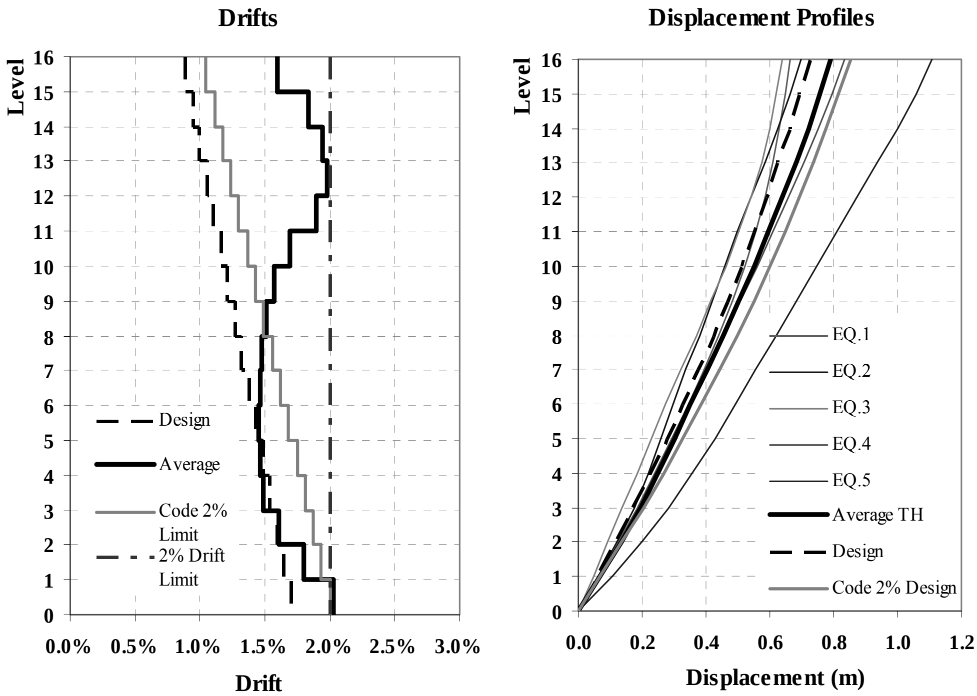

Figure 6-10. Time-history displacement profiles and maximum storey drift results for 16 storey frame designed using Eqs. (6.1), (6.2) and (6.5)

influence of the drift reduction factor is clearly seen in the displacement plot, where the average time-history profile follows between the decreased design values and the profile based on the original 2% drift design.

6.2.3.1 Application to short and intermediate height frames

Results shown in Figure 6-9 utilised frame designs for the two and four storey buildings that included the redistribution of base shear according to Eq.(6.2). Given the behaviour observed it is possible that this redistribution is not necessary as higher mode amplification is not particularly significant up to about 10 storeys (considering the 8 and 12 storey results presented and additional interpolation). Possibly the use of the drift reduction factor ω_θ would account of the dynamic response, such that designs could be considered sufficient for frames of 10 storeys or less without the use of Eq.(6.2). The time-history results in Figure 6-11 for the 8 storey structure without base shear redistribution show the dynamic performance to be very satisfactory.

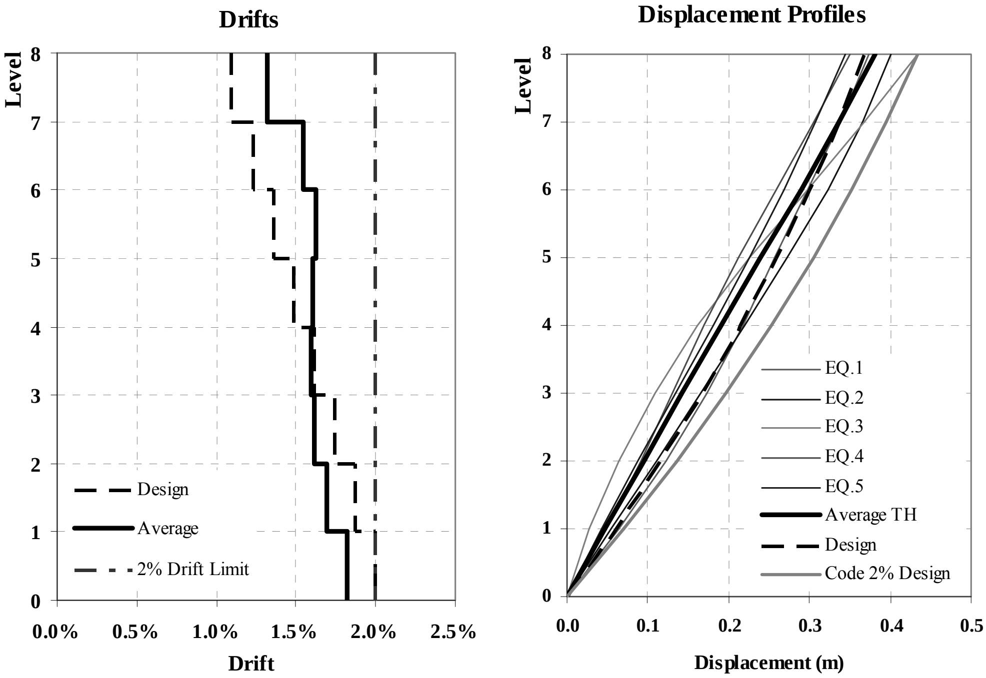

Figure 6-11. Maximum drift and displacement profiles; 8 storey frame designed with Eqs. (6.1) and (6.5) with no base shear redistribution according to Eq. (6.2)

6.3 SUMMARY OF PROPOSED CHANGES TO THE DIRECT DISPLACEMENT-BASED FRAME DESIGN PROCEDURE.

Sections 6.1 and 6.2 have shown that the previously described direct displacement-based design procedure for frames of the type studied in this research project, do not adequately account for some of the displacement response behaviour seen from inelastic time-history results. Primarily peak storey drifts were found to be excessive, especially in the taller frames investigated, where higher mode amplification became significant in the upper ¼ of the structure.

To account for these effects a series of changes and additions to the design procedure have been proposed and validated with respect to the structures identified as critical in these regions.

The design displacement profile used to approximate the inelastic first mode shape is modified to give a more linear shape for taller structures. For frames of four storeys or less the linear profile originally proposed is maintained. The proposed new equations are summarised as:

for n ≤ 4: $$\phi_i = \frac{H_i}{H_n} \tag{6.1a}$$

for n > 4: $$\phi_i = \frac{4}{3} \cdot \left(\frac{H_i}{H_n} \right) \cdot \left(1 - \frac{1}{4} \frac{H_i}{H_n} \right) \tag{6.1b}$$

Time-history trials indicated that for buildings of 10 storeys or more, the dynamic amplification of displacements and storey drifts rapidly increases as the second mode of vibration begins to participate to a greater extent. This observation has led to the conclusion that to adequately control this behaviour, the beam strength distribution is the most important factor to consider. Based on the simplified analysis method described in Section 4.1, the beam strength distribution is directly related to the equivalent lateral forces applied to the structure. For this reason the following equation is proposed as a means of maintaining more consistent behaviour over the building height.

for n ≤ 10: $$F_i = V_B \frac{\Delta_i m_i}{\sum_{i=1}^{n} \Delta_i m_i} \tag{6.2a}$$

for n > 10: $$F_i = F_t + 0.9 V_B \frac{\Delta_i m_i}{\sum_{i=1}^{n} \Delta_i m_i} \tag{6.2b}$$

Where F_t equals $0.1V_B$ at roof level and 0 at all other levels.

Preliminary results using the above equations indicated significantly more controlled dynamic response. However in general there is a tendency for critical storey drifts at the bottom level to match very closely or slightly exceed the assumed code limit of 2%. For this reason a drift reduction factor was found empirically by comparing the time-history results for the six frames assessed, and this takes the following form, with $\omega_\theta = 0.85$.

for all n: $$\Delta_{i,\omega} = \omega_\theta \cdot \Delta_i \tag{6.4}$$

Trial designs using these equations have given satisfactory improvement to the dynamic displacement behaviour of the structure. The following section provides a full development and application of these equations.

7. IMPLEMENTATION OF SUGGESTED DDBD PROCEDURES

The changes to the direct displacement-based design procedure for tube-frames suggested in Chapter 6 as a result of the initial inelastic time-history results, are adopted in this Chapter, with new designs generated for all six frames under consideration.

7.1 REVISED DIRECT DISPLACEMENT-BASED DESIGNS

The same basic parameters outlined in Section 4.2 were used for these updated designs, however due to the changes in structural demand resulting from alterations in the design displacement profiles and strength distributions, changes to structural geometries were necessary in order to accommodate the moment capacities required by these modifications. For the purposes of these analyses the beam depths have been kept constant over the height of each building, with a parametric study, described later in Chapter 9, used to verify that variations in member size do not produce significantly different results.

Table 7-1 shows the member geometries used for the new analyses. Compared with Table 4-4 the beam and column geometries have changed such that the shorter frames have larger column dimensions, while the taller structures have smaller column sizes. To simplify the interpretation of the results, beam depths are now constant for all buildings. As much as practicable, the beam sizes at critical levels have been limited to meet maximum steel ratio restrictions as defined in NZS 3101, which for beams is 2% for tension steel. Therefore assuming symmetrical reinforcement at the top and bottom of the sections (for simplicity and to minimise subjective decisions by the designer maintaining some amount of consistency) a total content of 4% is implied. For columns the limit was also set at 4% based on code considerations.

Table 7-1. Revised frame member geometries

n	Frame A				Frame B				Frame C				Frame D				Frame E				Frame F			
	Columns (square)		Beams		Columns (square)		Beams		Columns (square)		Beams		Columns (square)		Beams		Columns (square)		Beams		Columns (square)		Beams	
i	**1&2**	**3&4**	**b_w**	**h_b**	**1&2**	**3&4**	**b_w**	**h_b**	**1&2**	**3&4**	**b_w**	**h_b**	**1&2**	**3&4**	**b_w**	**h_b**	**1&2**	**3&4**	**b_w**	**h_b**	**1&2**	**3&4**	**b_w**	**h_b**
20																					850	850	400	1100
19																					850	850	400	1100
18																					850	850	400	1100
17																					850	850	400	1100
16																	800	800	400	1100	850	850	400	1100
15																	800	800	400	1100	850	850	400	1100
14																	800	800	400	1100	850	850	400	1100
13																	800	800	400	1100	850	850	400	1100
12													800	800	400	1100	800	800	400	1100	850	850	400	1100
11													800	800	400	1100	800	800	400	1100	850	850	400	1100
10													800	800	400	1100	800	800	400	1100	850	850	400	1100
9													800	800	400	1100	800	800	400	1100	850	850	400	1100
8									800	800	400	1100	800	800	400	1100	800	800	400	1100	850	850	400	1100
7									800	800	400	1100	800	800	400	1100	800	800	400	1100	850	850	400	1100
6									800	800	400	1100	800	800	400	1100	800	800	400	1100	850	850	400	1100
5									800	800	400	1100	800	800	400	1100	800	800	400	1100	850	850	400	1100
4					750	750	400	900	800	800	400	1100	800	800	400	1100	800	800	400	1100	850	850	400	1100
3					750	750	400	900	800	800	400	1100	800	800	400	1100	800	800	400	1100	850	850	400	1100
2	750	750	400	900	750	750	400	900	800	800	400	1100	800	800	400	1100	800	800	400	1100	850	850	400	1100
1	750	750	400	900	750	750	400	900	800	800	400	1100	800	800	400	1100	800	800	400	1100	850	850	400	1100

NB: b_w is the beam shear width; h_b is the total beam depth

Revised Direct Displacement-based Design Parameters and member design values

Following the same procedure of calculating yield displacements, ductility and equivalent viscous damping at each storey level, Table 7-2 summarises the important design parameters for each frame.

Table 7-2. Revised direct displacement-based design parameters

Frame	θ_d	$\theta_{d,\omega}$	Δ_d (m)	M_e (t)	H_e (m)	ξ_{eff} (%)	μ_Δ	T_e (sec)	K_e (kN/m)	V_b (kN)
A	2 %	1.7 %	0.096	550	5.7	20.0	2.72	0.68	46599	4496
B	2 %	1.7 %	0.174	1073	10.2	20.0	2.72	1.23	27957	4862
C	2 %	1.7 %	0.269	2235	19.0	20.0	2.72	1.90	24335	6550
D	2 %	1.7 %	0.395	3319	28.1	19.9	2.70	2.79	16846	6651
E	2 %	1.7 %	0.521	4400	37.2	19.9	2.69	3.68	12861	6697
F	2 %	1.7 %	0.647	5524	46.2	19.9	2.68	4.56	10479	6776

Following the method described in Section 4.1 column base design moments and beam moments were assigned to give the design strengths for each frame.

The resulting design distributions are summarised in Table 7-3 to 7-6 and Figure 7-1.

Table 7-3. Revised DDBD frame equivalent lateral forces, storey shears, overturning moments and displacements; Frames A, B & C

Storey	Frame A				Frame B				Frame C			
	F_i (kN)	V_{icol} (kN)	OTM (kNm)	Δ_i (m)	F_i (kN)	V_{icol} (kN)	OTM (kNm)	Δ_i (m)	F_i (kN)	V_{icol} (kN)	OTM (kNm)	Δ_i (m)
20												
19												
18												
17												
16												
15												
14												
13												
12												
11												
10												
9												
8									1129	1129	0	0.369
7									1255	2384	3952	0.336
6									1119	3502	12295	0.299
5									968	4470	24554	0.259
4					1720	1720	0	0.238	803	5273	40200	0.215
3					1571	3291	6020	0.179	624	5897	58657	0.167
2	2794	2794	0	0.119	1047	4338	17538	0.119	430	6328	79298	0.115
1	1702	4496	9780	0.060	524	4862	32722	0.060	222	6550	101444	0.060
0	0	4496	25516	0.000	0	4862	49740	0.000	0	6550	124368	0.000

Table 7-4. Revised DDBD frame equivalent lateral forces, storey shears, overturning moments and displacements; Frame D, E & F

Storey	Frame D				Frame E				Frame F			
	F_i (kN)	V_{icol} (kN)	OTM (kNm)	Δ_i (m)	F_i (kN)	V_{icol} (kN)	OTM (kNm)	Δ_i (m)	F_i (kN)	V_{icol} (kN)	OTM (kNm)	Δ_i (m)
20									1114	1114	0	0.904
19									516	1630	3899	0.873
18									496	2126	9602	0.841
17									476	2602	17043	0.807
16					1207	1207	0	0.725	455	3058	26151	0.771
15					627	1833	4223	0.694	434	3491	36854	0.734
14					597	2430	10639	0.661	411	3902	49074	0.696
13					565	2995	19144	0.626	387	4290	62732	0.656
12	1368	1368	0	0.547	532	3527	29627	0.589	363	4653	77747	0.615
11	808	2176	4789	0.515	497	4024	41972	0.551	338	4990	94032	0.572
10	754	2930	12404	0.481	460	4484	56056	0.510	311	5302	111498	0.527
9	697	3627	22659	0.444	422	4906	71752	0.468	284	5586	130054	0.481
8	635	4262	35352	0.405	382	5288	88924	0.423	256	5842	149605	0.434
7	570	4831	50268	0.363	340	5628	107433	0.377	227	6070	170053	0.385
6	500	5331	67177	0.319	297	5925	127133	0.329	197	6267	191297	0.334
5	427	5758	85836	0.272	251	6177	147871	0.279	167	6434	213231	0.282
4	349	6107	105989	0.223	205	6381	169489	0.227	135	6569	235749	0.229
3	268	6375	127364	0.171	156	6537	191823	0.173	103	6672	258741	0.174
2	183	6558	149676	0.116	106	6643	214704	0.117	69	6741	282092	0.117
1	93	6651	172628	0.060	54	6697	237954	0.060	35	6776	305686	0.060
0	0	6651	195906	0.000	0	6697	261392	0.000	0	6776	329403	0.000

Table 7-5. Revised beam design shear forces and bending moments

Storey	Frame A		Frame B		Frame C		Frame D		Frame E		Frame F	
	V_{bi} (kN)	M_{bi} (kNm)	V_{bi} (kN)	M_{bi} (kNm)	V_{bi} (kN)	M_{bi} (kNm)	V_{bi} (kN)	M_{bi} (kNm)	V_{bi} (kN)	M_{bi} (kNm)	V_{bi} (kN)	M_{bi} (kNm)
20											249	622
19											364	909
18											475	1187
17											581	1452
16									266	666	683	1707
15									405	1012	779	1949
14									536	1341	871	2178
13									661	1653	958	2394
12							296	741	779	1947	1039	2597
11							472	1179	888	2221	1114	2785
10							635	1587	990	2475	1184	2959
9							786	1965	1083	2708	1247	3118
8					234	586	923	2309	1168	2919	1304	3261
7					495	1237	1047	2617	1243	3107	1355	3388
6					727	1817	1155	2888	1308	3270	1399	3498
5					928	2319	1248	3119	1364	3409	1436	3591
4			319	797	1094	2736	1323	3309	1409	3522	1467	3666
3			610	1526	1224	3060	1381	3454	1443	3608	1489	3724
2	411	1027	804	2011	1313	3283	1421	3553	1467	3667	1505	3762
1	661	1652	902	2254	1359	3398	1441	3603	1478	3696	1513	3782
Column Seismic Tension Force	1072	-	2635	-	7374	-	12129	-	16489	-	21012	-

Table 7-6. Revised DDBD column design moment distributions for Outer (1 & 4) and Inner (2 & 3) columns (kNm; positive values are anticlockwise moments)

	Frame A		Frame B		Frame C		Frame D		Frame E		Frame F	
Storey	Outer	Inner	Outer	Inner	Outer	Inner	Outer	Inner	Outer	Inner	Outer	Inner
20											1672	193
19											-1010	1094
19											1919	725
18											-949	1157
18											2136	1216
17											-871	1239
17											2323	1666
16											-775	1340
16									1490	508	2482	2073
15									-772	886	-662	1458
15									1784	1138	2611	2439
14									-694	980	-534	1594
14									2035	1703	2712	2763
13									-589	1104	-390	1745
13									2242	2202	2784	3044
12									-460	1257	-232	1911
12							1348	876	2407	2637	2829	3283
11							-534	704	-308	1437	-60	2091
11							1712	1653	2529	3005	2845	3479
10							-418	860	-135	1643	124	2284
10							2005	2315	2610	3308	2835	3634
9							-262	1069	58	1872	319	2490
9							2226	2860	2650	3544	2798	3746
8							-69	1329	269	2123	525	2706
8					954	803	2377	3289	2650	3715	2735	3815
7					-283	501	158	1633	497	2393	741	2932
7					1519	1972	2459	3601	2610	3820	2647	3843
6					-101	781	416	1979	739	2681	964	3168
6					1918	2853	2472	3797	2531	3860	2533	3828
5					166	1192	700	2360	994	2983	1195	3410
5					2154	3447	2420	3878	2415	3835	2395	3772
4					506	1717	1006	2772	1260	3299	1433	3660
4			929	1463	2230	3755	2302	3845	2262	3745	2234	3673
3			94	524	908	2336	1331	3209	1535	3625	1675	3914
3			1431	2528	2152	3784	2122	3699	2073	3591	2049	3533
2			527	1273	1357	3028	1671	3665	1816	3959	1921	4172
2	1080	2000	1484	2749	1926	3538	1882	3441	1850	3374	1842	3353
1	582	1227	1097	2262	1839	3770	2020	4133	2102	4299	2169	4434
1	1070	2077	1157	2246	1559	3026	1583	3073	1594	3094	1613	3131
0	1605	3116	1736	3369	2338	4539	2374	4609	2391	4641	2419	4696

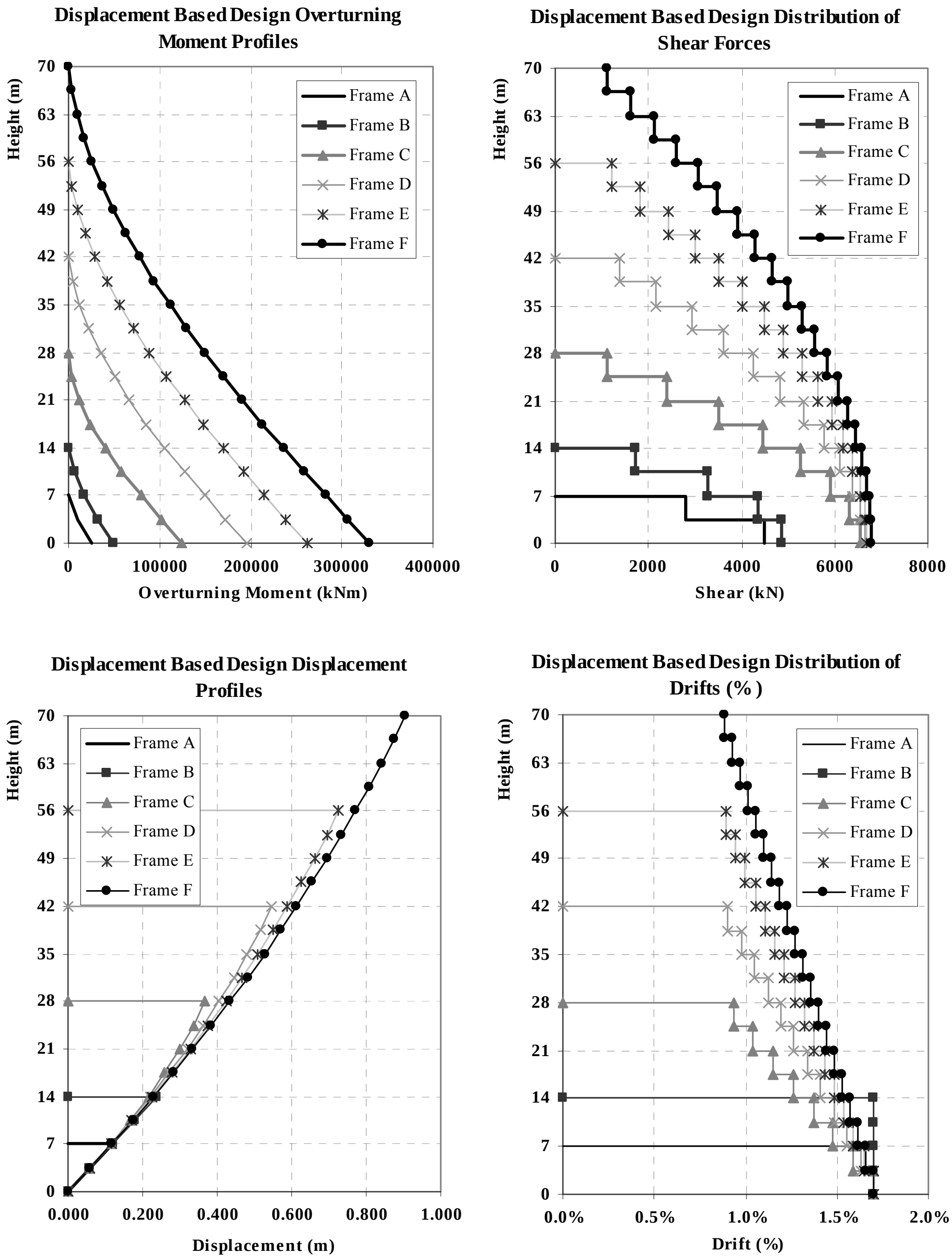

Figure 7-1. Revised displacement-based designs for Frames A to F

As with the original designs, Eqs.(4.11), (4.12) and (4.13), and the limiting material parameters as defined in Table 4-10, were used to calculate the section and member properties required for the input files used in Ruaumoko.

Table 7-7. Revised DDBD beam Yield Curvature, cracked second moment of area and bilinear flexural factor for frames A, B & C

	Frame A			Frame B			Frame C		
Level	ϕ_y	I_{cr}	r_ϕ	ϕ_y	I_{cr}	r_ϕ	ϕ_y	I_{cr}	r_ϕ
20									
19									
18									
17									
16									
15									
14									
13									
12									
11									
10									
9									
8							0.00348	0.0061	0.015
7							0.00348	0.0128	0.015
6							0.00348	0.0188	0.015
5							0.00348	0.0240	0.015
4				0.00425	0.0067	0.015	0.00348	0.0283	0.015
3				0.00425	0.0129	0.015	0.00348	0.0316	0.015
2	0.00425	0.0087	0.015	0.00425	0.0170	0.015	0.00348	0.0340	0.015
1	0.00425	0.0140	0.015	0.00425	0.0191	0.015	0.00348	0.0351	0.015
0	-	-	-	-	-	-	-	-	-

Table 7-8. Revised DDBD beam Yield Curvature, cracked second moment of area and bilinear flexural factor for frames D, E & F

	Frame D			Frame E			Frame F		
Level	ϕ_y	I_{cr}	r_ϕ	ϕ_y	I_{cr}	r_ϕ	ϕ_y	I_{cr}	r_ϕ
20							0.00348	0.0064	0.015
19							0.00348	0.0094	0.015
18							0.00348	0.0123	0.015
17							0.00348	0.0150	0.015
16				0.00348	0.0069	0.015	0.00348	0.0177	0.015
15				0.00348	0.0105	0.015	0.00348	0.0202	0.015
14				0.00348	0.0139	0.015	0.00348	0.0225	0.015
13				0.00348	0.0171	0.015	0.00348	0.0248	0.015
12	0.00348	0.0077	0.015	0.00348	0.0201	0.015	0.00348	0.0269	0.015
11	0.00348	0.0122	0.015	0.00348	0.0230	0.015	0.00348	0.0288	0.015
10	0.00348	0.0164	0.015	0.00348	0.0256	0.015	0.00348	0.0306	0.015
9	0.00348	0.0203	0.015	0.00348	0.0280	0.015	0.00348	0.0322	0.015
8	0.00348	0.0239	0.015	0.00348	0.0302	0.015	0.00348	0.0337	0.015
7	0.00348	0.0271	0.015	0.00348	0.0321	0.015	0.00348	0.0350	0.015
6	0.00348	0.0299	0.015	0.00348	0.0338	0.015	0.00348	0.0362	0.015
5	0.00348	0.0323	0.015	0.00348	0.0353	0.015	0.00348	0.0371	0.015
4	0.00348	0.0342	0.015	0.00348	0.0364	0.015	0.00348	0.0379	0.015
3	0.00348	0.0357	0.015	0.00348	0.0373	0.015	0.00348	0.0385	0.015
2	0.00348	0.0367	0.015	0.00348	0.0379	0.015	0.00348	0.0389	0.015
1	0.00348	0.0373	0.015	0.00348	0.0382	0.015	0.00348	0.0391	0.015
0	-	-	-	-	-	-	-	-	-

Table 7-9. Revised DDBD column concrete confinement values and M-ϕ bilinear approximation parameters

		f_{cc}' (MPa)	e_{cu}	N_{Grav} kN	M_y kNm	ϕ_y' /m	M_N kNm	ϕ_y /m	M_u kNm	ϕ_u /m	I_{cr} m4	r_ϕ
Frame A												
	Outer	48.2	0.0228	490	980	0.0052	1405	0.0070	1620	0.1150	0.0081	0.0099
	Inner	49.0	0.0223	980	1890	0.0058	2050	0.0078	2102	0.1050	0.0103	0.0020
Frame B												
	Outer	48.2	0.0227	1048	1262	0.0053	1594	0.0068	1802	0.1214	0.0085	0.0077
	Inner	49.1	0.0224	2096	1937	0.0060	2393	0.0074	2586	0.1115	0.0116	0.0057
Frame C												
	Outer	48.8	0.0200	2194	1905	0.0048	2347	0.0059	2598	0.1062	0.0144	0.0063
	Inner	49.1	0.0199	4388	3848	0.0057	4573	0.0067	4658	0.0748	0.0244	0.0018
Frame D												
	Outer	48.7	0.0200	3316	1996	0.0050	2386	0.0060	2526	0.1005	0.0143	0.0037
	Inner	49.1	0.0199	6632	3613	0.0051	4652	0.0065	4612	0.0659	0.0257	-0.0010
Frame E												
	Outer	48.7	0.0200	4438	2056	0.0053	2407	0.0062	2440	0.0914	0.0140	0.0010
	Inner	49.0	0.0199	8876	3389	0.0044	4694	0.0061	4657	0.0568	0.0277	-0.0009
Frame F												
	Outer	48.1	0.0192	5604	2319	0.0050	2647	0.0057	2616	0.0823	0.0166	-0.0009
	Inner	48.3	0.0191	11209	3680	0.0038	5151	0.0054	5071	0.0488	0.0345	-0.0019

7.2 INELASTIC TIME-HISTORY RESULTS USING REVISED DDBD METHODS

Using the designs developed in Section 0 with the implementation of the suggested design method revisions of Section 6.3, a series of inelastic time-history analyses at varying levels of earthquake intensity (*I*) were carried out for all six buildings.

The results are presented below as mean maximum values of storey shear, storey column moment sum (for moments at the top and bottom of the columns at each level), storey drift and centre of force (at the effective height of the building) displacement.

7.2.1 Description of results

The levels of intensity tested represent 0.5x, 1.0x and 2.0x the design earthquake level. Therefore it could be expected that the maximum centre of force displacements will be approximately equal to these ratios multiplied by the design displacements. In general the displacement profile results are seen to follow this well (Figure 7-3 to 7.8), and for intensities up to the design level, the average maximum storey drifts scale accordingly, with critical bottom storey drifts less than 2% for I = 1.0, and approximately 1% for I = 0.5.

The column bending moment "average maximum" time-history results are the outcome of summing across each floor level, at each column end (giving two sums per storey). To simplify the comparisons, the equilibrium derived design bending moments for each column (presented in Table 7-6) have been averaged above and below each beam-column joint level and then summed across each storey level *i* (at each column end), these results are thus termed "Design Storey Moment Sum" and "TH Storey Moment Sum" as shown in Figure 7-2.

A more practical approach could be to assume no column longitudinal reinforcement is terminated in a beam-column joint, in which case moment capacity above and below a joint could be assumed equal to the maximum design moment at each floor level (from moment values above and below the joint) based on Table 7-6.

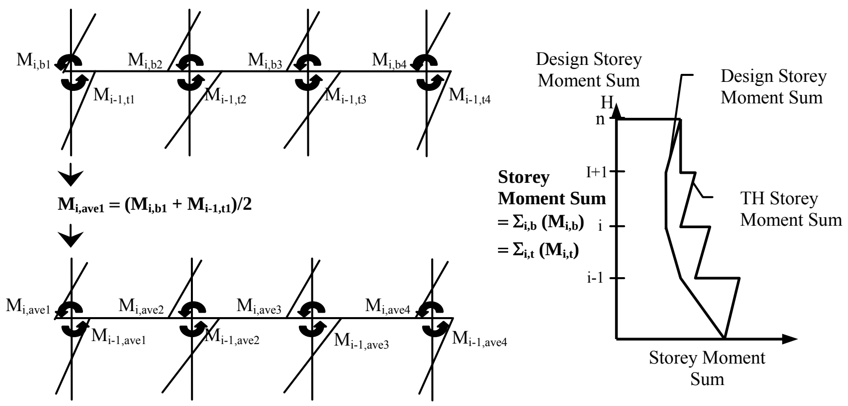

Figure 7-2. Schematic diagram showing the process used to develop the values of design storey moment sums that were used to compare time-history column moment maxima results

It should be noted that 20 storey building displacement and drift results are in fact for the same frame designed without use of the drift amplification factor ω_θ. This is because the time-history results using the reduction factor lowered the effective period into a portion of the displacement spectrum which exhibited mean characteristics for the earthquakes that gave excessively large displacement demands and therefore made interpretation meaningless (the shear force and moment results are however from the designs using ω_θ).

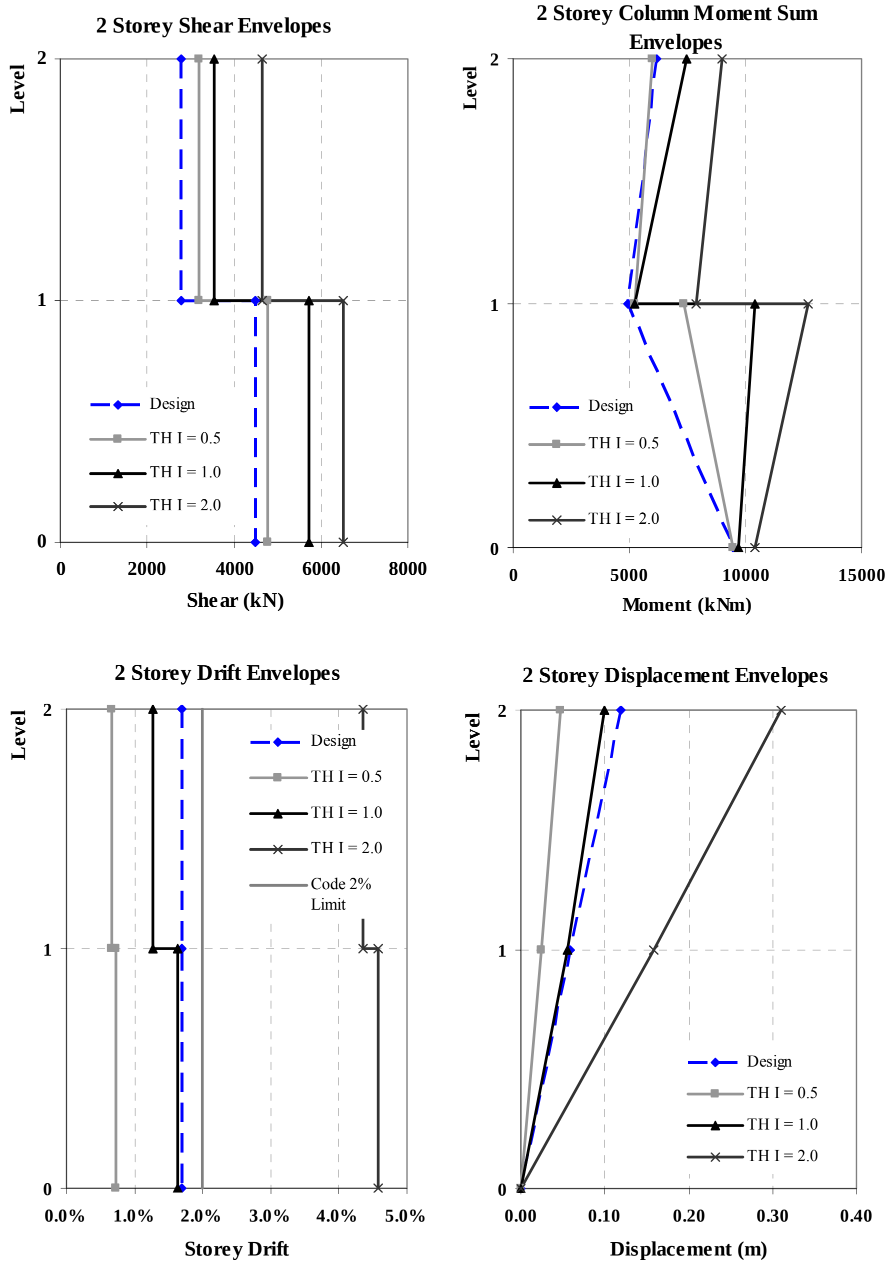

Figure 7-3. Average maximum time-history results at I = 0.5, 1.0 & 2.0 for 2 storey frame

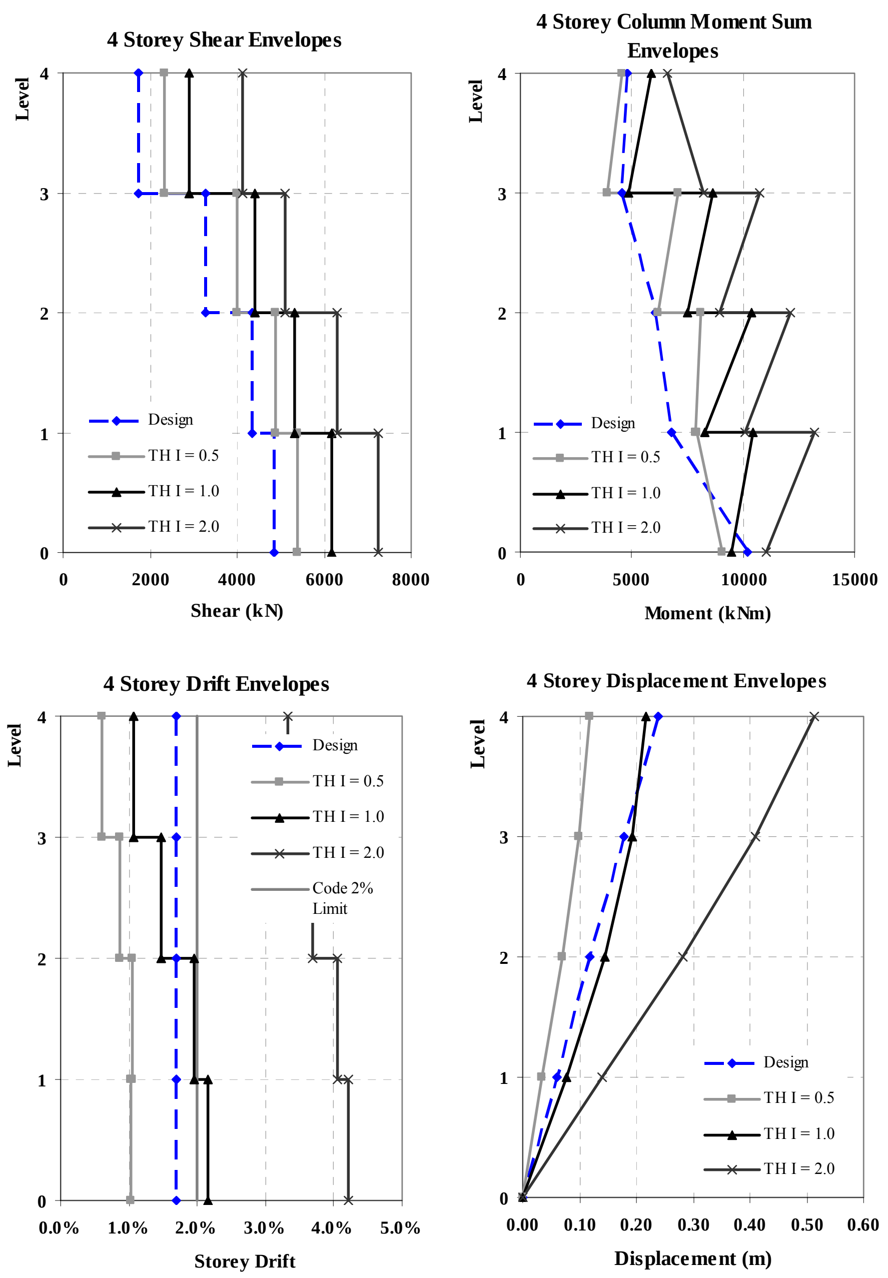

Figure 7-4. Average maximum time-history results at I = 0.5, 1.0 & 2.0 for 4 storey frame

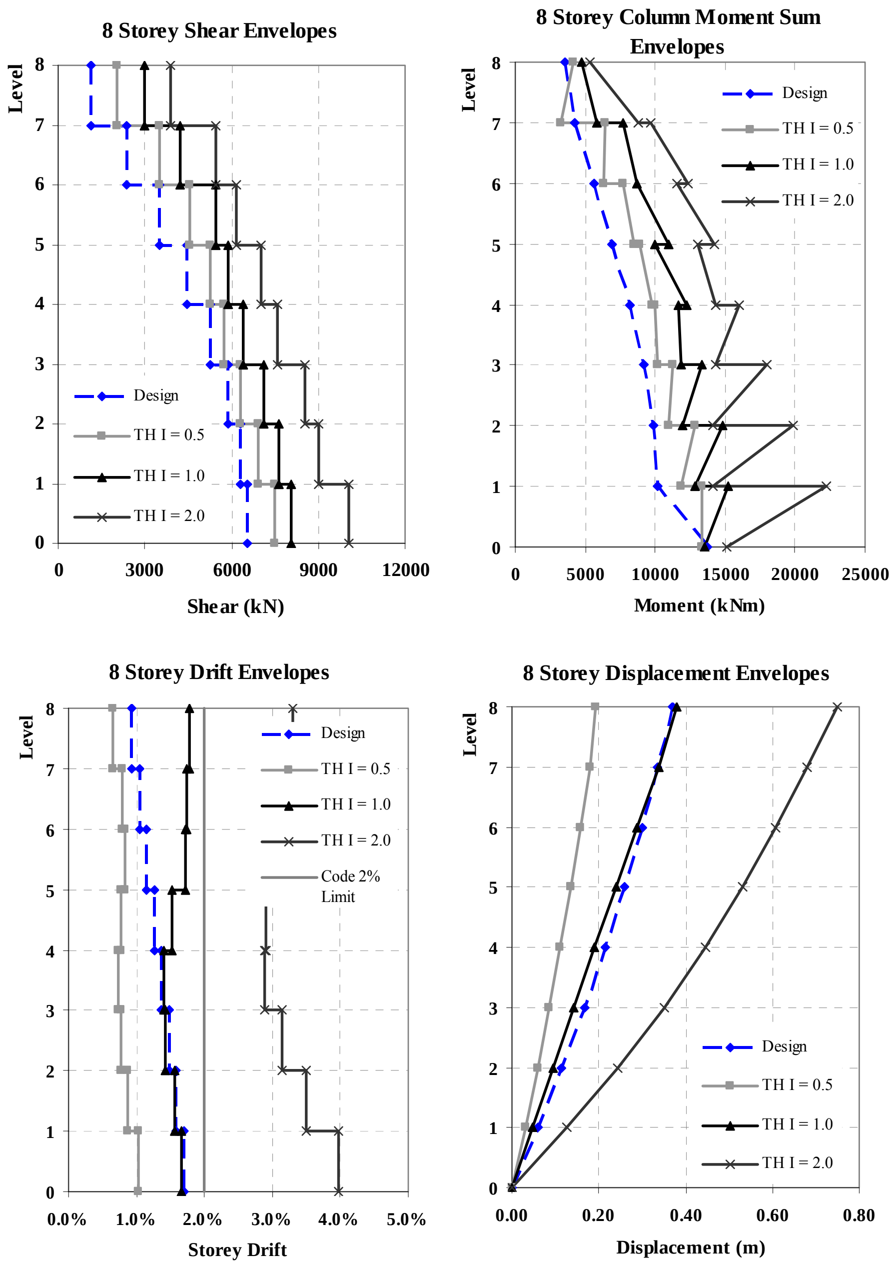

Figure 7-5. Average maximum time-history results at I = 0.5, 1.0 & 2.0 for 8 storey frame

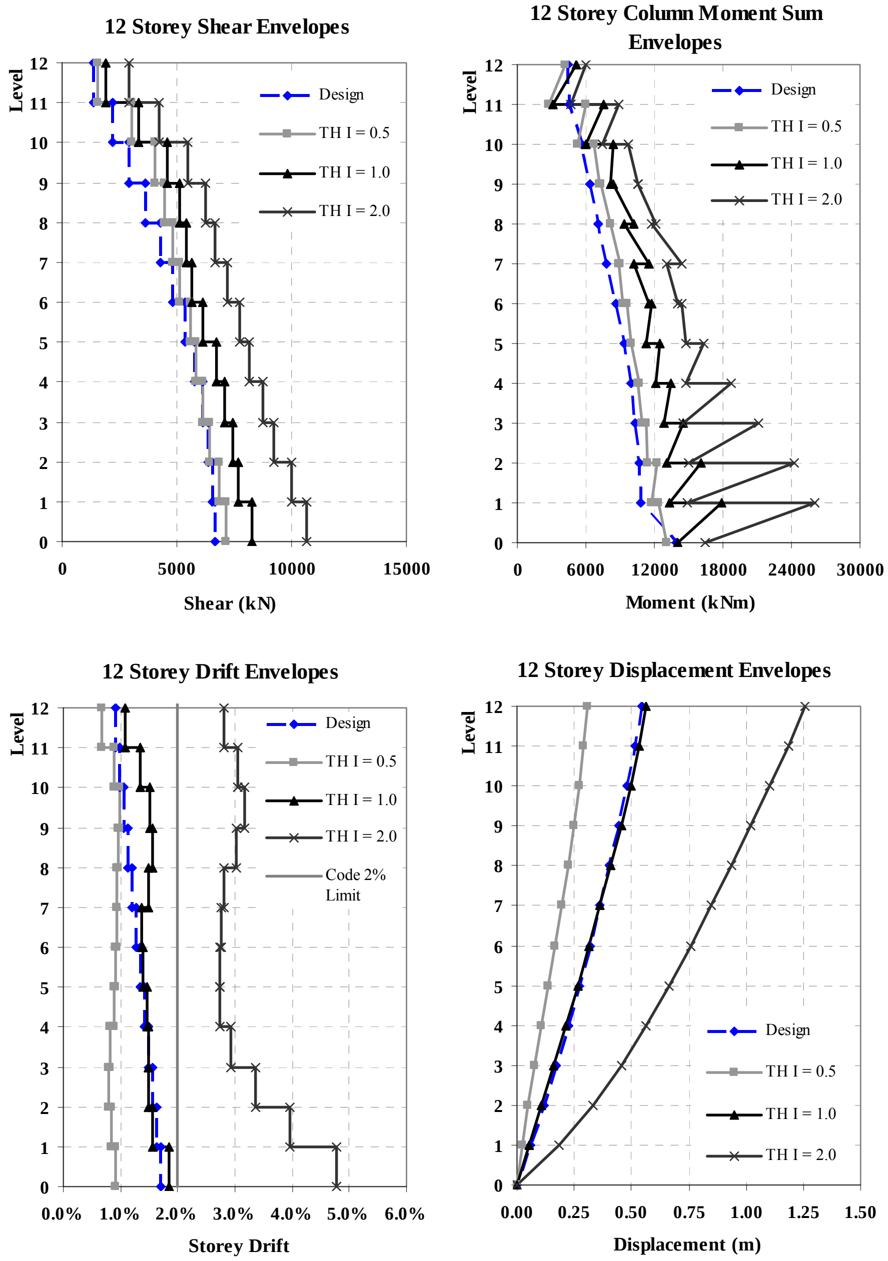

Figure 7-6. Average maximum time-history results at I = 0.5, 1.0 & 2.0 for 12 storey frame

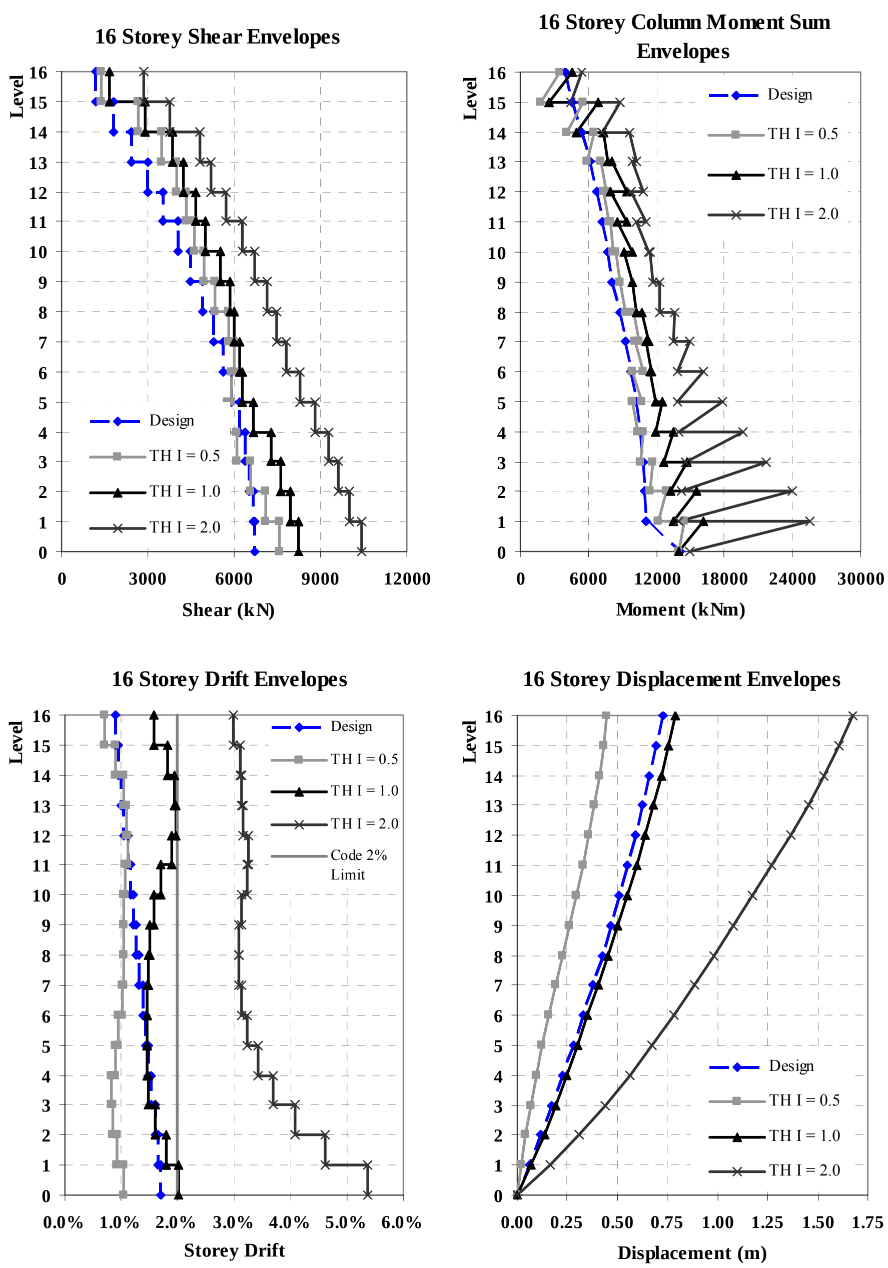

Figure 7-7. Average maximum time-history results at I = 0.5, 1.0 & 2.0 for 16 storey frame

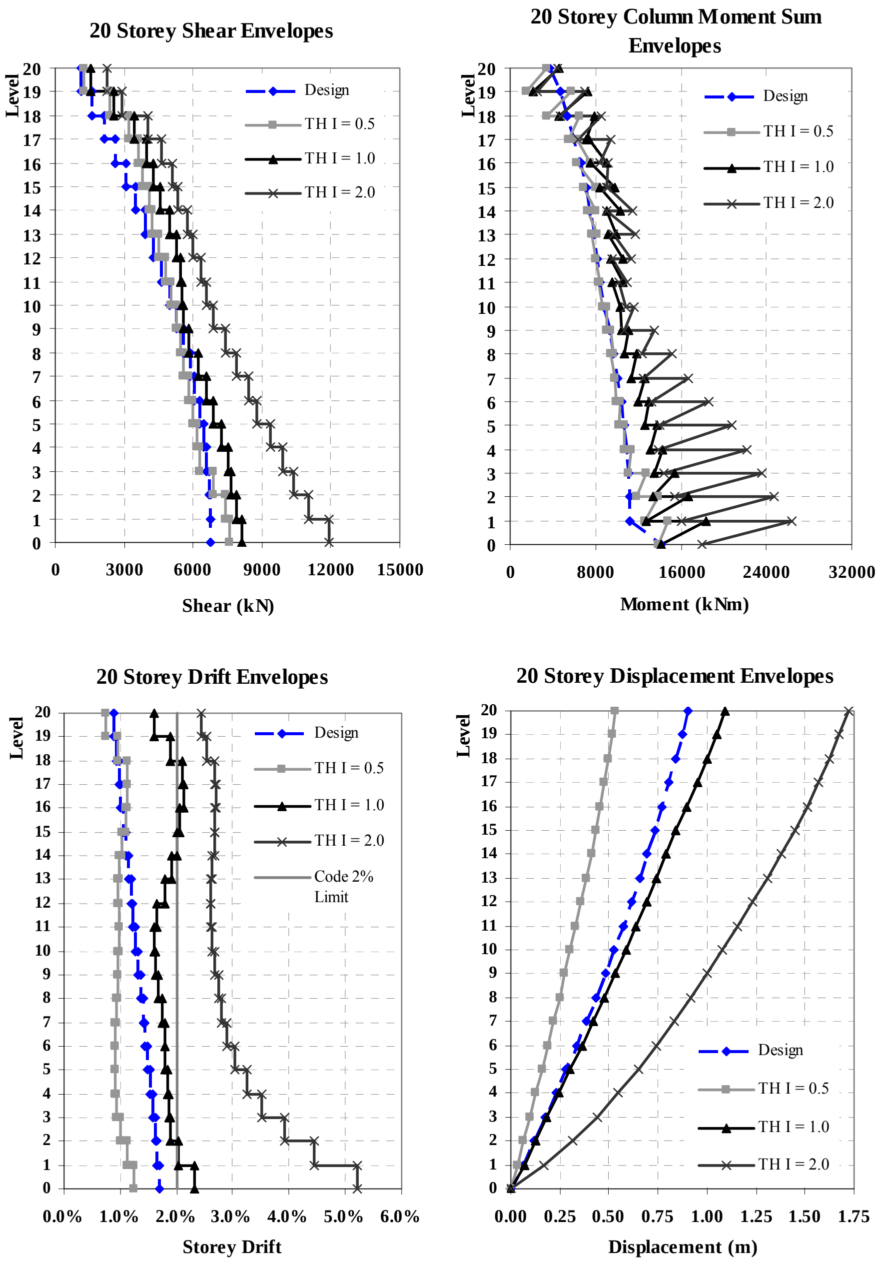

Figure 7-8. Average maximum time-history results at I = 0.5, 1.0 & 2.0 for 20 storey frame

7.2.2 Comments on results

Overall the behaviour of the frames is consistent between the different height buildings and with the design methodology assumptions. As mentioned in Section 7.2.1 the storey drift and displacement behaviour is generally acceptable at the design earthquake intensity. Peak drift demands closely match the design value at the assumed critical ground floor level, and centre of force displacements generally reflect the spectral displacement obtained at the design effective period.

The plots clearly show intensity dependence in all aspects of the frame behaviour. Comparison of the storey column shears and column moment sums suggest that in the shorter buildings the upper half of the structure is more influenced by intensity effects, while for the taller structures the increase in demand due to higher intensity motion is more noticeable in the bottom levels. As mentioned above, centre of force displacements generally reflect the intensity scaling.

It should be noted that the column bending moment and shear results contain some amount of overstrength behaviour due to steel strain hardening in the reinforcing as modeled in the beam hysteretic model (material overstrength has been removed by using expected strengths of concrete and steel as described in Section 4.2.1). For the results presented in Figure 7-3 – 7.8, the overall behaviour is of interest, however for the development of methods to account for the dynamic amplification some attempt at removing this content from the time-history results is made following the method outlined in Section 7.2.2.2.

In comparing the structures and the influence of intensity, it is also clear that higher mode effects become more dominant as the input motions are increased. This is more noticeable in the plots of storey drift (particularly for 8 storeys or more) in which values remain essentially constant over the height of the building for I = 0.5, but exhibit dynamic amplification for I = 1.0 with drift values increasing towards the 2% limit over the top half of the frames. An interesting observation is that behaviour does not continue to be accentuated in this fashion for I = 2.0. Drift amplification at this level is concentrated in the lower quarter of the buildings, and upper level drift profiles become essentially equal. The behaviour is very similar to what could be expected from the development of a "soft-storey" mechanism. However with no inelastic action permitted at the top of the bottom storey columns, the first floor beam behaviour is governing the response. Therefore at the higher intensity, these beams are subject to proportionally higher inelastic action than implied by the intensity level. It appears that the suggested inelastic first mode displacement profiles used in design do not reflect the higher intensity behaviour, and that the highly curved profiles seen from using Eq.(3.12) better reflect these results.

The dynamic amplification of storey shears and column moments is noticeable, particularly in the taller structures where clear differences exist between the design profiles and time-history maxima. Maximum storey shear averages maintain a consistent profile shape with amplification above the design level at all heights, in all buildings. However the amount of amplification is not constant as is shown in Figure 7-9, where the factor increases in the upper half of all the frames studied (if plotted with respect to normalised height the curves have very similar forms). An important result seen in this figure is the influence of the $0.1V_B$ assigned at the roof level in Eq.(6.2b). The curves for n = 4 and 8 show that without application of this extra proportion to the upper levels, the amplification becomes extreme in the upper storeys. For the three taller structures the amplification is somewhat limited, indicating that this approach not only helps to control storey drift demands, but in a similar fashion limits the dynamic shear amplification. This comparison reflects observations made by Medina (2004) that overall dynamic behaviour is sensitive to the pattern of distribution of design storey shear strength.

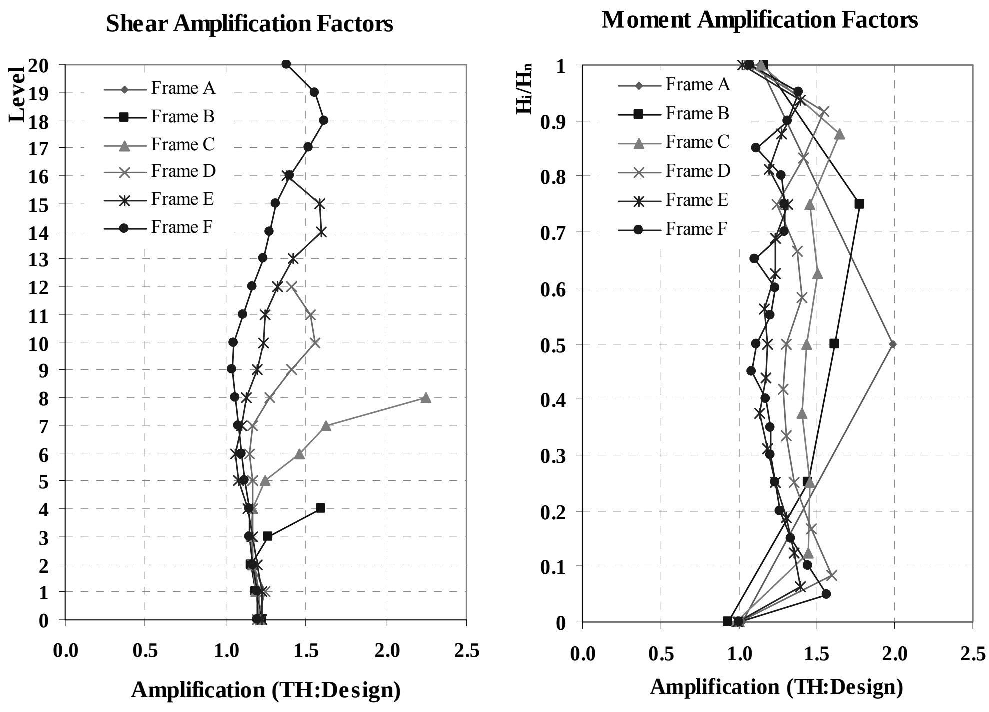

Figure 7-9. Inelastic time-history storey shear and column moment amplification (I = *1.0*)

The storey sum column moment amplification also shown in Figure 7-9 has been normalised with respect to height, this is in order to highlight the similarity in amplification distribution between all of the buildings. Principally amplification is important at the first floor level and the floor level below the roof (floor n-1). Over the rest of the building the factor is generally constant between 1.25 and 1.50 times the design value.

While dynamic amplification is found in all the results presented, it is not significant compared to the behaviour observed for structural walls using similar design methods. In the results presented by Priestley and Amaris (2002) the influence of higher modes is very significant due to the assumption (and general design requirement) that the wall remains elastic above the plastic hinge at the base. With respect to the storey shears and column moments, the dynamic amplification due to higher modes, is seen not to be particularly significant. Reasoning from the observed wall behaviour, this is clearly due to the distribution of inelastic action over the complete height of the building. Provided plastic hinges form in the beams at all levels of the structure, it can be expected that amplification due to higher mode dominance in the upper levels will be somewhat limited due to the ductility development.

To some extent this reasoning is verified by the observed drift behaviour mentioned above, in particular that increasing the intensity does not lead to greater participation of the higher modes in the upper levels of the structures. Instead drift amplification is limited to the lower levels, suggesting that the relative contribution of the significant modes has changed such that the higher modes have a reduced importance. In a similar respect the column moment profiles reflect such behaviour, thus the drift increases seen in the lower levels are due to the increased "softening" of the lower level beams through the greater inelastic action developed.

7.2.2.1 Scatter in Time-history results

The following plots (Figure 7-10) are included to show the extent of scatter in results seen for the six frames tested. These plots represent the behaviour at the design intensity. However it should be noted that at I = 0.5 the scatter was minimal, while for I = 2.0 the scatter was noticeably increased.

For all six buildings, the storey shear results are very consistent and show little scatter at all levels, it follows that column bending moments also exhibit minimal variation between records. The consistent results are also present in the profile plots of maximum centre of force displacement, where the design profile shape and magnitude are generally well represented by the individual earthquake results. Contrary to these observations, the storey drifts show large amounts of scatter at all heights, for all the buildings. The variation is particularly significant over regions where higher modes influence the response, such as in the top quarter of the 12, 16 and 20 storey frames.

7.2.2.2 Accounting for overstrength due to steel strain hardening

To identify the influence of dynamic behaviour on the structural demands and thus follow the general capacity design equation, it is necessary to remove the portion of action (bending moments and shear forces) overstrength corresponding to strain hardening in the reinforcing steel. Conceptually this is a relatively straight forward task to follow if the maximum moment for an element occurring in the time-history, is divided by the corresponding design moment. In reinforced concrete frames the primary source of overstrength is in the beam plastic hinges, from which the moments generated are transferred to the columns. Therefore evaluating the strain hardening at each beam level would give an estimate of the overstrength action transferred to the columns.

The difficulty in accurately assessing the overstrength and its influence is that maximum beam bending moments do not necessarily occur at the same time as the maximum column moments since the column moment development is significantly dependent on the variation in axial load due to the global structural behaviour under seismic load. To assume that the maximum beam overstrength can be removed directly from the maximum column moments and shear forces could be significantly non-conservative.

Therefore, it was decided for this study to account for flexural overstrength by evaluating the average ductility demand from the time-history results using the displacement profiles found at the time of the maximum centre of force displacement. As shown (Figure 7-3 – 7.8), the average results gave good approximation to the design profiles, so such an assumption does not seem unreasonable. Thus converting the modeled flexural (M-ϕ) bilinear factor r_ϕ to the equivalent force (F-Δ) bilinear factor using the following equation derived from Moment Area and Moment-Curvature considerations:

$$r_\Delta = \frac{1}{\dfrac{6L_p}{r_\phi L} + 1} \tag{7.1}$$

Where L_p is the calculated plastic hinge length from Eq.(5.1) and L is half the clear beam span. The assumed overstrength at maximum global response can then be found using Eq.(7.2) which was developed from basic Force-Displacement Ductility diagram (Figure 7-11) considerations:

$$\phi_o = 1 + r_\Delta\left(\mu_\Delta - 1\right) \tag{7.2}$$

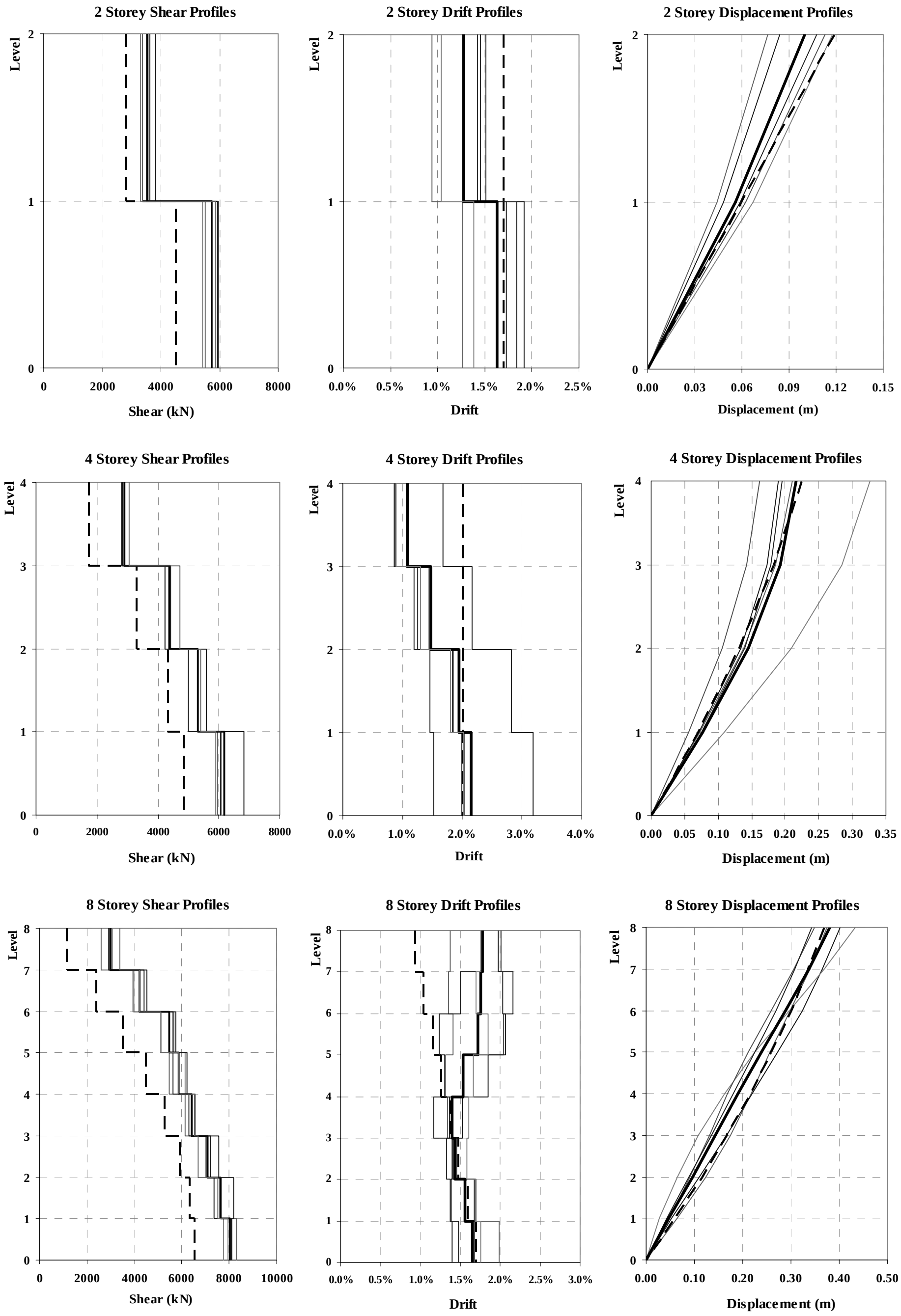

Figure 7-10. Time-history results (2, 4 & 8 storey frames) showing the individual record variation between results for storey shears, drifts and displacement profiles (I = 1.0).

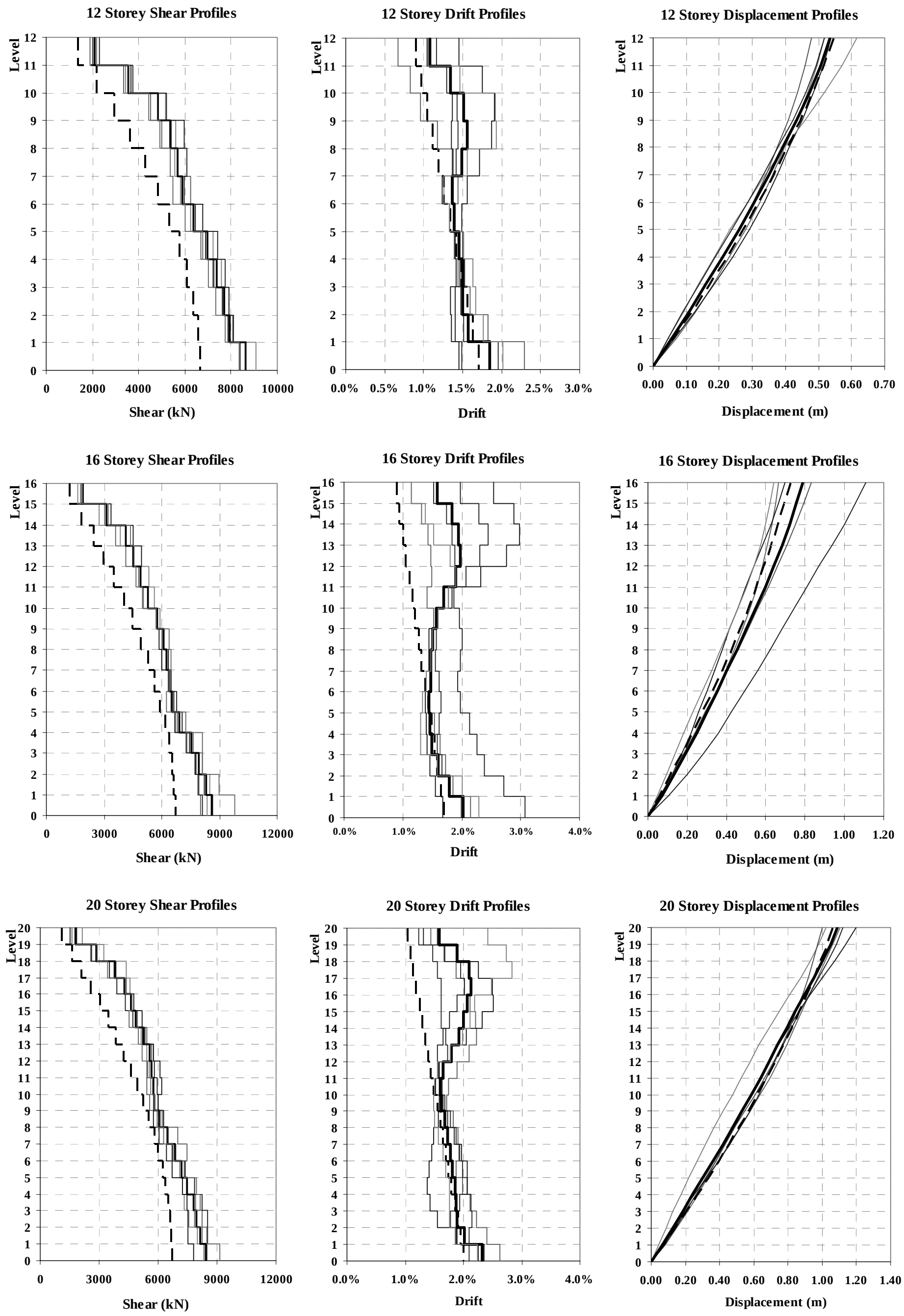

Figure 7.10. Time-history results (12, 16 & 20 storey frames) showing the individual record variation between results for storey shears, drifts and displacement profiles (I = 1.0) (cont.)

It should be noted that an error was found in the calculations after this equation was applied. The equation actually used was $\phi_o = 1 + r_\Delta(\mu_\Delta)$ which led to slight over-estimations of the overstrength value in the upper, less ductile levels, and minor under-estimations in the lower levels. While this had some influence on the final results used in Chapter 8 to develop methods of accounting for dynamic amplification, trials have shown that they are not significant and that the suggested equations in Section 8.2 remain valid.

A final consideration is that the maximum storey ductility could be calculated based on maximum drifts, however given that maximum drifts do not necessarily coincide with maximum shear or column moment development, such an approach could also be significantly in error.

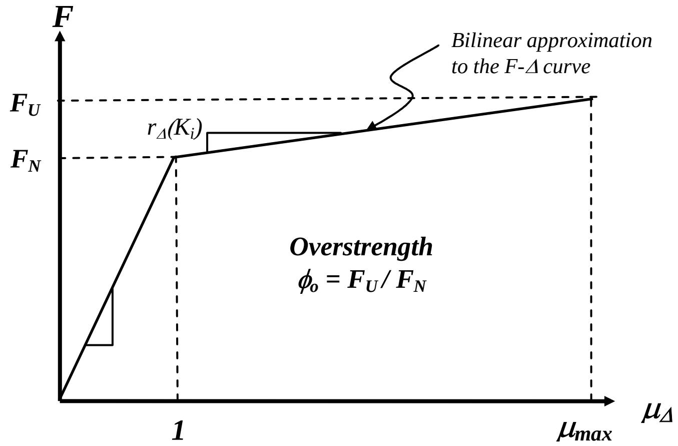

Figure 7-11. Determining overstrength factor ϕ_o from bilinear approximation to the Force - Displacement ductility response of an element

7.2.2.3 Results using real earthquake accelerograms

As mentioned in Section 5.2.6, a suite of five real earthquake records, with an average compatible with the EC8 displacement spectrum was used as a final verification of the methods developed.

The details of the accelerograms are included in Appendix A, however in general they represent far-field motions that do not include significant directivity effects. While four of the records maintain a fairly wide-band range of motion, it is noted that the record from the ChiChi 1999 earthquake (TCU047) is possibly influenced by site amplification due to basin geometry effects and the presence of soft-soils underlying the site. The result is that this accelerogram exhibits motion somewhat similar to expected near-field behaviour.

The average results at the design level intensity, presented in Appendix A, generally reflect those seen in Section 7.2.1, however as might be expected there is somewhat more scatter between the individual records. This is reflected by particular concentrations of excess demand. An example of this is the four storey frame for which the drift and displacement envelopes exceed the design levels, particularly in the bottom storey. This can be attributed to the TCU047 record, which has significantly higher displacement demands over the period range applicable to this frame.

The storey shear force and column bending moment amplification patterns are very similar to those seen when using the artificial accelerograms. This is to be expected given the ductility development throughout the building will tend to limit the internal forces (effectively desensitising the building from the form of ground motion, although not necessarily the intensity).

8. ACCOUNTING FOR DYNAMIC AMPLIFICATION

Using the inelastic time-history results presented in Section 7.2, the following sections look at methods of accounting for the dynamic amplification of column shear forces and bending moments as observed in the six frames analysed in this investigation.

8.1 APPLICATION OF EXISTING METHODS

As outlined in Section 2.2, force-based design can be applied either as an equivalent lateral force analysis with a later account for higher mode effects in the design phase, or a multi-modal analysis can be used to directly account for the influence of higher modes. This section looks at the application of the methods defined in Section 2.2.1.1 and 2.2.2 as well as the method proposed by Priestley and Amaris (2002) for wall structures.

8.1.1 FORCE-BASED AMPLIFICATION APPROACHES

The methods outlined in earlier sections were applied to the design profiles of storey shear, and where possible column moment, for each of the frames and compared with the time-history maxima presented in Section 7.2. It is important to note that without making assumptions of member cracked stiffness it is not possible to apply the multi-modal analysis method for bending moment distributions. Having assumed values of member stiffness the design strengths can be found and thus the more appropriate cracked stiffness values can be found from M-ϕ analyses. The iteration required to satisfactorily represent the section stiffness underlines the inherent problems with force-based design and the inappropriate methods of modelling required to apply such methods (Priestley, 2003). It should also be noted that the moment amplification equation is a function of the fundamental period of the structure, which has previously been determined using elastic periods based on assumed cracked section properties. It is expected that structures analysed under such assumptions will exhibit periods shorter than the true values. This is compared to the periods found from bilinear approximations to moment-curvature analyses, which tend to be longer for all building heights. Therefore it is expected that the amplified column moments seen in Figure 8-1 will be somewhat excessive.

The results shown in Figure 8-1 show that current methods used with force-based design do not give consistently adequate, or accurate account of the dynamic amplification of both column bending moments and shear forces.

The application of the modal superposition used the specifications in EC8, requiring a minimum total of 90% mass participation and a behaviour factor q calculated as shown below for the assumption of a medium ductility class (DCM) reinforced concrete frame structure to give fair comparison with respect to the relatively low design ductility found for the structures.

$$
\begin{aligned}
q &= q_o k_w \geq 1.5 \\
q_o &= 3.0\left(\frac{\alpha_u}{\alpha_l}\right) = 3.0(1.3) = 3.9 \\
q &= q_o k_w = (3.9)\cdot 1.0 = 3.9
\end{aligned}
\tag{8.1}
$$

It is clear in this development that the assumed reduction factor is significantly higher than the design ductility values found for direct displacement-based design, and that the application of the same assumed level of ductile behaviour for all building heights leads to significantly different design values that clearly do not meet the actual column shear demands. To reasonably compare the elastic modal superposition approach, a similar form using the design ductility rather than the assumed value of behaviour factor has been included in Figure 8-1. The results show that as the building height (and period) increase, the elastic modal superposition becomes increasingly non-conservative.

The equations presented by Paulay and Priestley (1992) for both column bending moments and column shear forces give relatively good approximations to the time-history results, however they tend to be inconsistent with shear force design envelopes being very accurate for the shorter frames, but becoming less accurate (and non-conservative) in the top half of the taller buildings due to higher mode amplification exceeding the 30% upperbound of Eq.(2.9a). The column moment envelopes tend to underestimate the required amplification for the shorter frames and significantly overestimate the demands of the taller structures through the mid-height floor levels, while peak demands in the first and second floor levels are not well anticipated.

It can be concluded that current methods of dynamic amplification used in force-based design are not applicable for use with displacement-based design, and that a method that can be applied to the direct displacement-based procedure, with an account for intensity is required.

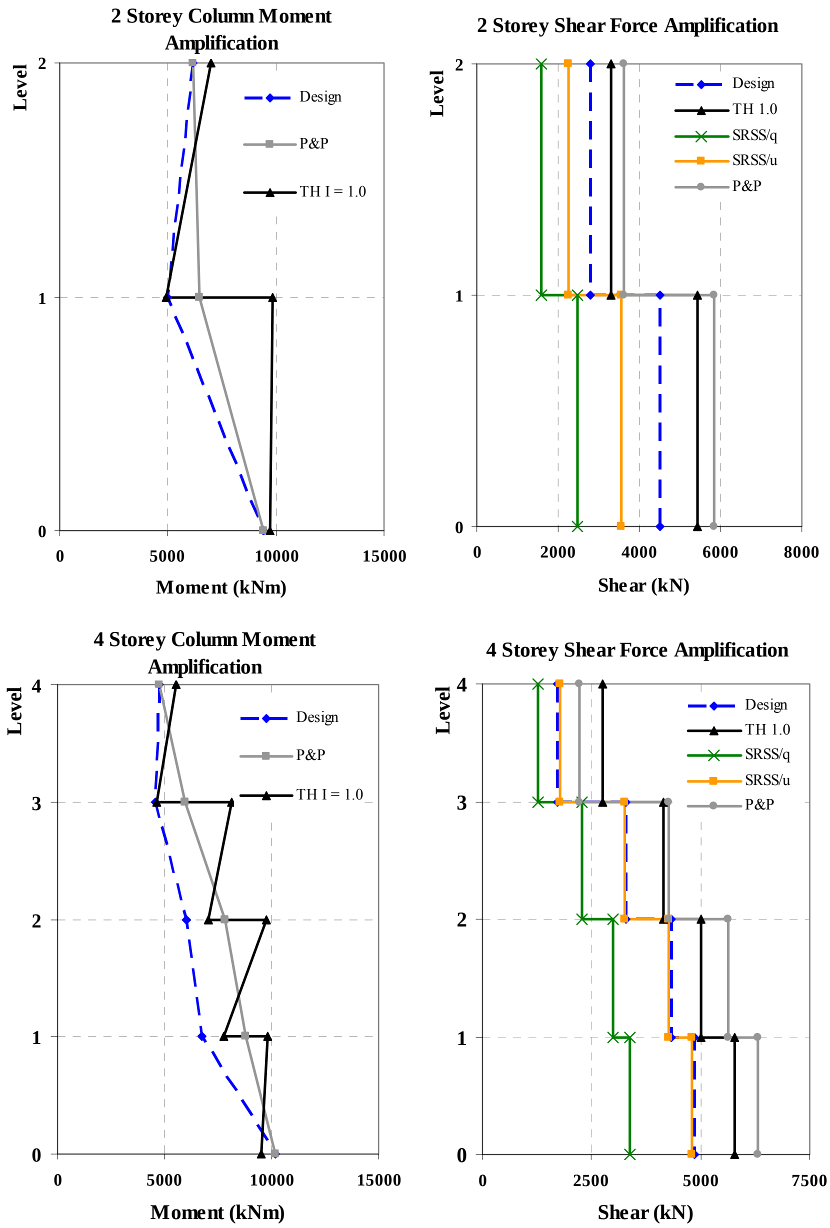

Figure 8-1. Current methods of accounting for dynamic amplification using Eqs. (2.6a) and (2.9a) (Paulay and Priestley, 1992) labelled 'P & P'; Elastic Modal Superposition divided by the EC8 behaviour factor q labelled as 'SRSS/q'; Elastic Modal Superposition divided by the design ductility factor labelled as 'SRSS/μ'

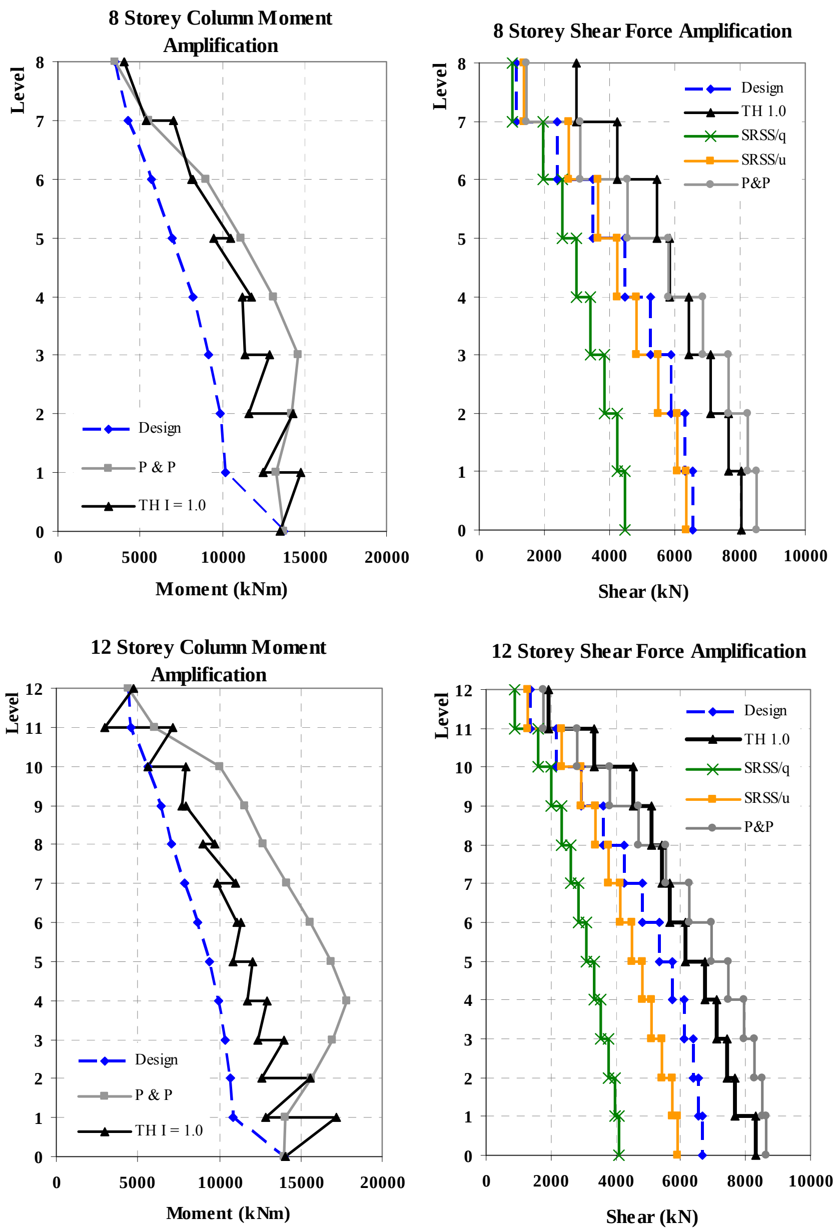

Figure 8.1. Current methods of accounting for dynamic amplification using Eqs. (2.6a) and (2.9a) [Paulay and Priestley (1992)] labelled 'P & P'; Elastic Modal Superposition divided by the EC8 behaviour factor q labelled as 'SRSS/q'; Elastic Modal Superposition divided by the design ductility factor labelled as 'SRSS/μ' (cont.)

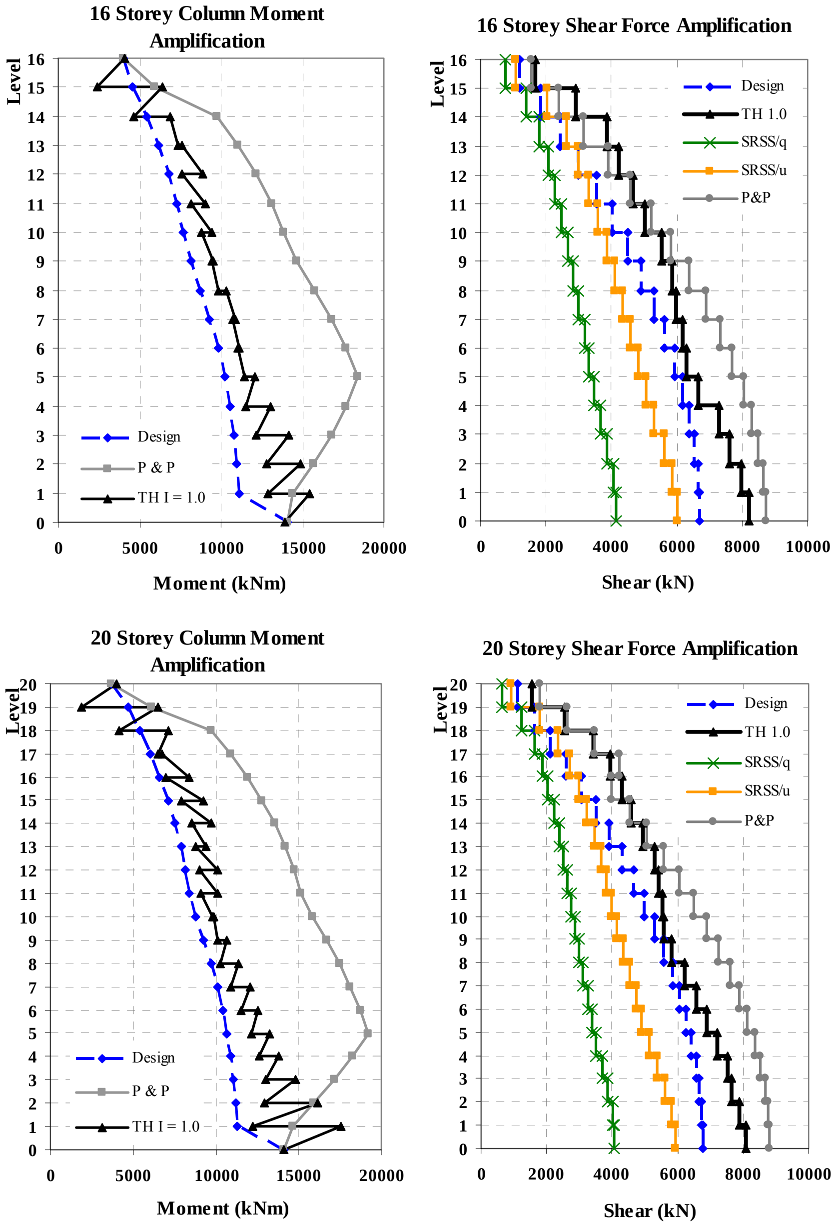

Figure 8.1. Current methods of accounting for dynamic amplification using Eqs. (2.6a) and (2.9a) [Paulay and Priestley (1992)] labelled 'P & P'; Elastic Modal Superposition divided by the EC8 behaviour factor q labelled as 'SRSS/q'; Elastic Modal Superposition divided by the design ductility factor labelled as 'SRSS/μ' (cont.)

8.1.2 DDBD DYNAMIC AMPLIFICATION METHOD: MODIFIED MODAL SUPERPOSITION

Priestley and Amaris (2002) proposed a method of accounting for dynamic amplification that utilised the concepts of an intensity dependent multi-modal superposition. This Modified Modal Superposition (MMS) has the variation that the direct displacement-based design shear forces or moments were substituted for the first mode response in the superposition procedure.

The proposed equations therefore take the form of a SRSS combination, with the DDBD shear forces and moments substituted in place of the first mode elastic forces, while all other modes required are taken as the elastic modal analysis forces.

$$V_i = \left(V_{1i}^2 + V_{2Ei}^2 + V_{3Ei}^2 + \ldots\right)^{1/2} \tag{8.2}$$

$$M_i = 1.1 \times \left(M_{1i}^2 + M_{2Ei}^2 + M_{3Ei}^2 + \ldots\right)^{1/2} \tag{8.3}$$

This method was found to give very satisfactory estimates of the dynamic amplification in structural walls.

Based on the good results found for wall structures it is a logical progression to try applying the method to frame structures as the direct displacement-based design process is essentially the same. In a preliminary investigation by Priestley (2003), the results of this application were inconsistent, and did not reproduce the close agreement with time-history results seen for structural walls. To further verify this, trials were carried out using Eq.(8.2) on each of the six frames, with Figure 8-2 and 8.3 showing the comparative results for storey shear force. As found by Priestley the method tends to become excessively conservative as the number of storeys increases and the estimated participation of the elastic higher modes becomes more dominant. The result is that for shorter buildings the method is slightly non-conservative, while for taller buildings it is over conservative for most of the building.

As suggested by Priestley (2003), the reason for this conservatism in the method is that frame structures have vibration modes that have more closely spaced natural periods. The result is that as the structure experiences inelastic behaviour, not only does the fundamental mode shift into longer periods, but some of the higher modes will also tend to reduce in influence (leading to decreased excitation as they follow down the constant velocity slope of the acceleration spectrum) as shown in Figure 8-4. This is in contrast to structural walls where the first mode period is substantially longer than the higher modes, therefore the first mode reduces in influence, while the higher modes tend to remain close to the constant acceleration plateau.

The use of the elastic forces for the higher modes as applied in Eqs.(8.2) and (8.3) is thus clearly not appropriate for reinforced concrete frame structures, and some revision of the method to account for this difference could be expected to give better results with respect to the time-history profiles.

A further consideration regarding frame behaviour in general, is that the assumed inelastic mechanism under the application of capacity design utilises beam hinging at all levels of the structure. Therefore it can be considered that ductility would influence the structure at all heights, leading to a limitation of the forces that can develop in the upper level of the building, and therefore reducing the additional demands due to higher mode excitation. This is evidently so, when compared to structural walls which are assumed to remain elastic above the base level plastic hinge. Assuming that the higher modes do not significantly alter the ductility in the beams (at the time of maximum centre of force response), it is possible that use of the direct displacement-based design ductility in some way may reduce the higher mode contributions to the MMS procedure.

8.2 DEVELOPMENT OF DYNAMIC AMPLIFICATION PROCEDURES FOR FRAME DESIGN

The concept of approximating the global response of a structure by applying the assumed inelastic first mode design forces in the MMS approach appears conceptually reasonable, and is validated in the results seen for wall structures. Therefore a modification to the MMS procedure is a logical step in trying to develop a consistent method of accounting for dynamic magnification effects.

The observed higher mode response is somewhat muted in effect compared to the behaviour of structural walls, due to the development of plastic hinges at all heights of the building and period shift of the higher modes. As mentioned this distribution of inelasticity acts to limit the amplification of the induced actions over the whole height, and therefore a reasonable first approach is to apply this ductile reduction over the full extent of the building using the MMS approach rather than the elastic modal superposition already shown to be inadequate. This ductile MMS procedure will be referred to as the DMMS approach from here onwards to distinguish between that applied to walls and that developed for frames.

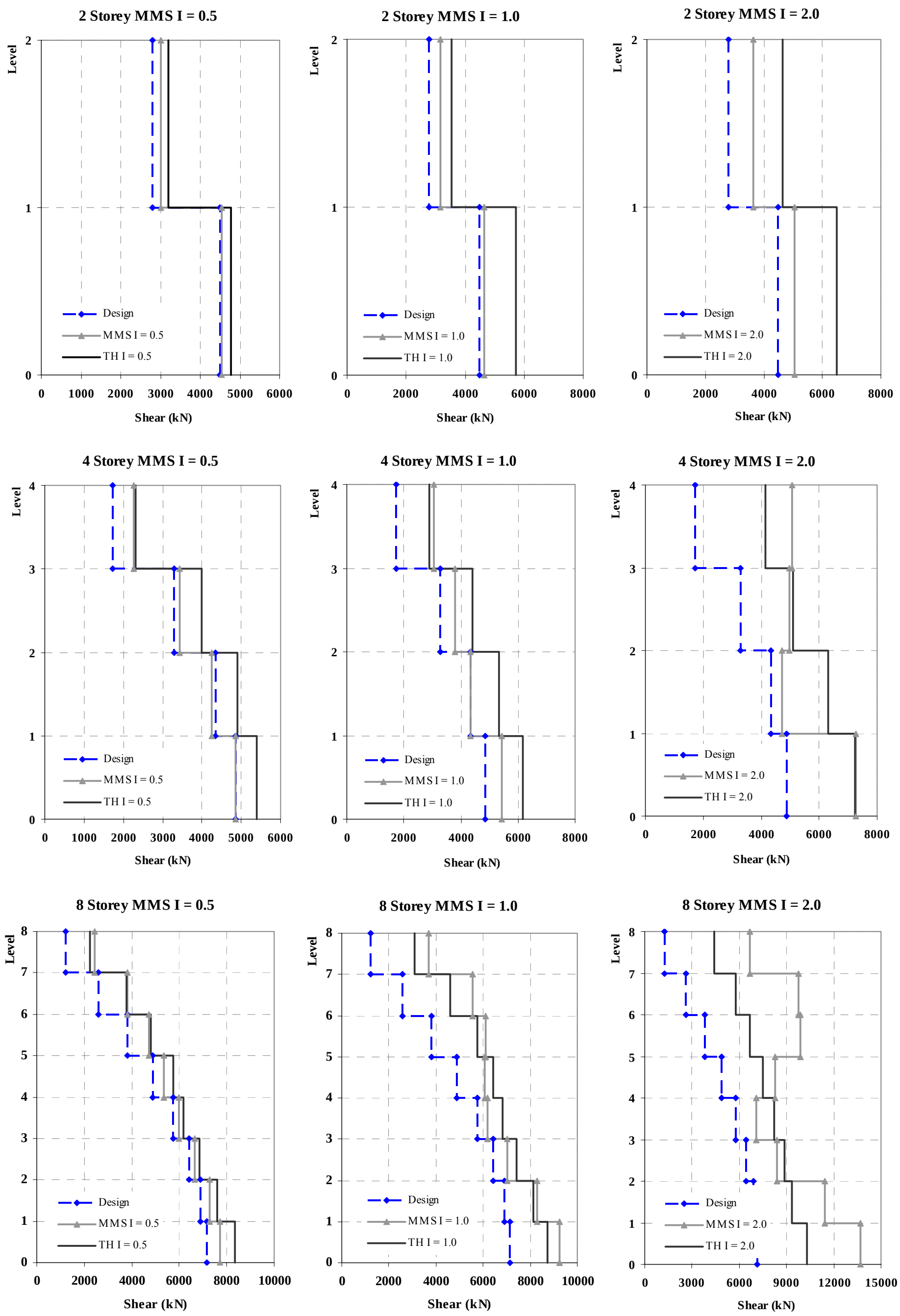

Figure 8-2. Storey shears from MMS compared with design and time-history results for 2, 4 and 8 storey frames at 0.5x, 1.0x and 2.0x the design intensity

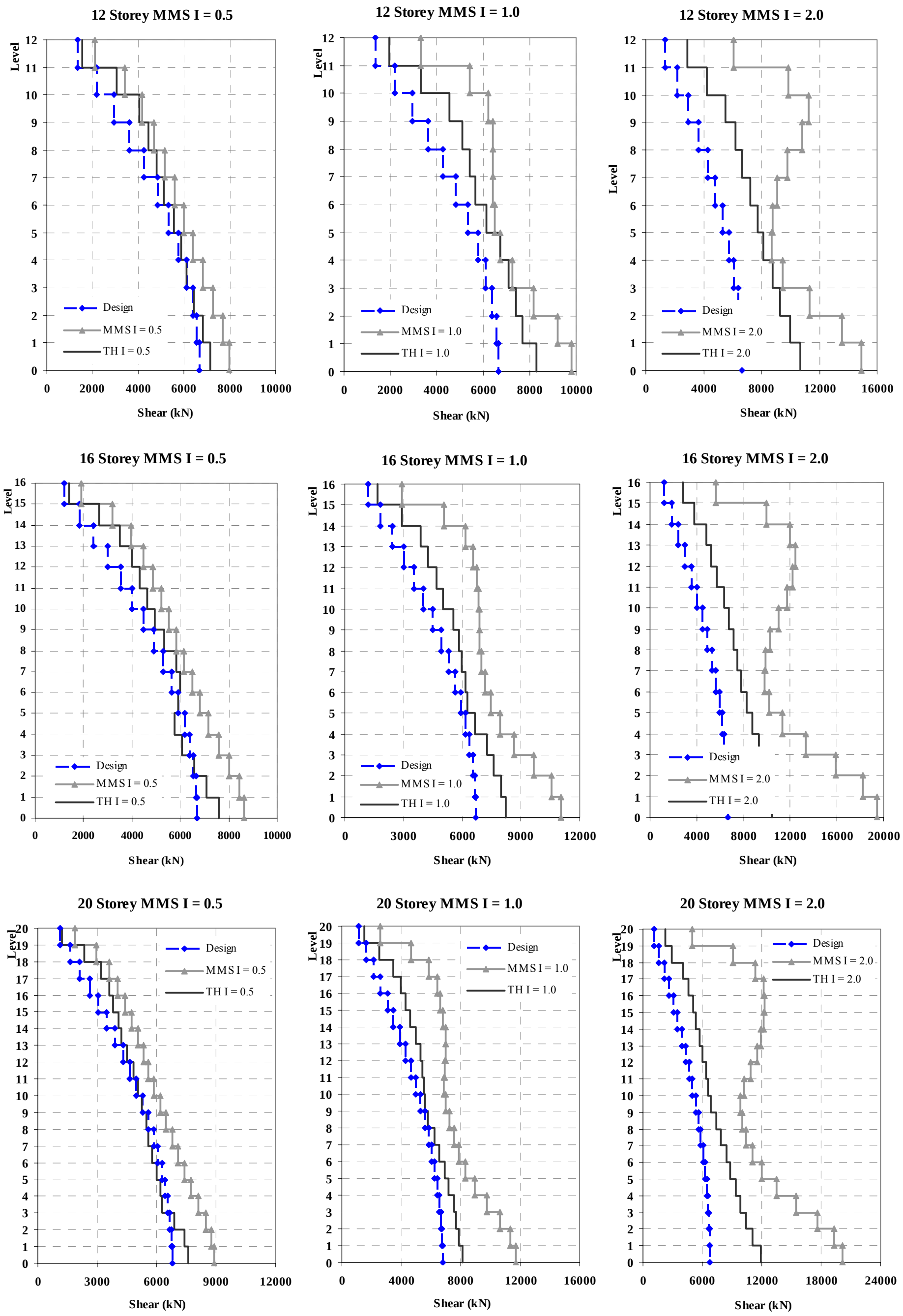

Figure 8-3. Storey shears from MMS compared with design and time-history results for 12, 16 and 20 storey frames at 0.5x, 1.0x and 2.0x the design intensity

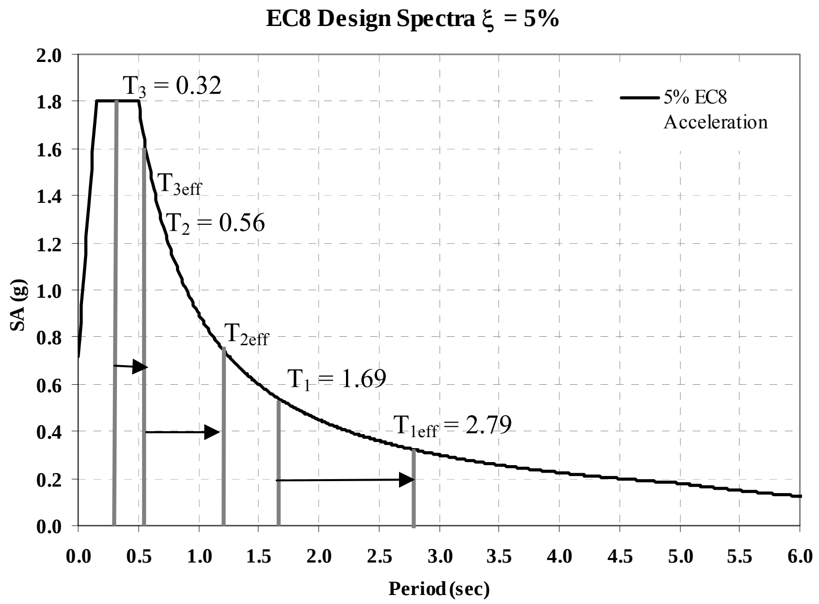

Figure 8-4. Design spectrum showing conceptually how the closer spacing of frame building natural periods leads to the higher modes decreasing influence as the structure becomes inelastic

8.2.1 Column shear force amplification

Considering the column shear behaviour, the above concept can be combined with the MMS procedure to give a more logical application of the so called reduction factor (or behaviour factor) as the predominant inelastic action is still derived from the inelastic first mode design forces. Such a method would take the following proposed form with the requirement of 90% mass participation (as described in Section 2.2.2).

$$V_i = \left(V_{1i}^2 + \left(\frac{V_{2Ei}}{\mu_D} \right)^2 + \left(\frac{V_{3Ei}}{\mu_D} \right)^2 + \ldots \right)^{1/2} \tag{8.4}$$

Provided a structure behaves with similar characteristics as those assumed by the design displacement equations, the use of the design ductility in this form should give good reflection of the force reductions that occur due to inelastic action. The definition of the design displacement ductility needs consideration however, as the value gained using the substitute structure can potentially be different from that found by calculating the design ductility at each storey level, due to changes in beam depth and the parabolic displacement profiles giving variable ductility up the height of the building.

If Eq.(8.4) is first considered using the substitute structure design ductility value, that is the global ductility factor, the results at the design intensity are consistently lower than the values obtained for the time-history average maximum storey shears, as shown in Figure 8-5.

It is initially difficult to tell what the reasons are for the consistent underestimation of storey shear. However as mentioned in Section 7.2.2.2, the difficulty in accounting for overstrength action due to strain hardening and the column moment capacity dependence on axial load could cause such effects. The influence of column axial load can not be directly evaluated from the column bending moment results shown earlier, because the models only utilised axial load – moment interaction curves in the ground level columns. Investigation of the global overturning moments from the time-history results showed a consistent amplification above the design profile over the whole building height. Given that the external column axial force couple dominates the overturning response, a general estimate of the axial force influence on the dynamic behaviour can be found from these results. Typically at the design intensity the amplification was approximately 20% for all the frames, therefore it is possible that this value could be used as an indirect account for the dynamic axial behaviour, and thus the potential column shear force amplification.

An interesting consideration is the use of the storey design ductilities in Eq.(8.4) instead of the substitute structure ductility. This gives an account of the parabolic displacement profile (and beam depth changes), and therefore the variation in ductility distribution over the building height. Figure 8-6 shows the result of applying such an approach.

This approach follows a more logical path with respect to the assumed design distribution for the inelastic first mode response as this is determined assuming the ductility developed over the height of the building is not constant (by distributing with respect to the force vector as found using the design displacements). In this case the upper level results are better, but in general there is not a significant improvement.

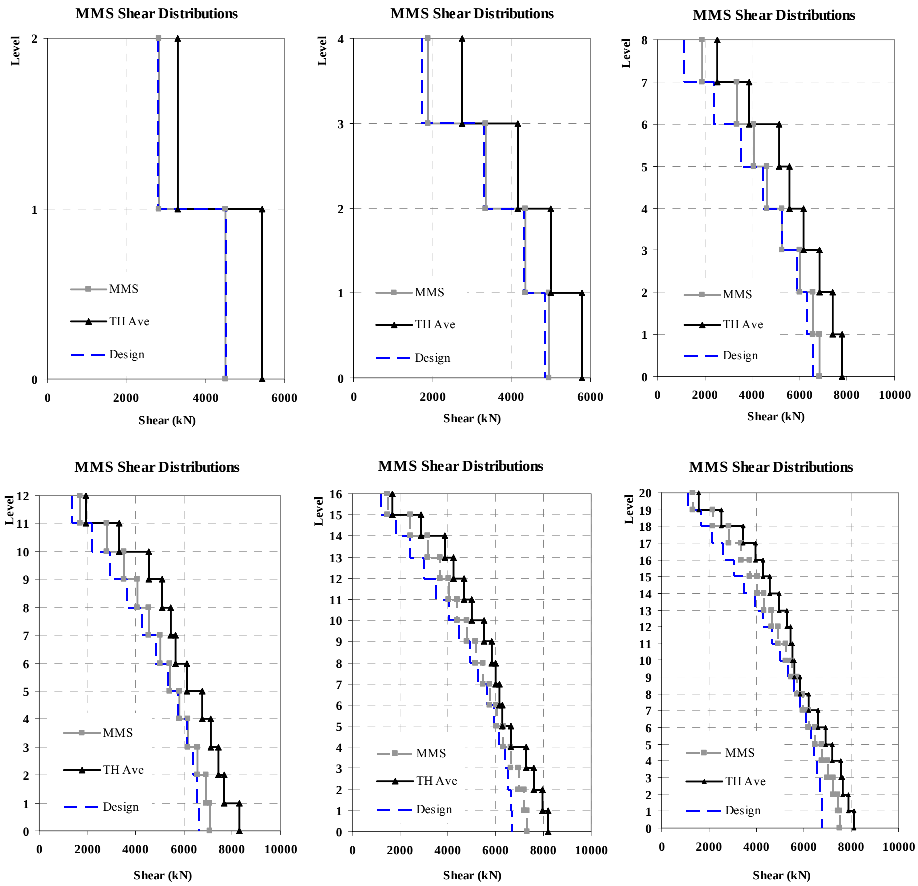

Figure 8-5. Application of Eq. (8.4) using the Substitute Structure design ductility; as compared to the direct displacement base design profile and time-history average maxima at the design intensity

As mentioned there is reduction in higher mode participation due to the eventual shift down the constant velocity slope as a result of inelastic behaviour. It is known that the effective period Te approximately scales in proportion to the elastic period T_1 as $\sqrt{\mu_\Delta} \cdot T_1$; therefore a third option would be to divide by the square root of the design ductility in Eq.(8.4). Trials using the same modal analysis results show that this maintains too much of the second mode influence and does not reproduce the time-history results accurately. This can be explained by the higher modes not increasing in period by the same scaling amount as the first mode (possibly they increase more due to the changes in displacements they induce), and the fact that the acceleration spectrum is non linear beyond 0.5 seconds, hence the first mode shift falls on a flatter part of the spectrum, while the higher modes are on a steeper descending portion of the constant velocity curve.

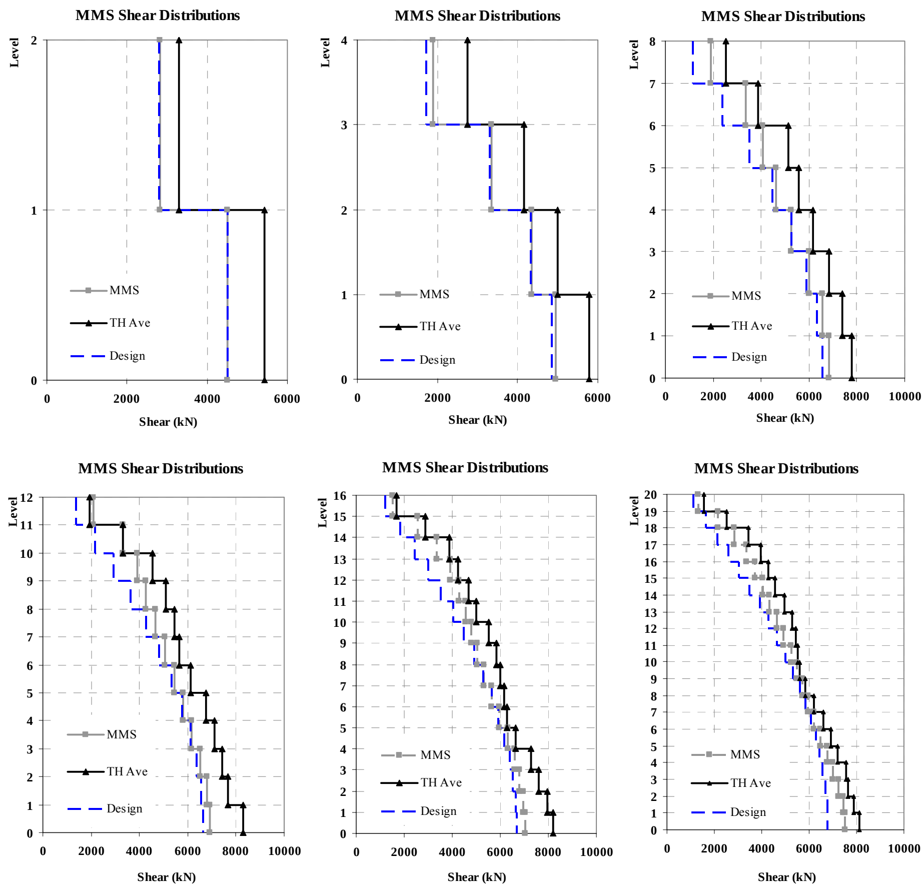

Figure 8-6. Application of Eq. (8.4) using the individual design storey ductility at each level; and compared to DDBD storey shear profiles and time-history maxima

It is proposed here to maintain the suggested form of Eq.(8.4), but with the addition of a factor ω_v that scales the DMMS profiles to account for the underestimation seen, giving the following form in Eq.(8.5). The value of the suggested factor was determined by trial and error based on the results in Figure 8-5 and 8.6. For simplicity, the substitute structure design ductility μ_D was adopted in Eq.(8.5) on the basis that this is known at the start of the design process:

$$V_i = \omega_v \left(V_{1i}^2 + \left(\frac{V_{2Ei}}{\mu_D} \right)^2 + \left(\frac{V_{3Ei}}{\mu_D} \right)^2 + \ldots \right)^{1/2} \tag{8.5}$$

Considering the form of Eq.(8.4) there is inherently a problem noted by Priestley (2003) regarding the application of the modal superposition method to varying levels of intensity. For example if the intensity is doubled, the design ductility (or reduction factor) is also assumed to double, therefore the resulting combination of design actions is independent of intensity. This clearly opposes the time-history results presented in Section 7.2.1. Hence to allow the proposed form of Eq.(8.5), the factor ω_v should be intensity dependent to scale the DMMS results appropriately. A simple investigation of the three intensity levels considered, showed the required factor was well approximated by the following:

$$\omega_v = \sqrt{\frac{\mu_\Delta}{2}} \geq 1.0 \tag{8.6}$$

For design ductilities around 2.7 (as found for all the frames investigated) this factor is approximately 1.16, while at twice the intensity it becomes 1.64. The value of 1.16 gives a noted agreement with the overturning moment amplification mentioned earlier.

While the form of Eqs.(8.4) and (8.5) is very similar to the elastic modal superposition using a design ductility (as shown in Figure 8-1) the importance of using the DDBD first mode shear forces must be noted. As seen in Figure 8-1 the elastic modal superposition significantly underestimates the shear demands in the lower half of the taller buildings, while generally giving a much better approximation in the shorter structures.

Two considerations explain the behaviour seen in Figure 8-1 and the importance of using the inelastic first mode design shear forces in Eq.(8.5). The inelastic design displacement profile is significantly different from the elastic profile found with a modal analysis, and when combined with the redistribution of base shear proposed in Section 6.3, the distribution of shear force differs from the elastic modal superposition.

The second factor considers (Figure 8-4) in which the inelastic periods of the important (to include up to 90% mass participation) modes are shown to shift along the constant velocity portion of the design acceleration spectrum. Looking at the second mode period shift, it is seen that the change in the spectral acceleration value of the second mode is significantly greater than that for the first mode. A constant division using the design ductility (i.e. the SRSS/μ) does not account for the decreasing slope of the spectrum, and leads to the first mode contribution being excessively diminished.

With these considerations the gradual reduction in accuracy of the SRSS/μ curve as the fundamental period increases (seen in Figure 8-1) can be explained, and the importance of using the DDBD shear force profile justified.

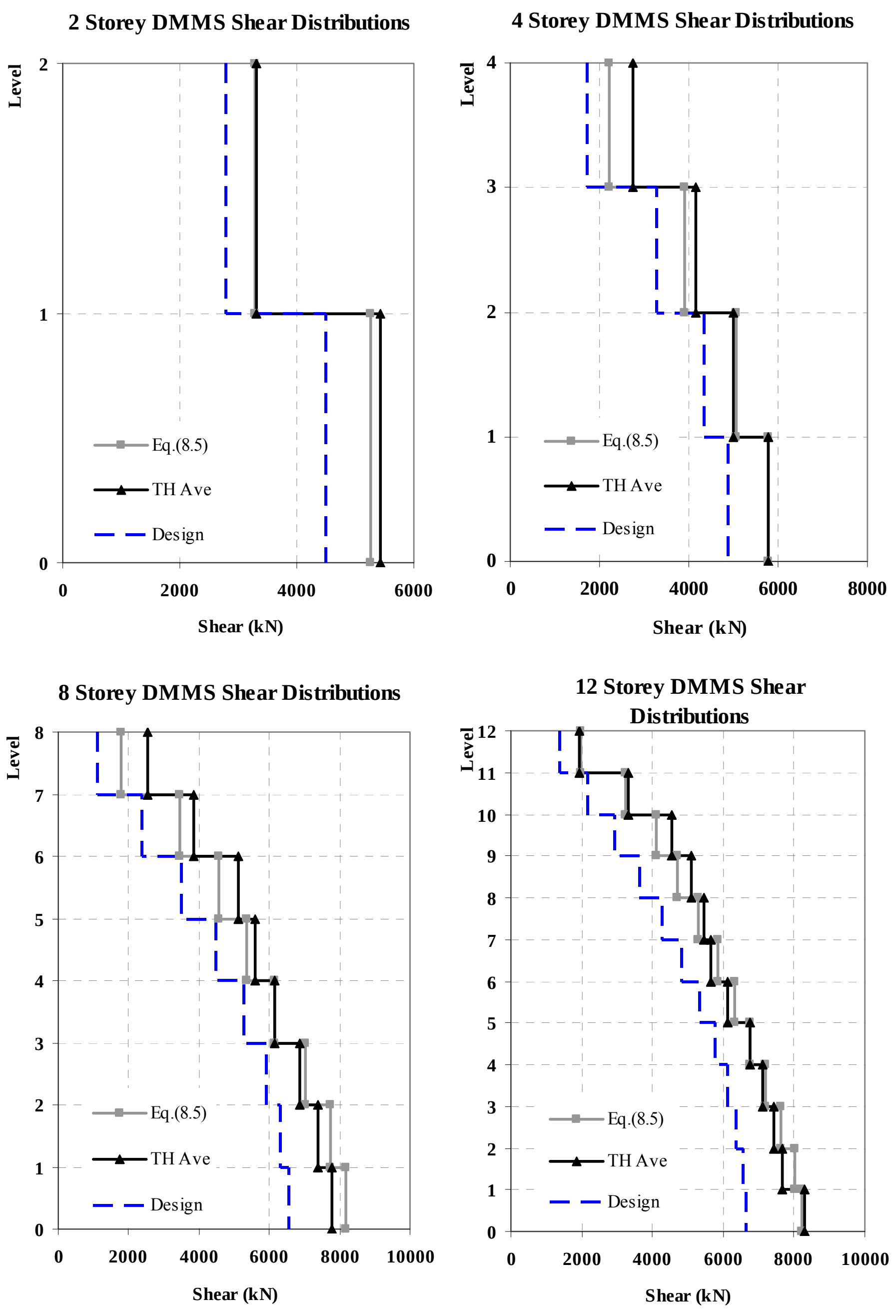

Figure 8-7. Application of Eq. (8.5) to account for dynamic amplification of storey shear forces

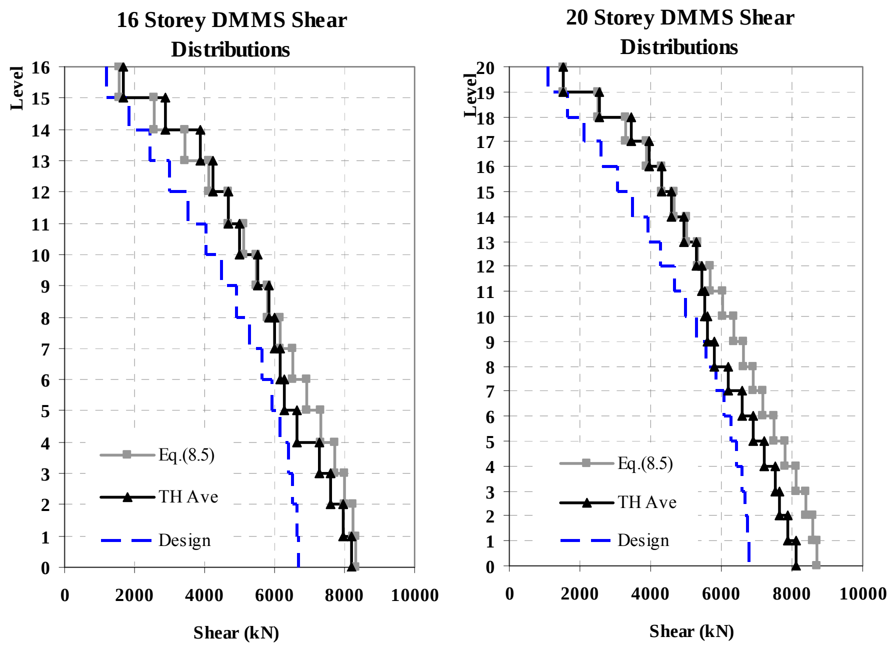

Figure 8.7. Application of Eq. (8.5) to account for dynamic amplification of storey shear forces (cont.)

The results show that the method predicts the column shear force amplification at all levels with reasonable accuracy. As the buildings tend more towards elastic behaviour (i.e. the taller frames) the participation of the second mode is notably more significant in the time-history shear profile shape. There is increased overestimation in the shears at lower levels using Eq.(8.5), but it is generally conservative and of an acceptable level.

Figure 8-8 compares the proposed method with time-history results at one half and twice the design earthquake intensity. This implies that while the higher modes used in the superposition have increased excitation due to the direct scaling of the elastic spectral accelerations, the design ductility used in Eq.(8.5) is also increased by a factor of two. It can be seen that the proposed method gives similar results (to Figure 8-7) at half the intensity, while generally being conservative at twice the level of excitation. Clearly the scaling factor in Eq.(8.6) produces the desired effect, allowing the dependency and variation on earthquake intensity to be adequately reproduced.

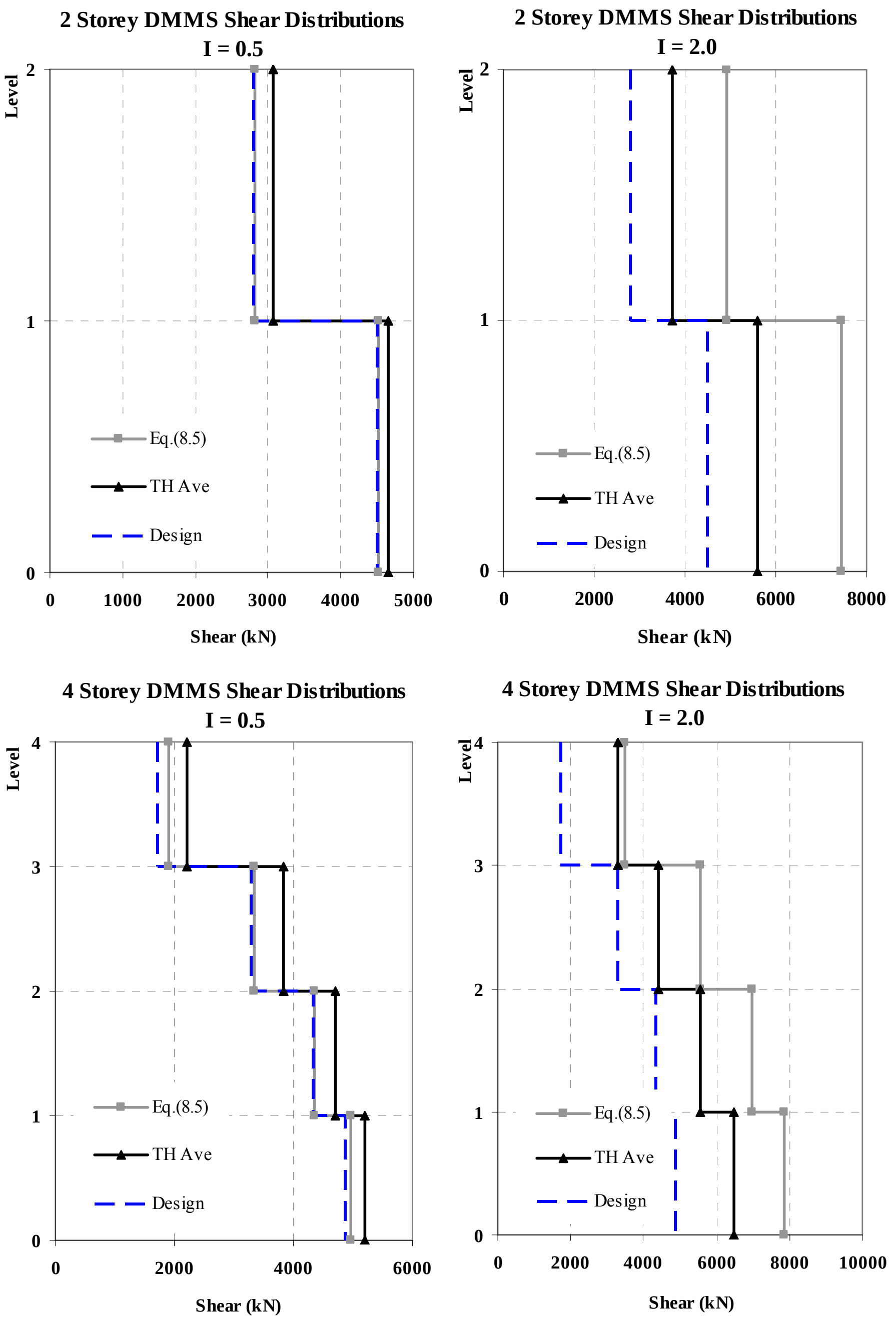

Figure 8-8. Application of Eq. (8.5) to account for dynamic amplification of storey shear forces at 0.5x and 2x the design intensity, implying the same variation in ductility development

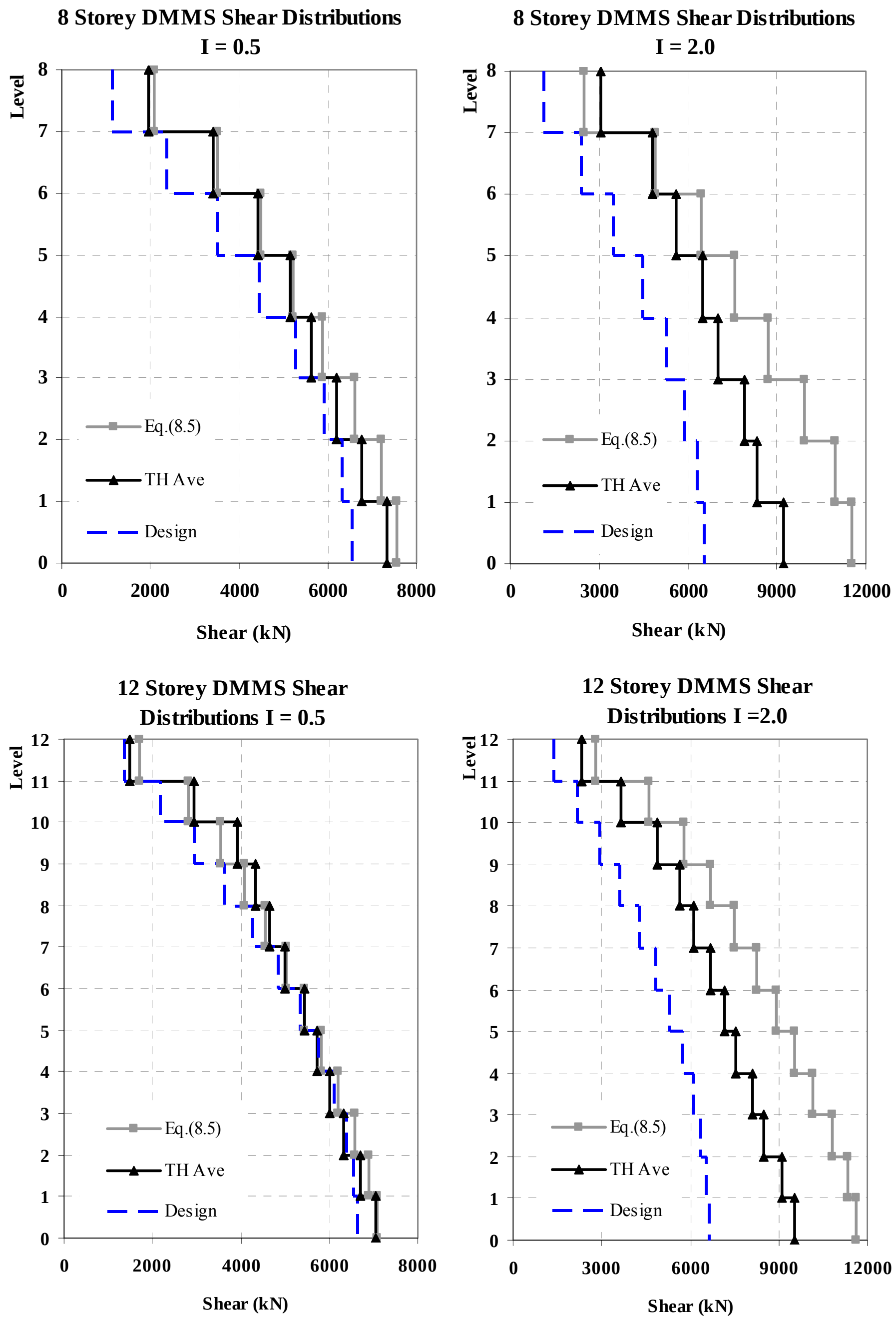

Figure 8.8. Application of Eq. (8.5) to account for dynamic amplification of storey shear forces at 0.5x and 2x the design intensity, implying the same variation in ductility development (cont.)

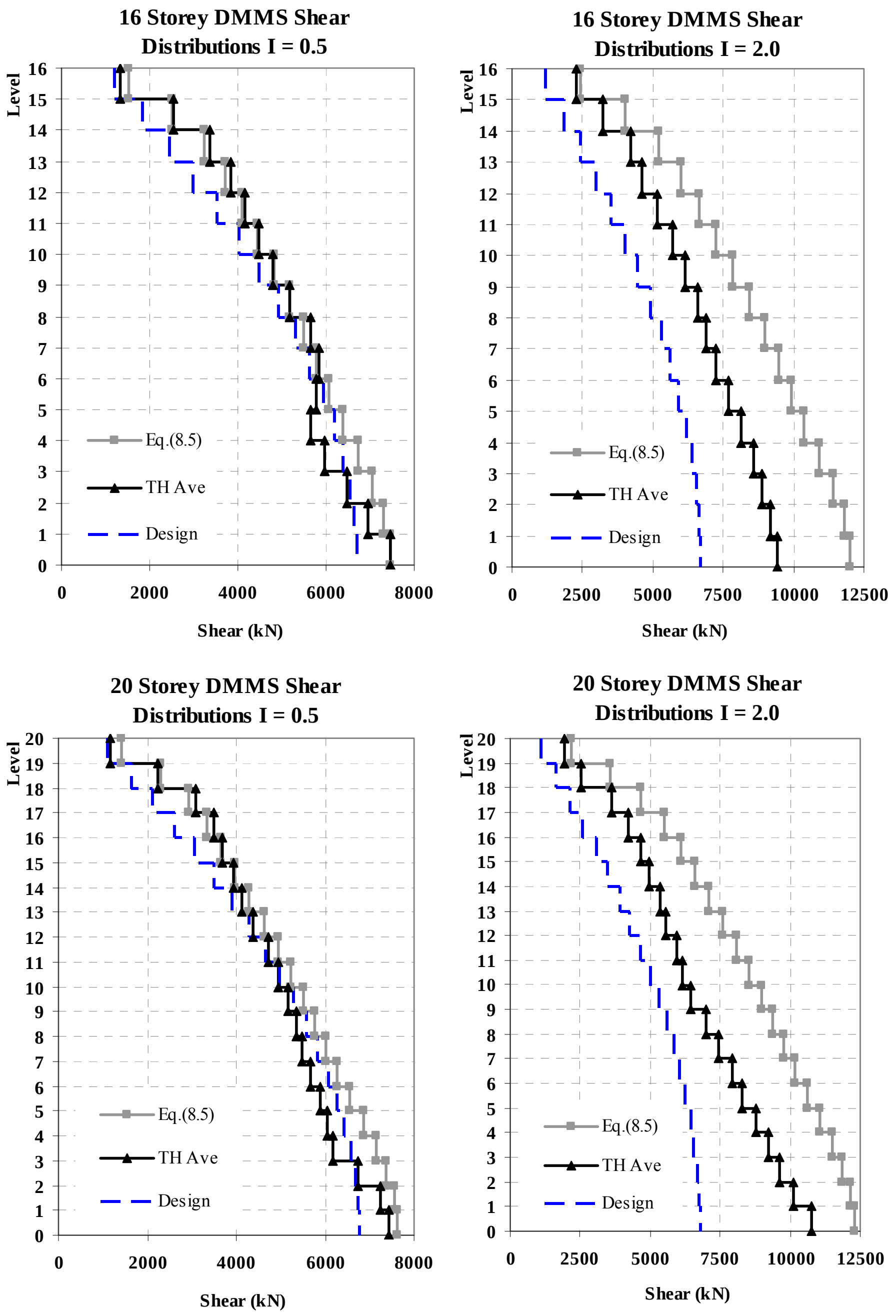

Figure 8.8. Application of Eq. (8.5) to account for dynamic amplification of storey shear forces at 0.5x and 2x the design intensity, implying the same variation in ductility development (cont.)

8.2.2 Column bending moment amplification

As shown in Section 8.1, existing methods of column moment dynamic amplification are in general inconsistent and do not adequately represent higher mode effects as obtained from time-history analyses. Clearly the development of a moment amplification method for displacement-based design is required.

It is conceptually possible to investigate the application of a similar modification of the MMS method as presented for column shear forces. However the time-history results (Figure 7-3 to 7.8) show that the amplification is nearly constant over the height of the buildings and therefore a scaling factor equation that changes with respect to intensity and building height (to account for the peak amplification at the first floor) would be appropriate and somewhat easier to apply.

In seeking to develop such an equation it is worth noting that the moment demands do not scale directly with intensity, since the average amplification as seen in Figure 7-9 is between 1.2x - 1.5x the design value. This approximately corresponds to the square root of the design ductility, giving the basis to develop the scaling equation.

It is evident from Figure 7-9 that column moments at the first floor in nearly all cases exhibit the largest dynamic amplification, which would not be accounted for if using a constant factor based on the overall building amplification average. Therefore some account of this particular spike could be made based on normalized height, giving the equation the form:

$$\omega_m = \sqrt{\mu_\Delta} + f\left(H_i / H_n \right) \tag{8.6}$$

Trials show that the square root of the ductility gives a good estimate of the first floor amplification but to apply this as a constant value over the height of the building would lead to excessive conservatism in the middle to upper levels. Height dependence is therefore introduced to reduce the value of ω_m up the height of the building. The normalized height ratio can be multiplied by a factor x, which could be determined from the time-history amplification results. By trial and error the best fit to the time-history results was found to be $x = -0.15$, giving the following amplification equation for all levels i except the roof and ground for which ω_m = 1. The minimum factor of 1.3 is particularly necessary for buildings not expected to develop significant ductility.

$$\omega_m = \sqrt{\mu_\Delta} - 0.15\left(H_i / H_n \right) \geq 1.3 \tag{8.7}$$

Where μ_Δ is taken to be the design ductility for the substitute structure as used in Eq.(8.5), again for simplicity and consistency in the methods suggested. The resulting amplification curves at the design intensity for each frame are shown in Figure 8-9.

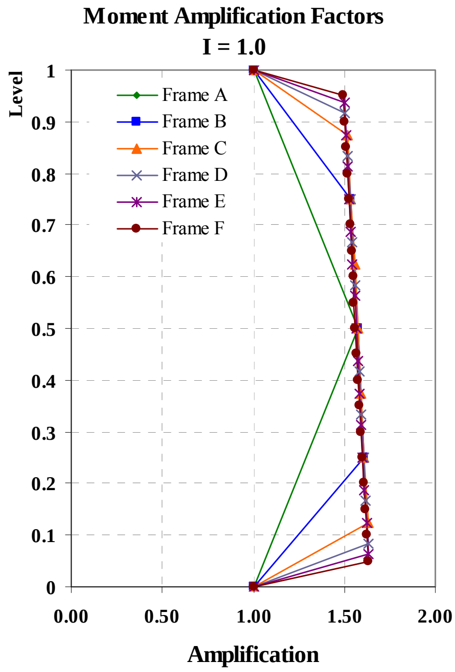

Figure 8-9. Column moment amplification curves using Eq. (8.7) normalised with respect to height

The proposed method was applied to the design moment profile (sum of storey moments at each column end) assuming the beam moments are distributed equally to the columns above and below the beam level (as mentioned in Section 7.2.1). Figure 8-10 shows that the equation gives a good representation of the dynamic amplification of column moments. It is seen that in the upper levels some of the time-history moment maxima exceed the amplified design profile. While this is undesirable in the context of the capacity design philosophy, it should be remembered that these plots are for the sum of the column storey moments and that the sum being greater than the design value does not necessarily indicate a soft storey mechanism has developed.

It is suggested that allowing minor inelastic column flexural action, at places other than at column bases may not be a significant problem, provided hinges do not form simultaneously at the both ends of all columns in a storey level. The effects of such behaviour are not well known, suggesting a further line of study, to verify the acceptability of this influence.

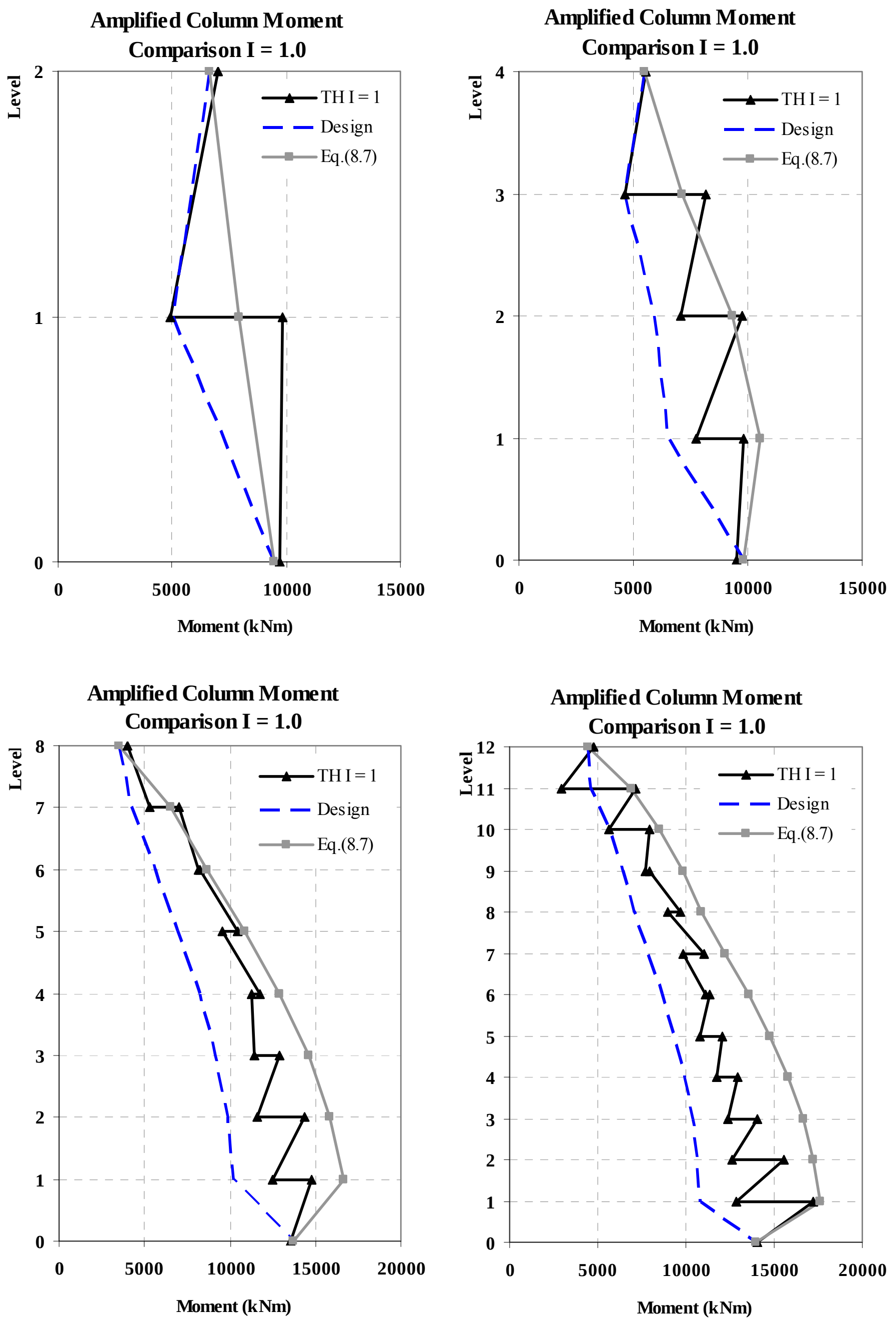

Figure 8-10. Application of Eq. (8.7) for column bending moment amplification at the design intensity

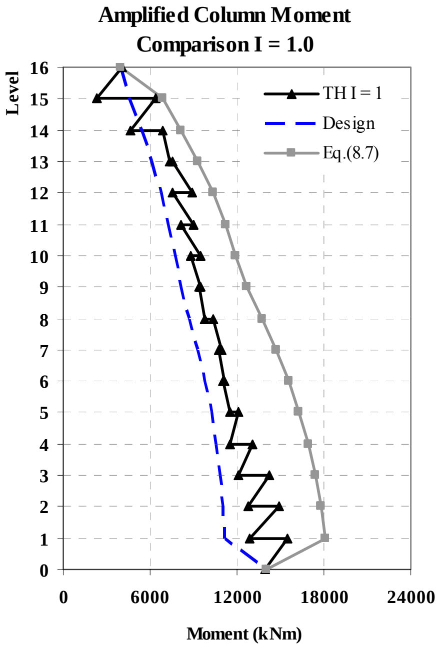

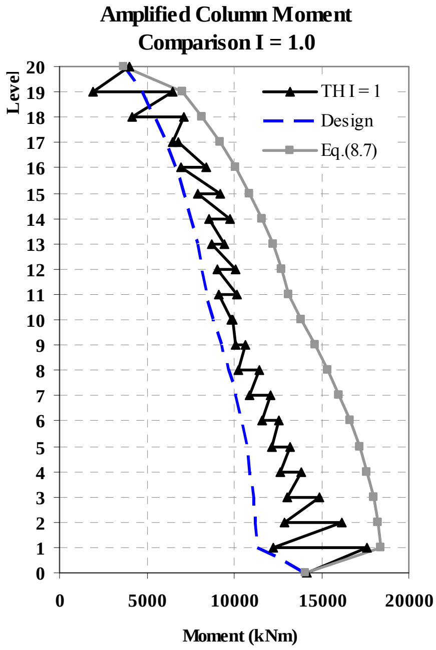

Figure 8.10. Application of Eq. (8.7) for column bending moment amplification at the design intensity (cont.)

As noted earlier, the column moments developed are dependent to some extent on intensity. To further investigate the application of Eq.(8.7) at one half and twice the design intensity (equivalent to one half and twice the design ductility), predictions are compared with the corresponding time-history results in Figure 8-11.

In both Figure 8-10 and 8.11 the proposed amplification equation gives a good envelope of the maximum moments developed from the time-history analyses. At the design intensity the match is particularly consistent with the first floor maximum and not excessively conservative over the height of the buildings. Similarly the minimum factor of 1.3 as required at half the intensity gives a very good approximation in all cases, while for twice the intensity the amplified envelope is somewhat more conservative but again satisfies the first floor maxima. The principal underestimation at the higher intensity, is the ground level moment sum that exceeds the design value in all cases. Again this can be attributed to the greater axial load variations that lead to increased moment capacity variations in the columns. This exceedance is more significant for the taller buildings, which is consistent with this idea of axial demand leading to increased moment capacity. To account for this, it is possible to specify that the ground level column moments should be scaled by a fixed factor, possibly extending the minimum of 1.3 to the ground level, however given that inelastic action is expected (and accepted) at the ground level, the only reason to include such a factor is to provide additional stiffness to the columns, that would act to control the bottom storey drifts.

8.3 VERIFICATION WITH REAL EARTHQUAKE ACCELEROGRAMS

As described in Section 7.2.2.3 the six frames were tested using the suite of real records described in Appendix A. The proposed shear and moment amplification methods were also applied to the average inelastic time-history results, to ensure that they were applicable to a range of different earthquake motions.

The results are shown in Appendix A at the design intensity. The DMMS consistently approximates the column shear force amplification over the height of the buildings, with the same level of accuracy as seen in Section 8.2.1, and is therefore an effective means of allowing for the dynamic shear force behaviour under a wide range of broad-band motion.

Application of Eq.(8.7), in general gives similar results to those in Section 8.2.2, however it is noted that the 20 storey frame exhibits a significant exceedance at the top of the bottom storey columns. Investigation of the individual earthquake results shows this to be heavily influenced by one record (TCU047), and therefore it could be discounted (along with the minimum record). However this is an important result to note, as this suggests that the column moment demands in the bottom storeys could be significantly higher under near-field pulse type motions. This would therefore require further investigation to ensure that design methods were adequate to allow for such extreme demands.

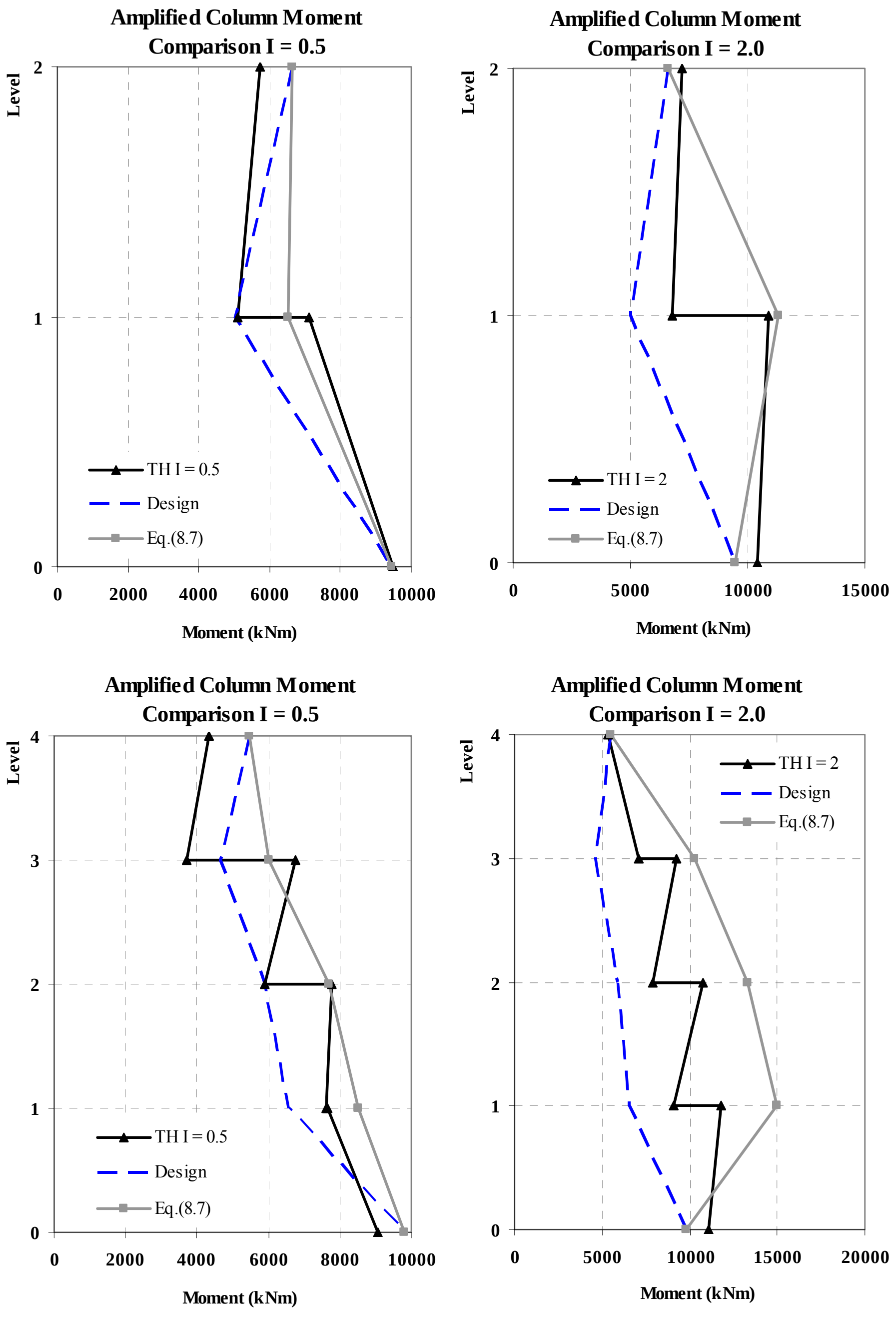

Figure 8-11. Application of Eq. (8.7) at 0.5x and 2.0x the design earthquake intensity.

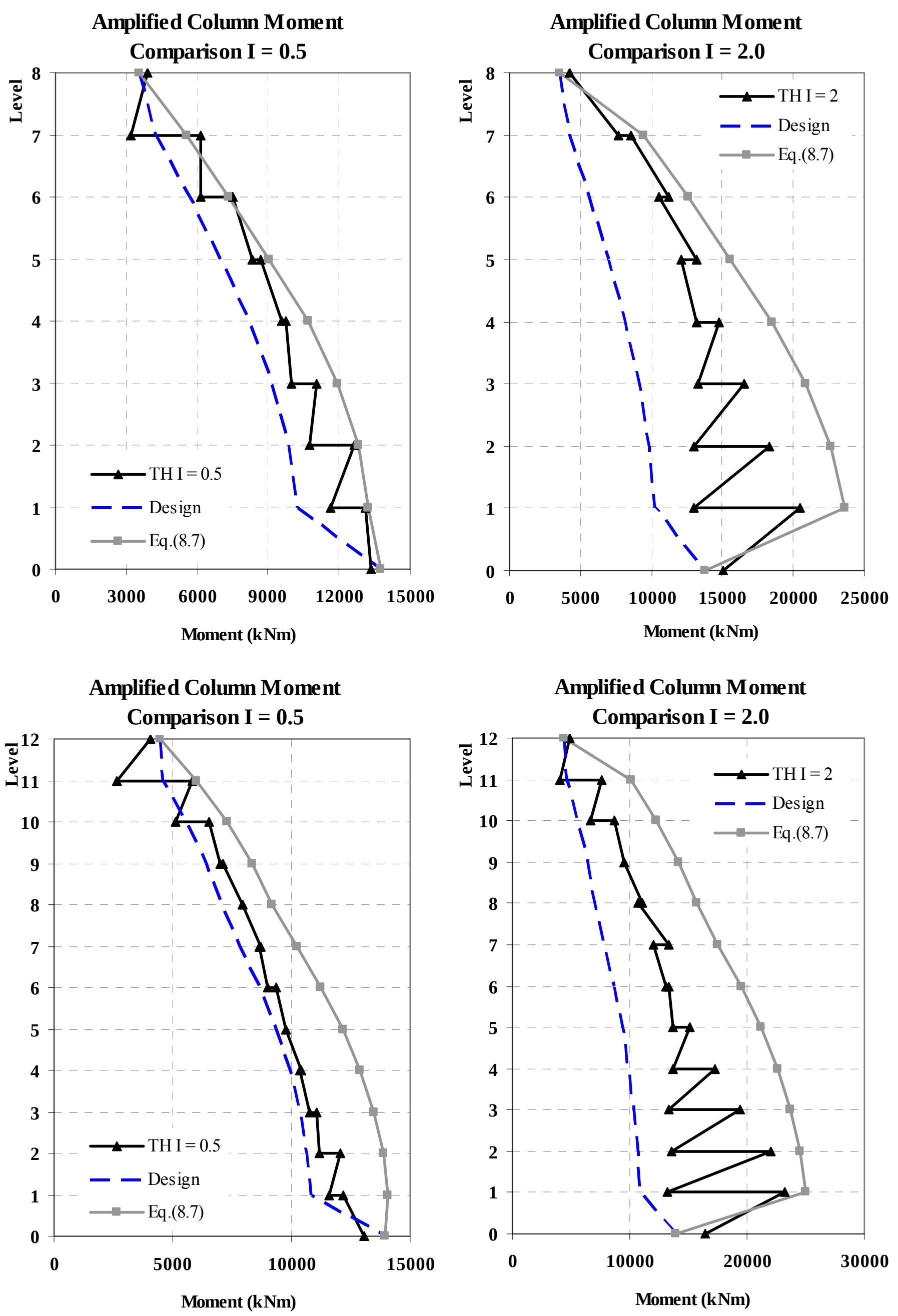

Figure 8.11. Application of Eq. (8.7) at 0.5x and 2.0x the design earthquake intensity (cont.).

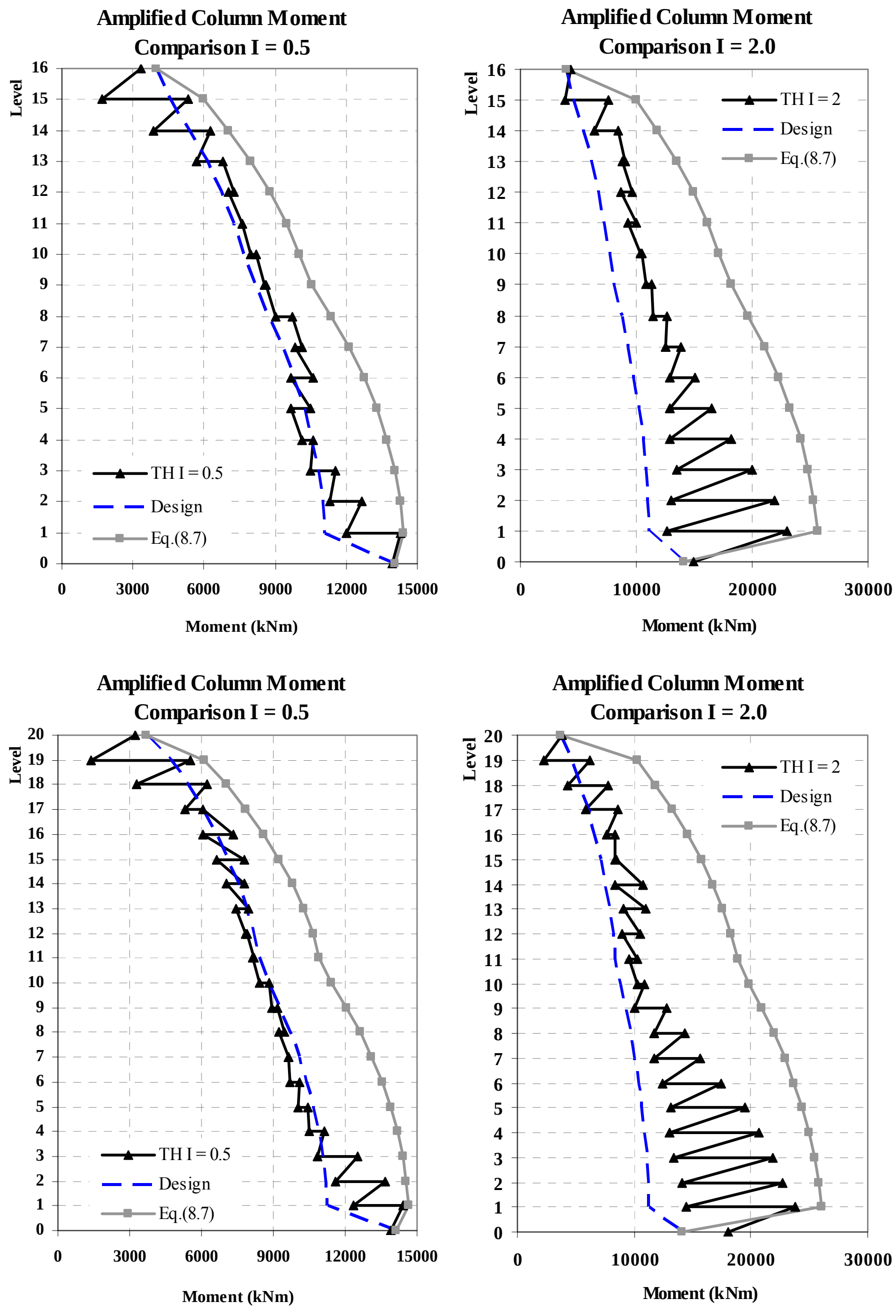

Figure 8.11. Application of Eq. (8.7) at 0.5x and 2.0x the design earthquake intensity (cont.).

8.4 MODIFICATION FOR TWO-WAY FRAMES

In applying the above methods of dynamic amplification, consideration must be given to column behaviour when subjected to simultaneous earthquake forces in the two principal directions. The potential for development of beam plastic hinges from sources in orthogonal directions (as is the case for beams framing into corner or internal columns) should be assessed, however the probability of concurrent magnification from such effects reduces as the number of sources increases (Paulay and Priestley, 1992).

Applying the approach of Paulay and Priestley (1992) to column shear forces, and assuming that beams framing into a column from two directions have the same strength, the resultant shear force could be $\sqrt{2}$ times the unidirectional shear force. For bi-directional shear forces the DMMS procedure can be modified to include this factor, such that Eq.(8.5) becomes:

$$V_i = \omega_v \left(V_{1i}^2 + \left(\frac{V_{2Ei}}{\mu_D} \right)^2 + \left(\frac{V_{3Ei}}{\mu_D} \right)^2 + \ldots \right)^{1/2} \text{ with } \omega_v = \sqrt{\mu_\Delta} \tag{8.5b}$$

Similarly Paulay and Priestley (1992) suggest that a column section with moment applied about the section diagonal, is approximately 90% efficient (with respect to bending about a principal axis) in resisting the moment. Using the assumption of equal moments in both orthogonal directions, the intensity dependent part of Eq.(8.7) can be scaled by a factor equal to $\sqrt{2}/0.9 \approx 1.5$, which can also be taken as the minimum amplification amount to give:

$$\omega_m = \sqrt{1.5\mu_\Delta} - 0.15\left(H_i / H_n \right) \geq 1.5 \tag{8.7b}$$

Following Paulay and Priestley (1992) it is also suggested that the value of ω_m be made equal to 1.1 (instead of 1.0) at the column base and roof level.

The frame can then be assessed as an effective one-way frame using Eqs.(8.5b) and (8.7b) applied in each principal direction to estimate the moment demand.

8.5 SUMMARY OF PROPOSED METHODS OF ACCOUNTING FOR DYNAMIC AMPLIFICATION

As shown in Section 8.1, existing methods of accounting for dynamic amplification of column bending moments and shears do not provide acceptable results with regards to reinforced concrete frame design. Therefore the following methods developed in Section

8.2 are proposed for use with reinforced concrete frames designed using direct displacement-based methods.

For column shear force amplification, the following adaptation of the Modified Modal Superposition, as originally proposed by Priestley and Amaris (2002) for structural walls has been found to give acceptable results for one-way frames when an intensity dependent factor ω_v is applied. For two-way frames a similar form is suggested based on a simplified mechanics approach.

$$V_i = \omega_v \left(V_{1i}^2 + \left(\frac{V_{2Ei}}{\mu_D} \right)^2 + \left(\frac{V_{3Ei}}{\mu_D} \right)^2 + \ldots \right)^{1/2}$$

$$\text{with} \quad \omega_v = \sqrt{\frac{\mu_\Delta}{2}} \quad \text{for one-way frames} \qquad (8.5a\ \&\ b)$$

$$\text{and} \quad \omega_v = \sqrt{\mu_\Delta} \quad \text{for two-way frames}$$

For column bending moment amplification the following intensity dependent equation provides reasonably consistent results that account for dynamic amplification, principally due to the axial load variation in the column under dynamic loading. Eqs.(8.7a & b) are applied at all levels *i*, excluding the column bases and roof level, where the value of ω_m is taken as 1.0 for one-way frames and 1.1 for two-way frames.

$$\omega_m = \sqrt{\mu_\Delta} - 0.15\left(H_i / H_n \right) \geq 1.3 \qquad (8.7a)$$

$$\omega_m = \sqrt{1.5\mu_\Delta} - 0.15\left(H_i / H_n \right) \geq 1.5 \qquad (8.7b)$$

In both cases the ductility factor is the design ductility of either the equivalent substitute structure, or the weighted average of individual storey design ductilities, both of which are approximately equal.

9. PARAMETRIC INVESTIGATION AND FURTHER DISCUSSION

To assess the extent of application for the methods developed in the preceding sections, a brief parametric study was carried out using three new frame designs. These included variations in the beam depths over the height of both a 16 and 20 storey building, and a 12 storey building with beam spans 30% greater than those used for the previous designs.

9.1 VARIATION OF BEAM DEPTH

The two designs utilised a sensible reduction in beam depth based on design beam moment demands. The level at which the depths could be changed was still governed by maximum steel limits as mentioned in earlier sections, with the result that the following geometric variations were used for the two frames.

Table 9-1. Design geometries for 16 and 20 storey frames using changing beam depths

16 Storey					**20 Storey**				
Level i	**Column (square)**		**Beams**		**Level** i	**Column (square)**		**Beams**	
	1/2	**3/4**	$\mathbf{b_w}$	$\mathbf{h_b}$		**1/2**	**3/4**	$\mathbf{b_w}$	$\mathbf{h_b}$
					16 – 20	850	850	400	900
11 – 16	800	800	400	900	**9 – 15**	850	850	400	1000
1 – 10	800	800	400	1100	**1 – 8**	850	850	400	1100

From Eq.(3.6) it is seen that decreasing the beam depth leads to larger yield drifts at individual floor levels. It is necessary to calculate these individual yield drifts at each level in order to evaluate the change in design ductility, and therefore equivalent viscous damping due to these geometric effects (and the parabolic design displacement profile). Having calculated the storey values an appropriate weighted average of the equivalent viscous damping is found using Eq.(3.15), or (using a similar weighted average approach) by finding the average beam depth as weighted with respect to the design storey drift at each level to reflect the beam level participation in the inelastic first mode shape and global damping (as damping is a function of ductility developed which is directly related to beam rotations or storey drift). This weighted average therefore has the form shown by Eq.(9.1) and can be used to evaluate the equivalent viscous damping of the substitute structure.

$$h_{b,eff} = \frac{\sum_{i=1}^{n} h_{b,i}^{2}\theta_{D,i}}{\sum_{i=1}^{n} h_{b,i}\theta_{D,i}} \tag{9.1}$$

With this addition to the design method the following parameters for direct displacement-based design were determined (Table 9-2).

Table 9-2. DDBD parameters for 16 and 20 storey frames with variable beam depths.

Frame n	θ_d	$\theta_{d,\omega}$	Δ_d (m)	M_e (t)	H_e (m)	ξ_{eff} (%)	μ_Δ	T_e (sec)	K_e (kN/m)	V_b (kN)
16	2 %	1.7 %	0.520	4384	37.1	19.39	2.57	3.63	13117	6822
20	2 %	1.7 %	0.646	5500	46.2	19.17	2.53	4.49	10762	6953

Principally, the reduced average beam depth has resulted in a slight decrease in system ductility (the values from Table 7-2 were 2.69 and 2.68 for the 16 and 20 storey frames respectively), therefore the design base shear has increased slightly

9.1.1 Time-history results and application of amplification methods

The time-history results for these two frames show very similar behaviour to that seen in Figure 7-7 and 7.8, although there is an average drift exceedance at the base (2.2% and 2.4% vs. design 2% limit), and around the ¾ height (2.15% and 2.1% vs. design 2% limit) of both frames. These drift results are however significantly influenced by single records that give large drifts, thus they are within the expected scatter. In each case removal of the two records giving the maximum and minimum results from the respective averages, gives envelopes that do not exceed 2% drift in the upper levels, but still exceed the drift limit at the bottom storey. The maximum displacement profiles in both cases match the inelastic first mode design profile very closely.

The column shear and bending moment profiles are consistent with the expected behaviour from the previous designs and the dynamic amplification equations from Section 8.5 give generally good results when compared with the time-history maxima. As in Section 8.2.1 the DMMS approach closely reflects the upper storey shear force maximums at each level with increasing conservatism down the building in both cases. The suggested equation for column moment amplification is reasonable in both cases, but for the 20 storey building the moment maximum at the top of the ground floor column is slightly underestimated (a result that is reflected by the larger drifts at the bottom level).

These results show that the change in geometry has very little effect on the dynamic behaviour of the frames and that the dynamic amplification methods summarised in Section 8.5 remain applicable.

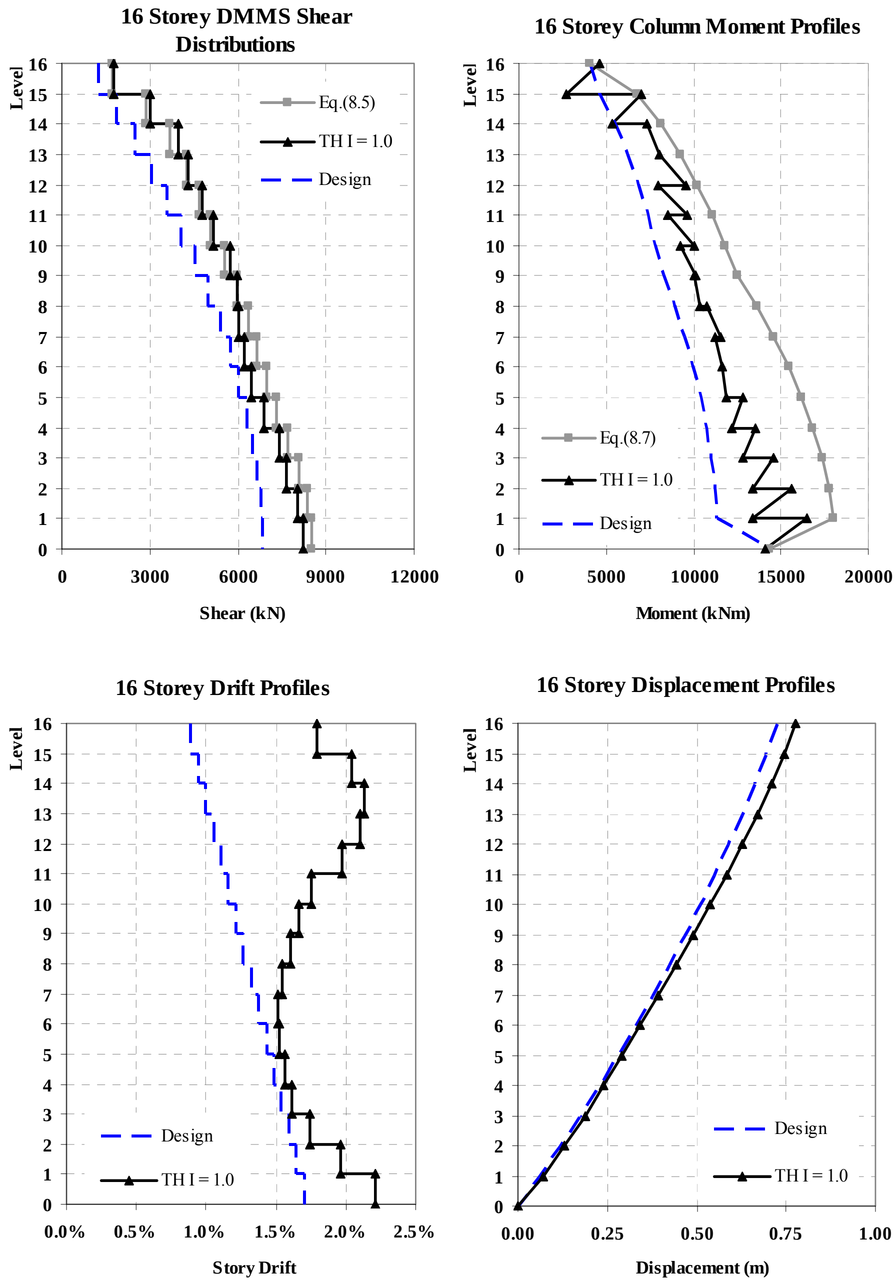

Figure 9-1. Average time-history results and application of dynamic amplification Eqs. (8.5) and (8.7) for a 16 storey frame with variable beam depths

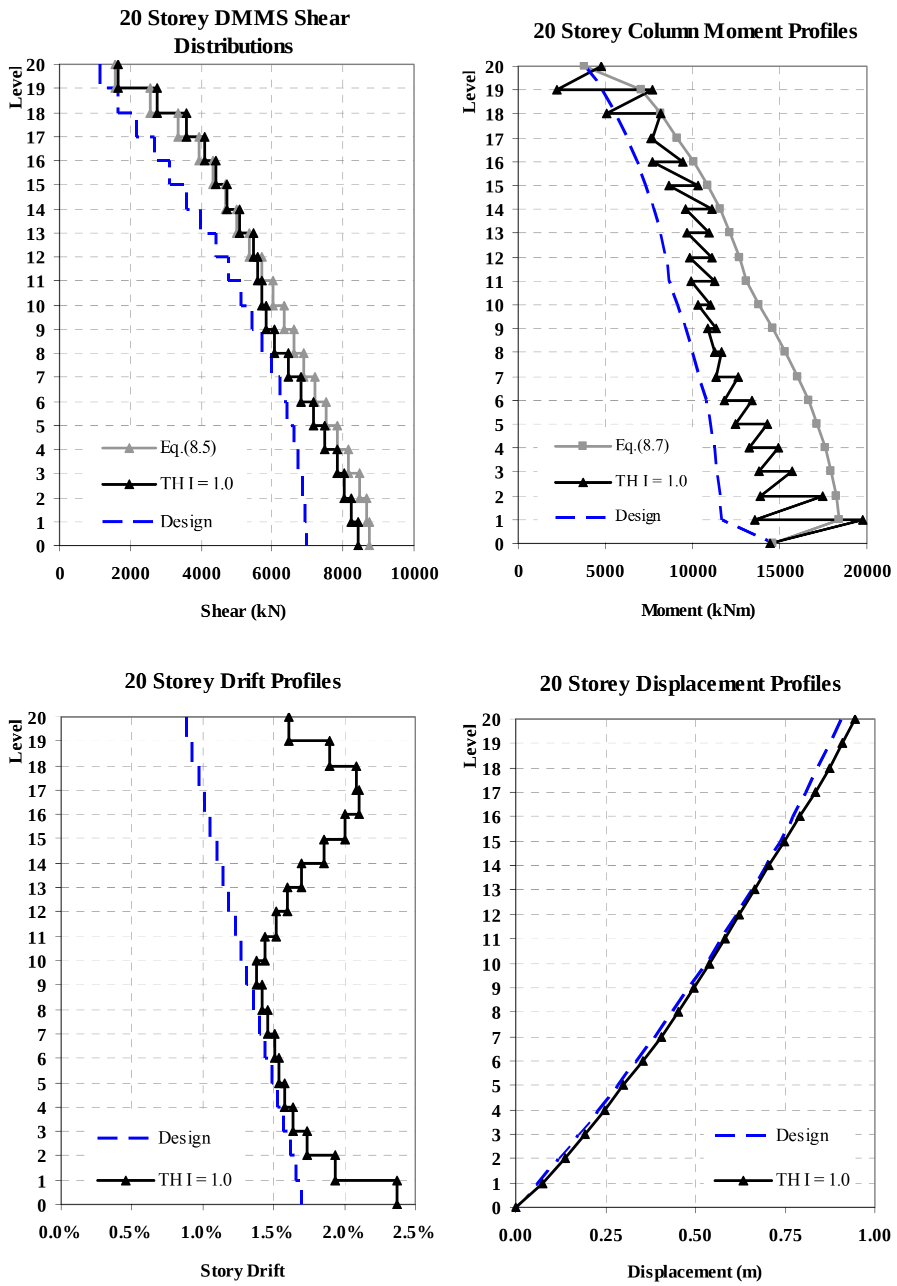

Figure 9-2. Time-history results and application of dynamic amplification Eqs. (8.5) and (8.7) for a 20 storey frame with variable beam depths

9.2 INCREASED BEAM SPANS

As described in Section 1.1 this study has looked primarily at the design procedures and dynamic behaviour of perimeter frame structures ('tube-frames') that exhibit greater ductility due to the deeper sections used in both the beam and column designs, and shorter beam spans. It has been seen that the proposed changes to the design method and the resulting dynamic amplification equations, work well for stiff frames, but it remains unclear whether the methods are applicable to more flexible frames that might have shallower beams, or beams of greater span. To briefly test the applicability, a single trial was made using the revised direct displacement-based design approach, in which the beams were increased in length by 30% to 6.5m.

Increasing the beam length increases the yield displacement [Eq.(3.6)] and so reduces the design ductility (and equivalent viscous damping). The result is a frame that can be expected to exhibit behaviour reflecting the reduced ductility, and accordingly the higher mode amplification may be more significant.

Importantly, that the increased base shear leads to greater beam design moments and thus to satisfy the maximum steel requirements in the lower level beams, the beam depth must be increased to maintain some amount of realism in the design application. In this case the beam depths were kept constant at 1150 mm over the building height to isolate the effects resulting from the increased beam length, while the required column depth and width was 850 x 850. While the beam depth has increased the span to depth ratio has still been increased by 27% and therefore the geometric proportions have changed. The DDBD parameters are given in Table 9-3.

Table 9-3. DDBD parameters for 12 storey frame with 6.5m long beams

Frame n	θ_d	$\theta_{d,\omega}$	Δ_d (m)	M_e (t)	H_e (m)	ξ_{eff} (%)	μ_Δ	T_e (sec)	K_e (kN/m)	V_b (kN)
12	2 %	1.7 %	0.395	3401	28.1	17.27	2.17	2.64	19335	7634

The time-history results presented in Figure 9-3 show very good behaviour with respect to the proposed column action amplification equations. The amplified design shear force profile is consistently conservative, while the column moment amplification closely reflects the lower level maxima, and slightly underestimates the upper level maximum values, possibly due to greater higher mode effects as suggested above. The maximum displacement profile closely follows the design displaced shape, and storey drift behaviour is well controlled and does not suggest any significant development of increased higher mode behaviour due to the structure being more elastic.

From the limited study carried out in this section it appears that the direct displacement-based design developments for tube frame structures would also be applicable to flexible frame buildings. To further verify this result it would be necessary to investigate in greater detail the behaviour of frames with lower seismic loading (multiple frame structures rather than tube-frames) and taller frames that exhibit design ductilities less than two.

9.3 DRIFT AMPLIFICATION DEPENDENCY ON INTENSITY

The time-history results presented in Chapter 7 showed the intensity-dependence of the frame dynamic behaviour. Particularly the lower storey displacement and drift behaviour that produced somewhat unexpected results, and that differed significantly from the consistent behaviour of the maximum centre of force displacement profiles.

The displacement profiles increase roughly in proportion to the intensity scaling for the design displacements. However the maximum drifts do not show such proportionality, particularly when the intensity is increased above the design level. Figure 7-3 to 7.8 show that the bottom storey drift in particular is very sensitive to the intensity level, particularly for the frames of eight or more storeys. At twice the earthquake intensity the drift behaviour for these four frames indicates apparent soft-storey behaviour with high bottom storey drifts and almost constant drifts over the upper levels. Given the method of modelling does not allow inelasticity at the top of the ground floor columns, this drift amplification is attributed to the concentration of inelastic rotations in the lower level beams.

Further to this it is clear that the frames of longer fundamental period are somewhat more susceptible to these effects and that the suggested constant value for the drift reduction factor of ω_θ = 0.85 may not be sufficiently conservative for these taller structures, and possibly excessively conservative when applied to the shorter frames.

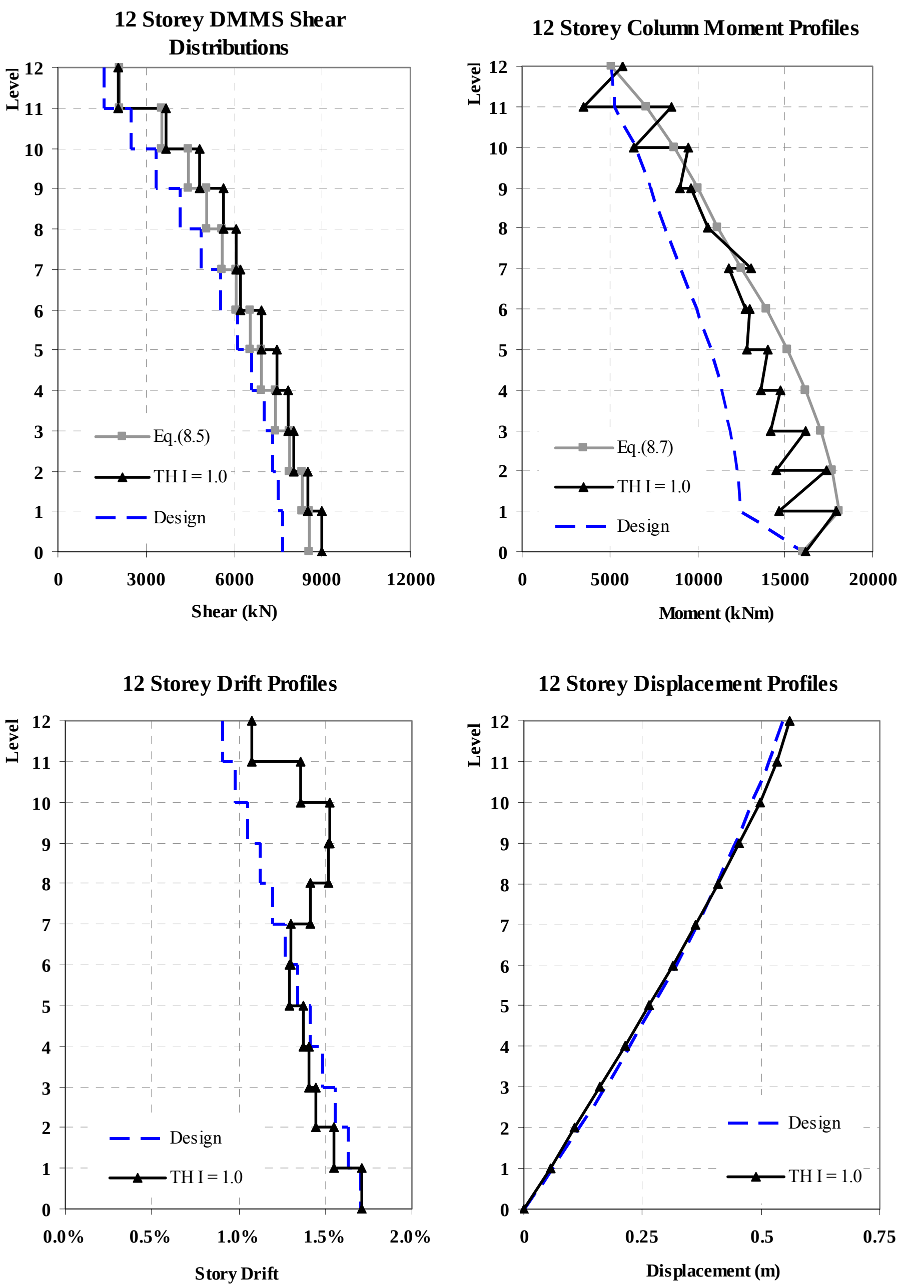

Figure 9-3. Time-history results and application of dynamic amplification Eqs. (8.5) and (8.7) for a 12 storey frame with 6.5m long beams

The conclusion that can be drawn from these observations is that the proposed drift reduction factor ω_θ may in fact need to be intensity dependent, and to some extent period or height dependent. This possibility has been investigated to a limited extent to develop a possible solution, for which it was found that such a method cannot be a function of period as the point of application for the factor is prior to the calculation of the structures fundamental period (be it elastic or effective period), unless an iterative approach is adopted. Therefore an equation based on total height (to approximately reflect period characteristics) and design drift (that scales directly with intensity) was derived by comparing the critical drift with the design limit 2% drift as shown in Figure 9-4. Assuming a linear trend of these ratios with respect to height and scaling the results to remove the included 15% reduction, Eq.(9.2) results, which produces the reduction factors in Figure 9-5 and design drifts in Figure 9-6.

$$\omega_\theta = 1 - 0.01\frac{H_T}{\theta_d}\cdot I \tag{9.2}$$

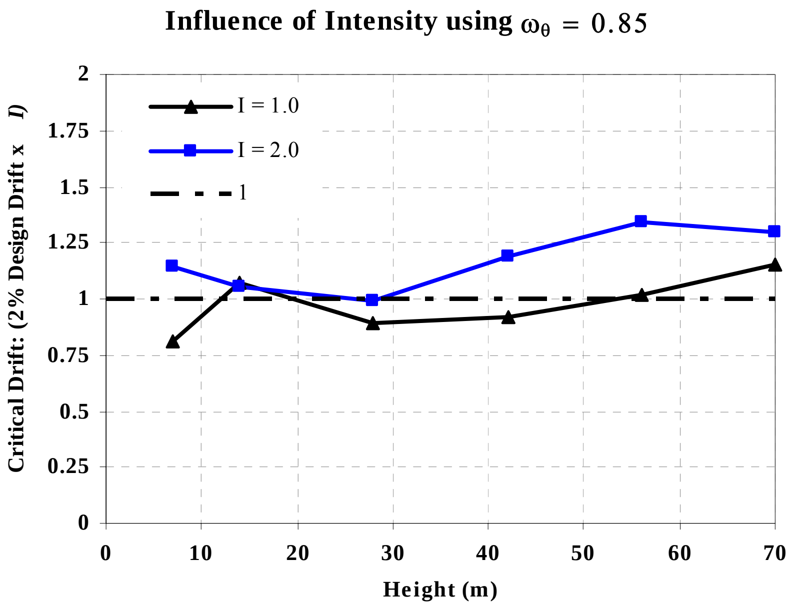

Figure 9-4. Ratio of Critical drift: (2% Design drift limit x *I*); from final results in Section 7.2.1

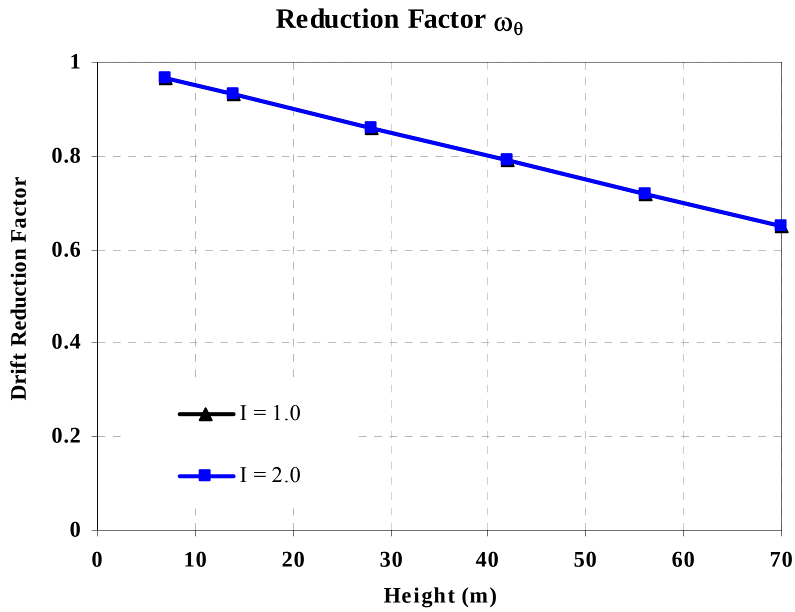

Figure 9-5. Variation of the Drift Reduction factor ω_θ using Eq. (9.2) at 1x and 2x the design intensity

A final solution to controlling the bottom storey drifts would be to provide guidelines for altering the distribution of lateral forces as suggested in Section 6.2.3. Provided equilibrium is maintained any distribution is valid, allowing designers to assign strength to critical regions as seen necessary with regards to design restrictions. Such an approach is somewhat more involved, and lies beyond the scope of this research project

9.4 SUMMARY OF PARAMETRIC STUDY

To briefly assess the applicability of the methods proposed in Chapters 6 and 8, a parametric study using two frames of 16 and 20 storeys, both with a realistic variation in beam depth over the height is carried out. Further to this a 12 storey frame is designed using longer beam spans of 6.5 meters to ensure a design ductility significantly lower than that found for each of the six frames designed in Chapter 7.

The inelastic time-history results show that the dynamic behaviour of these frames is not significantly different from that seen previously in Chapter 7, and that the proposed changes to the design method (as outlined in Section 6.3) and the application of the dynamic amplification equations for column shear forces and bending moments (Section 8.5) are valid for such frame designs.

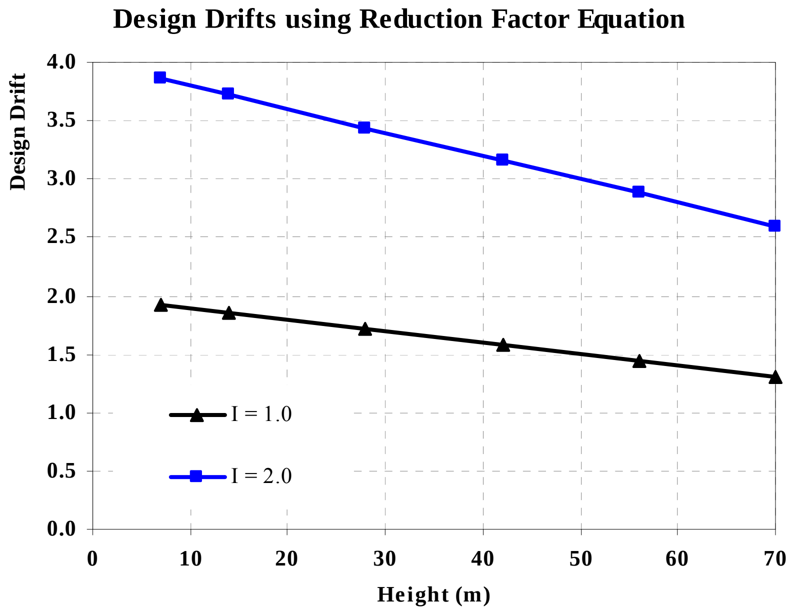

Figure 9-6. Critical design storey drifts from applying Eq. (9.2) at 1x and 2x the design intensity

From these results (and considering those presented in Section 7.2) it is suggested that the drift amplification factor ω_θ could be intensity and period (or height) dependent. Thus a simple equation utilizing these parameters is developed in the following form:

$$\omega_\theta = 1 - 0.01\frac{H_T}{\theta_d} \cdot I \qquad (9.2)$$

Where θ_d is the design drift limit (intensity dependent) and H_T is the total height of the frame.

.

10. CONCLUSIONS

The work presented in this dissertation has been used to evaluate the application and effectiveness of the direct displacement-based design method to reinforced concrete tube-frames. Using a set of six uniform structures of 2, 4, 8, 12, 16 and 20 storeys in height, the design method and the inelastic dynamic behaviour have been critically assessed, and where needed procedures have been revised or added to the DDBD process in order to develop a method capable of meeting the specified performance based requirements.

10.1 DDBD PROCESS: REVIEWS AND DEVELOPMENTS

The application of the DDBD method to reinforced concrete frames as demonstrated in this work, shows that the procedure when combined with a simplified method of analysis to determine member design actions provides a simple approach to seismic design. The use of 'hand methods' to determine the seismic design actions allowed a clearer insight to the dynamic response of the structures.

By applying the design procedures as developed in earlier work (Loeding et al., 1998; Priestley and Kowalsky, 2000), it has been found that the previously assumed first mode inelastic displacement profiles do not accurately represent the inelastic displacement behaviour of the tube frames that result from inelastic time-history analyses. Principally for buildings greater than 12 storeys in height the average time-history profiles were significantly more linear than the original design profiles. Thus a first development in this project has been a re-evaluation of the profile for structures greater than four storeys in height, so that the profile has a constant shape with respect to the normalised frame height [Eq.(6.1b)], while for buildings of four storeys or less the profiles are still assumed linear [Eq.(6.1a)].

for $n \leq 4$: $$\phi_i = \frac{H_i}{H_n} \qquad (6.1a)$$

for $n > 4$: $$\phi_i = \frac{4}{3} \cdot \left(\frac{H_i}{H_n} \right) \cdot \left(1 - \frac{1}{4} \frac{H_i}{H_n} \right) \qquad (6.1b)$$

The new design displacement profiles give better reflection of the time-history behaviour (when compared to the displacement profile at the time of maximum center of force displacement), however higher mode response is seen to significantly amplify the maximum storey drifts above the first mode shape. This was particularly extreme for the 16 and 20 storey frames, and for this reason the distribution of lateral forces (from the design base shear) has been revised to apportion a greater amount of strength to the upper levels [Eq.(6.2b)]. The resulting distribution is seen as similar to that proposed by Paulay and Priestley (1992) for use with simplifed equivalent lateral force based design, and the effect has been to introduce significantly more control of the upper level drifts, such that the assumed 2% drift limitation is no longer exceeded.

for n ≤ 10: $$F_i = V_B \frac{\Delta_i m_i}{\sum_{i=1}^{n} \Delta_i m_i} \tag{6.2a}$$

for n > 10: $$F_i = F_t + 0.9 V_B \frac{\Delta_i m_i}{\sum_{i=1}^{n} \Delta_i m_i} \tag{6.2b}$$

Finally, a measure of conservatism has been introduced to reduce the possibility of drift exceedance at all levels. The implementation of a drift amplification factor [Eq.(6.4)] used to reduce the design displacement at each level by 15% has been found to give consistent storey drift results, that in general do not exceed the code limitations.

for all n: $$\Delta_{i,\omega} = \omega_\theta \cdot \Delta_i \quad \text{with} \quad \omega = 0.85 \tag{6.4}$$

Further consideration was given to the form of the drift reduction factor required due to the observed tendency for drift limit exceedance in the 16 and 20 storey frames. The result was an intensity and height dependent equation that while not tested, would increase the conservatism in for taller frames and reduce the excessive conservatism in shorter frames.

for all n: $$\omega_\theta = 1 - 0.01 \frac{H_T}{\theta_d} \cdot I \tag{9.2}$$

With the three suggested changes the dynamic behaviour of column shear forces and bending moments has been investigated. Comparison with the design profiles shows that dynamic amplification is present, although not to the extent seen for similarly designed wall structures. Checks made using accepted methods of accounting for dynamic amplification showed that existing procedures used in force based design are not adequate and that the Modified Modal Superposition found to work well with structural walls (Priestley and Amaris, 2002), gave excessive over-estimation of the higher mode influence on these actions.

10.2 DDBD METHODS OF ACCOUNTING FOR DYNAMIC AMPLIFICATION IN FRAMES

Preliminary studies on frame behaviour using DDBD suggested that the MMS procedure did not work well for frames because the more significant higher modes tended to reduce in contribution, in a similar fashion to the first mode as inelasticity developed throughout the building. The time-history results reflected this with very little evidence of the second mode being seen in the moment and shear results, although it is clearly evident in the storey drift results. The shear and moment results can be explained by the beam plastic hinges limiting the dynamic input to the columns. Thus a logical development for use in shear strength design, already used in current force based design, was to include a reduction of the higher modes, through dividing by the design ductility. Therefore the ductile MMS (DMMS) combination maintained the same form with the design inelastic first mode being used, however the modes required above this to include a mass participation of 90% are divided by the DDBD ductility factor [Eq.(8.5)].

$$V_i = \omega_v \left(V_{1i}^2 + \left(\frac{V_{2Ei}}{\mu_D} \right)^2 + \left(\frac{V_{3Ei}}{\mu_D} \right)^2 + \ldots \right)^{1/2}$$

$$\text{with} \quad \omega_v = \sqrt{\frac{\mu_\Delta}{2}} \quad \text{for one-way frames} \qquad (8.5a \,\&\, b)$$

$$\text{and} \quad \omega_v = \sqrt{\mu_\Delta} \quad \text{for two-way frames}$$

The results were significantly improved, with upper level amplification accurately reproduced and lower level results increasing in conservatism to an acceptable amount as building height increased.

To account for the amplification of column bending moments an intensity dependent scale factor was developed that utilised the design ductility, while including a slight reduction over the building height to account for the reduced amplification in the upper levels [Eq.(8.7)]. Comparison of the design profiles with the time-history results showed that the maximum moment developed at the top of the ground floor columns was accurately accounted for, and over the height of most frames the results were also acceptable. In some instances the amplified design moments were exceeded, but the extent is not significant. Given that the method was compared to the moment sum at each column end, at each level, it is likely that these results would not imply a soft storey mechanism.

$$\omega_m = \sqrt{\mu_\Delta} - 0.15\left(H_i / H_n\right) \geq 1.3 \tag{8.7a}$$

$$\omega_m = \sqrt{1.5\mu_\Delta} - 0.15\left(H_i / H_n\right) \geq 1.5 \tag{8.7b}$$

Finally the methods developed were applied in a short parametric study to confirm that variations in beam depth and increased beam spans do not significantly alter the ability of the procedures to accurately predict time-history behaviour. It was found that in all three cases the dynamic behaviour was very consistent with that observed previously, and as a result the proposed design amplification methods also agreed well with the time-history results.

10.3 FUTURE DEVELOPMENTS

For the frames studied, the revisions to the direct displacement-based design method and the resulting methods of accounting for dynamic amplification have given very satisfactory results. However to better define the dynamic characteristics of reinforced concrete frames and the extent of application for the proposed methods, there remains some amount of investigation to be carried out.

- As mentioned the results for column moments have been evaluated with respect to storey moment sums. This implies that some column moment redistribution is allowed under seismic attack, and therefore that inelastic action is permitted. While this goes against the underlying philosophy of capacity design for frames, it is proposed that allowing some inelastic action to occur in columns above the ground level plastic hinge is acceptable provided that plastic hinges do not form at both ends of all columns on a given storey level. It is of interest to know what influence such effects would have on the frame behaviour, particularly with respect to the expected increases in storey drifts and potential for soft storey development. This could be investigated using inelastic column members over the full height of the buildings.

- The parametric study carried out to test the applicability of the proposed methods to more flexible frames exhibiting longer beam spans (and potentially shallower beam depths) was limited to a 12 storey frame. Clearly this needs to be extended to include a greater range of building heights, particularly for taller frames that tend towards elastic behaviour when using direct displacement-based design. The possibility of quantifying the shift in higher mode periods based on first-mode ductility, and therefore the decreased modal forces and participation, would be likely to produce a more general solution.

- The possibility that near-field ground motions will significantly alter the frame behaviour seen in this study needs to be considered and if required, modifications to the design approach developed to ensure that such motions do not generate excessive localised demands.

- Suggestions have been made for dynamic amplification in two-way frames, however the methods remain to be tested using inelastic time-history analysis.

- This study has concentrated on tube-frame behaviour, thereby utilizing short beam spans that are dominated by seismic action. The methods proposed therefore may not be applicable to frames with longer beam spans that tend to be dominated by gravity induced actions.

- The influence of P-Δ effects has not be investigated with respect to the proposed design and dynamic amplification methods. This is particularly important for the frames of low ductility where such second-order effects may reduce the stability of the structural response.

- The other important second-order effect not considered was the influence of torsion on building behaviour. The need for 3-dimensional modelling of such behaviour is significant, particularly to investigate the distribution of ductility demands in structures where base shear strength is unsymmetrical.

REFERENCES

1. Paulay, T., and Priestley, M.J.N., "Seismic Design of Reinforced Concrete and Masonry Buildings" John Wiley and Sons, New York, 1992, 744pp

2. Paulay, T., "Seismic Design of Ductile Moment Resisting Reinforced Concrete Frames, Columns – Evaluation of Actions", Bulletin, NZ National Society for Earthquake Engineering, Vol.10, No.2, June 1977, pp. 85-94.

3. New Zealand Standard NZS4203:1992 "Code of Practice for General Structural Design and Design Loadings for Buildings" NZ Standards Association, Wellington, 1992

4. New Zealand Standard NZS3101:1995 "New Zealand Concrete Structures Standard", NZ Standards Association, Wellington, 1995

5. Priestley, M.J.N., and Amaris, A.D., "Dynamic Amplification of Seismic Moments and Shear Forces in Cantilever Walls" Report No. ROSE 2002/01, European School for Advanced Studies in Reduction of Seismic Risk, Pavia, June 2002, 86pp.

6. Priestley, M.J.N., "Myths and Fallacies in Earthquake Engineering, Revisited" The Ninth Mallet Milne Lecture, IUSS Press, Pavia, May 2003, 118pp.

7. CEN (Comité Europèen de Normalisation), 2003. prEN 1998-1- "Design of structures for earthquake resistance. Part 1: General rules, seismic actions and rules for buildings." Draft No. 5 Doc CEN/TC250/SC8/N317, Brussels, Belgium, May 2002.

8. Sullivan, T.J., Calvi, G.M., Priestley, M.J.N., and Kowalsky, M.J., "The Limitations and Performances of Different Displacement-based Design Methods", Journal of Earthquake Engineering, Vol. 7, Special Issue 1, 2003, pp 201-241.

9. Priestley, M.J.N., and Kowalsky, M.J., "Direct displacement-based design of concrete buildings" Bulletin, NZ National Society for Earthquake Engineering, Vol.33, No.4, December 2000, pp 421-444.

10. Shibata, A., and Sozen, M., "Substitute Structure Method for Seismic Design in Reinforced Concrete", Jour. Structural Division, ASCE, Vol 102, No.12, 1976, pp 3548-3566.

11. Priestley, M.J.N., Calvi, G.M., and Kowalsky, M.J., "Direct Displacement-Based Seismic Design of Structures" IUSS Press, Pavia (in preparation) 2004.

12. Priestley, M.J.N., "Brief Comments on Elastic Flexibility of Reinforced Concrete Frames, and Significance to Seismic Design", Bulletin, NZ National Society for Earthquake Engineering, Vol.31, No.2, June 1998, pp 246-259.

13. Faccioli, E., Paolucci, R., and Rey, J., "Displacement Spectra for Long Periods", Earthquake Spectra, Vol.20, Issue 2, May 2004, pp 347-376.

14. Loeding, S., Kowalsky, M.J., and Priestley, M.J.N., "Direct Displacement-Based Design of Concrete Buildings", Structural Systems Research Report No.SSRP 98/08, University of California, San Diego, 1998.

15. ICBO "Uniform Building Code UBC '97" International Conference of Building Officials, Whittier, Ca.1997.

16. Mander, J.B., Priestley, M.J.N., and Park, R., "Theoretical Stress-Strain Model for Confined Concrete", Journal of Structural Engineering, ASCE, Vol. 114, No. 8, August 1988, pp. 1804 – 1826.

17. Carr, A.J., "Ruaumoko Program for Inelastic Dynamic Analysis – Users Manual", Department of Civil Engineering, University of Canterbury, Christchurch, New Zealand, 2002.

18. Otani, S. "Hysteretic Models for Reinforced Concrete for Earthquake Analysis". Jour. Faculty of Architecture, University of Tokyo, Tokyo, Vol.XXXVI, No.2, 1981, pp 125-159.

19. Medina, R.A., "Design Storey Shear Strength Patterns for Performance-Based Design of Regular Frames". ISET Journal, Special Issue: Performance Based Engineering, 2004.

20. Priestley, M.J.N., "Myths and Fallacies in Earthquake Engineering – Conflicts Between Design and Reality" Bulletin, New Zealand National Society for Earthquake Engineering, Vol. 26., No.3, Sept. 1993, pp 329-341.

21. Grant, D.N., Priestley, M.J.N., and Blandon, C.A., "Modelling Inelastic Response in Direct Displacement-Based Design" Report No. 2005/03, European School for Advanced Studies in Reduction of Seismic Risk, Pavia, July 2005, 104pp.

APPENDIX A
TIME-HISTORY RESULTS USING 5 REAL ACCELEROGRAMS

The following figures and tables summarise the real earthquake records used as a final verification for the methods presented in the report. The results shown are the average maxima for the column shear forces, bending moments, inter-storey drifts and displacement envelopes at the design intensity (I = 1.0).

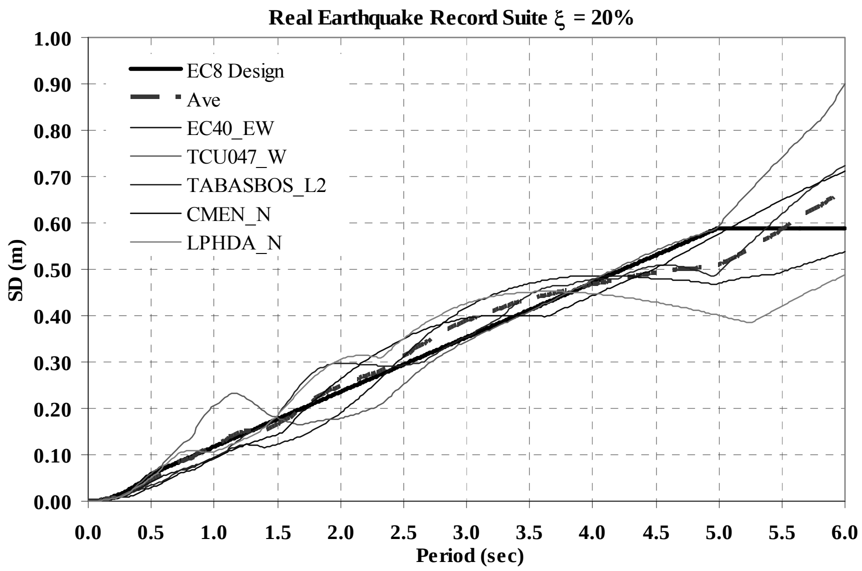

20% damping displacement spectra for the five real earthquake records used for method verification (note this is shown for a 0.5g PGA)

Summary table for the five real earthquake records

ID	Event	Year	M_w	Station	Component	Soil Type (NEHRP)	$R_{closest}$ (km)	Duration Orig. (sec)	Duration Used (sec)	Scaling	Scaled PGA (g)
EQ1	El Centro	1940	6.9	Imperial Valley	S90W	D	12.2	53.7	30	2.34	0.49
EQ2	Taiwan ChiChi	1999	7.6	TCU047	W	D	29.4	90	35	2.7	0.82
EQ3	Tabas	1978	7.4	Boshrooy	L2	C	26.1	35.0	34	5.51	0.48
EQ4	Cape Mendocino	1992	7.1	Fort – Fortuna Blvd.	000	C	23.6	44.0	30	3.62	0.42
EQ5	Loma Prieta	1989	6.9	Hollister Diff. Array	165	D	25.8	39.6	25	2.32	0.62

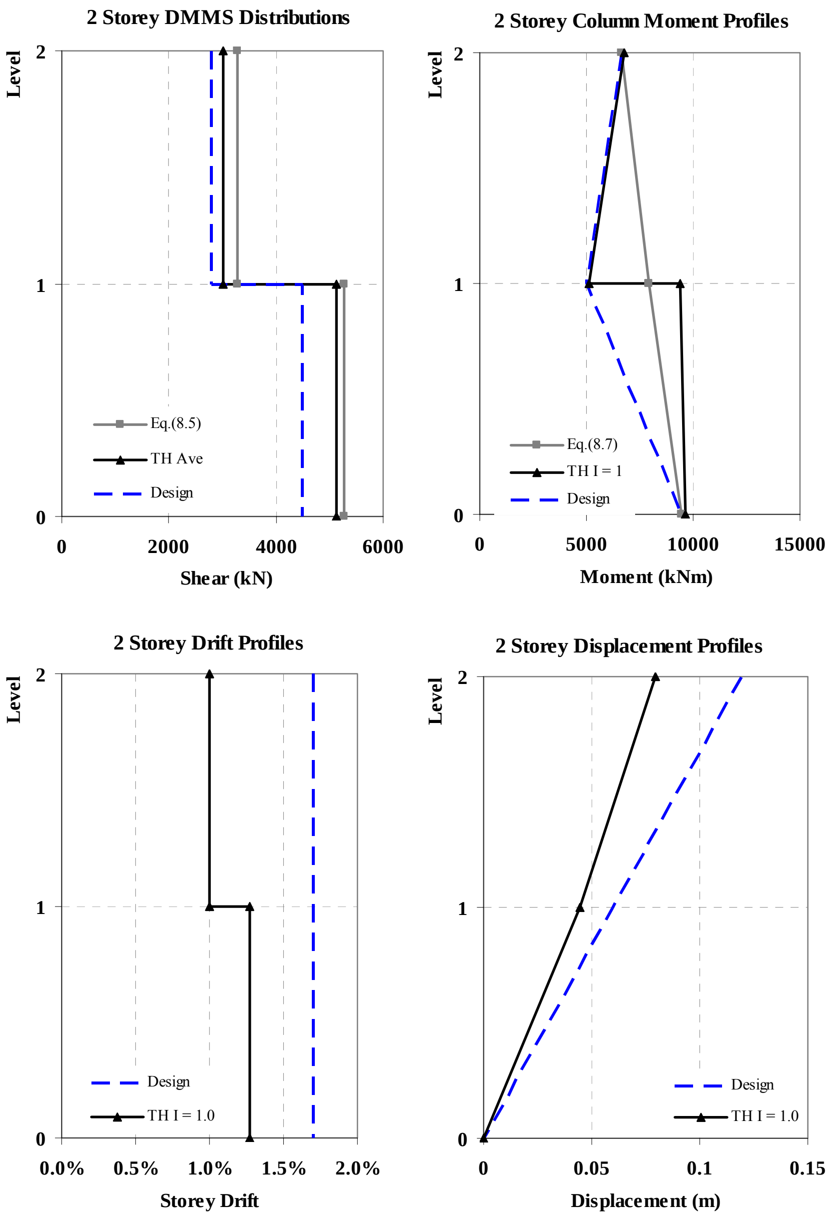

2 storey time history average results for column shear forces, storey column moment sums, inter-storey drifts and displacement envelopes. Also shown are the proposed DMMS for column shear forces, and moment amplification design curves.

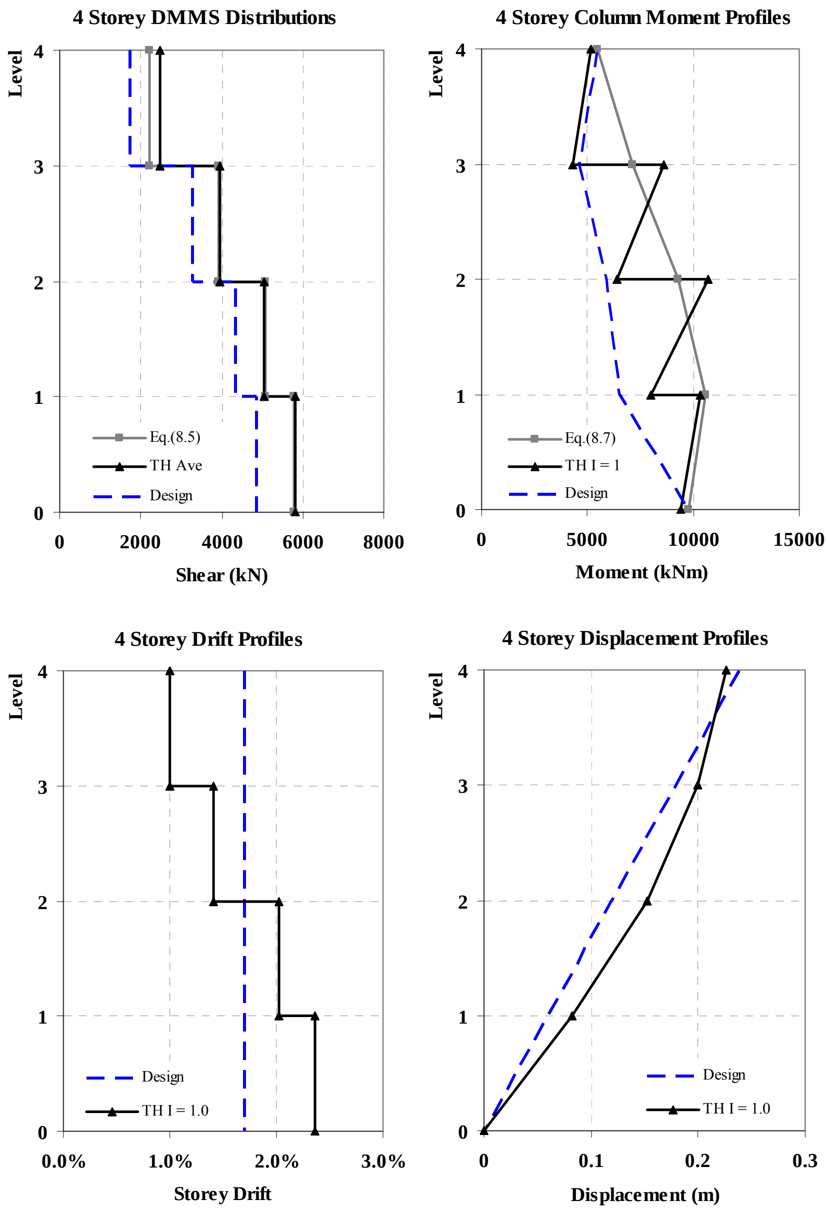

4 storey time history average results for column shear forces, storey column moment sums, inter-storey drifts and displacement envelopes. Also shown are the proposed DMMS for column shear forces, and moment amplification design curves.

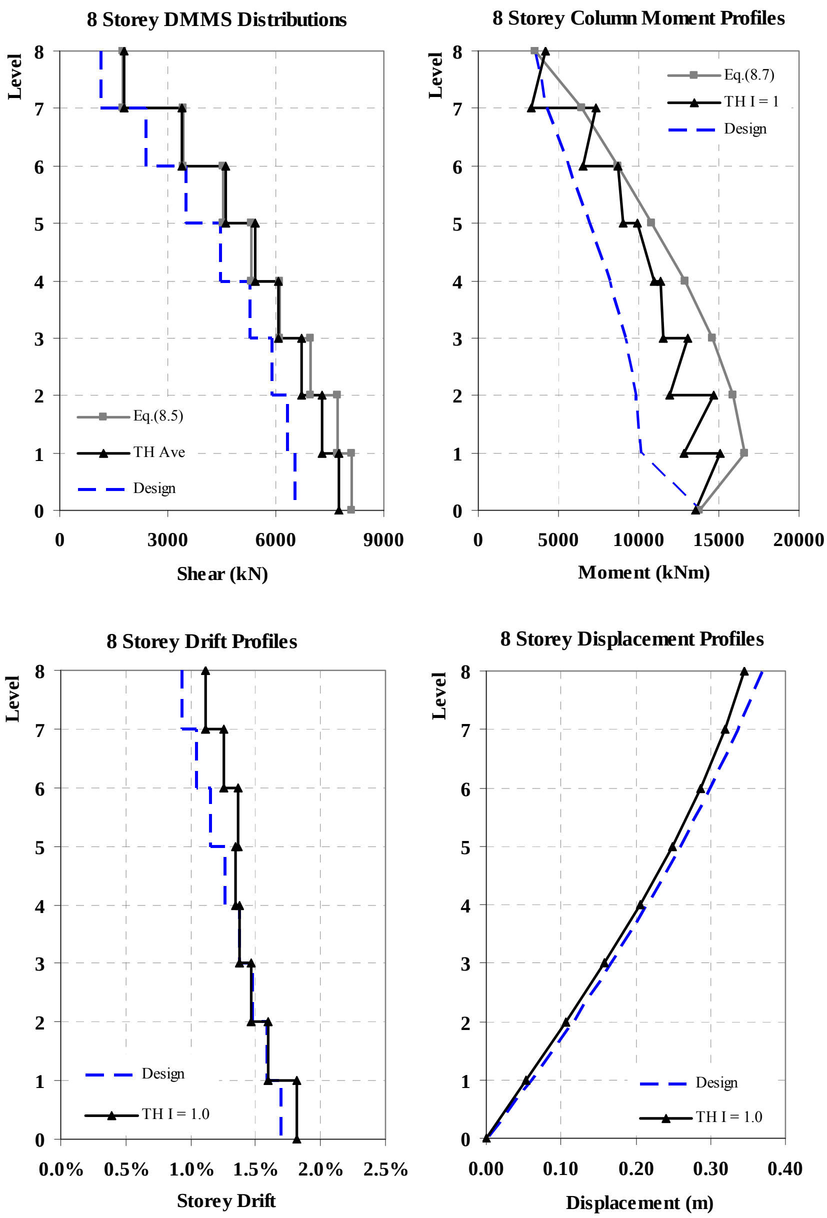

8 storey time history average results for column shear forces, storey column moment sums, inter-storey drifts and displacement envelopes. Also shown are the proposed DMMS for column shear forces, and moment amplification design curves.

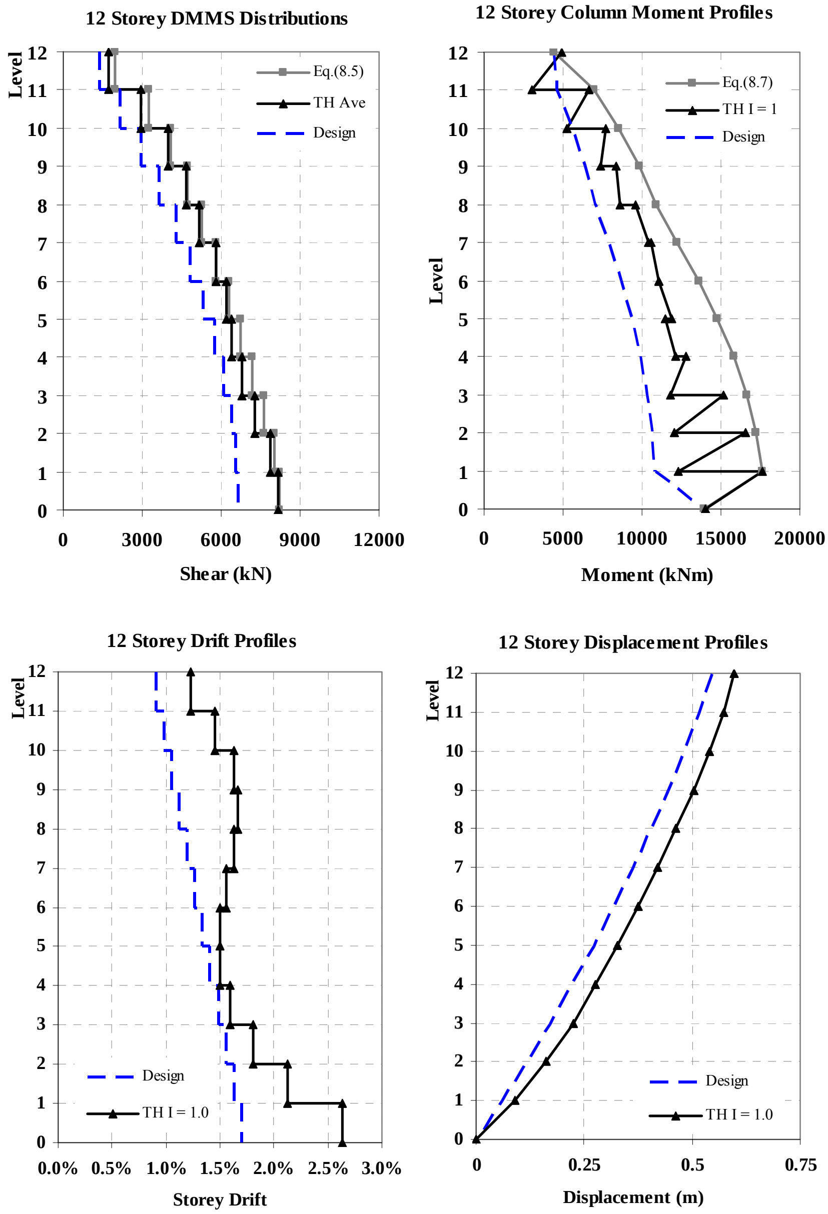

12 storey time history average results for column shear forces, storey column moment sums, inter-storey drifts and displacement envelopes. Also shown are the proposed DMMS for column shear forces, and moment amplification design curves.

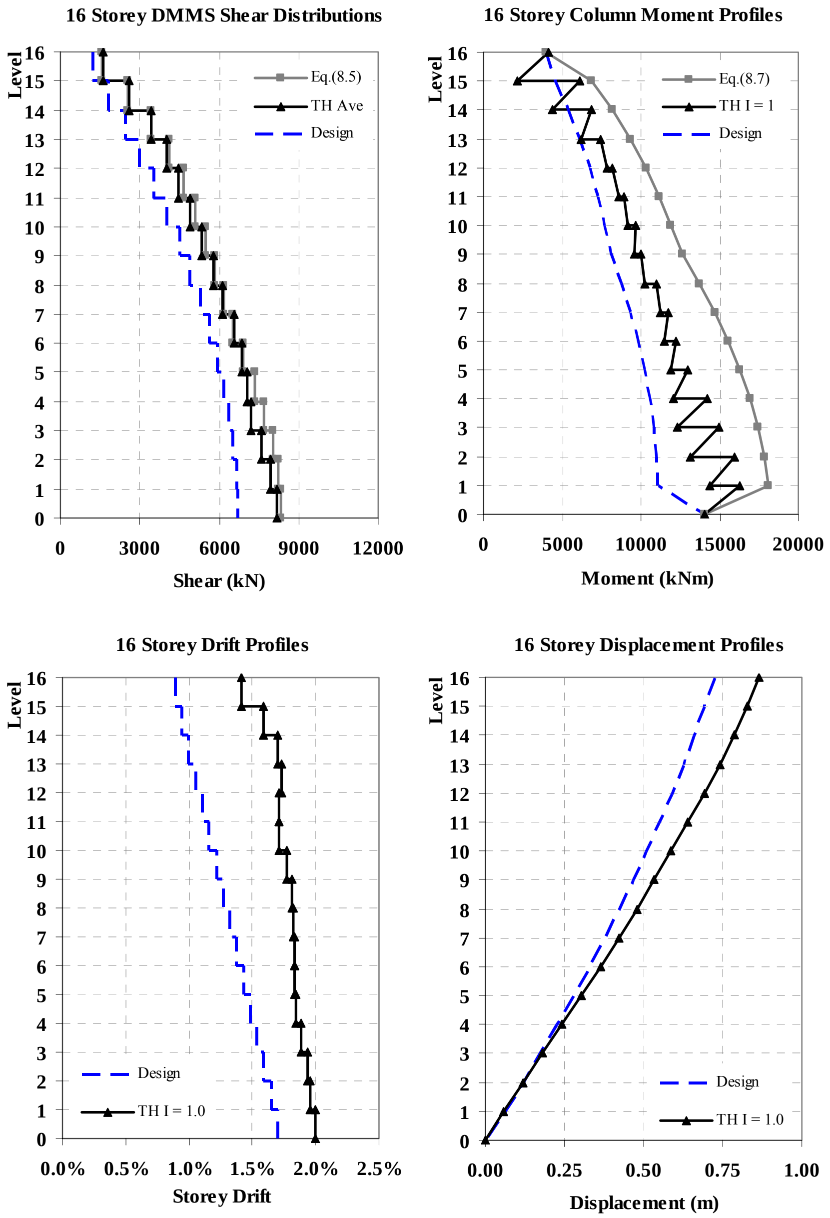

16 storey time history average results for column shear forces, storey column moment sums, inter-storey drifts and displacement envelopes. Also shown are the proposed DMMS for column shear forces, and moment amplification design curves.

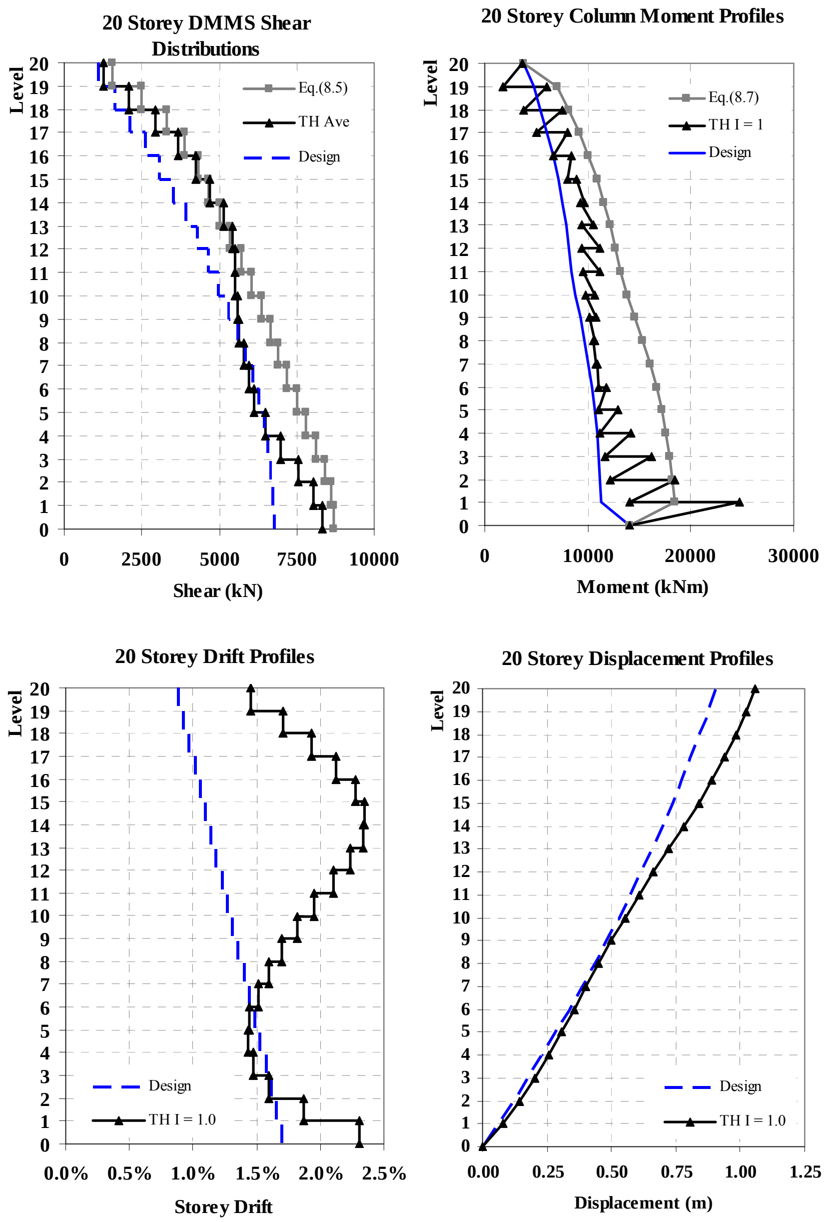

20 storey time history average results for column shear forces, storey column moment sums, inter-storey drifts and displacement envelopes. Also shown are the proposed DMMS for column shear forces, and moment amplification design curves.